The Pennsylvania State University

The Graduate School

Department of Mechanical and Nuclear Engineering

Ignition and Combustion of Nickel Coated and Uncoated Aluminum Particles in Hot Post-Flame Gas Environment

A Thesis in

Mechanical Engineering

by

Eric R. Boyd

Submitted in Partial Fulfillment
of the Requirements
for the Degree of

Master of Science

May 2009

The thesis of Eric R. Boyd was reviewed and approved* by the following:

Kenneth K. Kuo
Distinguished Professor of Mechanical Engineering
Thesis Advisor

Adri van Duin
Professor of Mechanical Engineering

Karen A. Thole
Head of the Department of Mechanical and Nuclear Engineering

*Signatures are on file in the Graduate School

ABSTRACT

An experimental study of ignition and combustion of isolated, Ni-coated, and uncoated aluminum particles was conducted. Ni-coated Al particles are of particular interest for two reasons. The Ni-coating prevents the particles from forming agglomerates due to the protective nickel layer. Intermetallic reactions between the nickel and aluminum are exothermic, giving an additional energy feedback to start the Al particle ignition. Two particle sizes (nominally 32 μm and 9 μm in diameter) were examined in this study. Since the coated and uncoated particles are from the same batch any differences between the ignition and combustion behaviors can be directly attributed to the effect of the Ni-coating. The ignition and combustion properties of the aluminum particles were examined in the post-flame zone of a multi-diffusion flat-flame (a modified Hencken burner) at atmospheric pressure. Isolated, single particles are burned in this experimental setup so the exothermic heating from the Ni-Al intermetallic reaction is of particular interest. This study shows that the applied nickel coating decreased the ignition temperature of the Al particles by 750 K on average for 32 μm particles and by 300 K for smaller 9 μm particles. These results are plotted against an effective oxidizer factor that takes into account the strength of O_2, H_2O, and CO_2 in the oxidation reaction of aluminum. Combustion times were measured by optical techniques to determine how the applied nickel coating would affect the combustion time. While there was significant data scatter, due to a broad particle size distribution, the results still showed that the combustion times for different sized particles were not noticeably affected by Ni-coating.

TABLE OF CONTENTS

LIST OF FIGURES

LIST OF TABLES

NOMENCLATURE

SYMBOL	DESCRIPTION	UNITS
F_d	Drag Force	[N]
C_d	Drag Coefficient	[-]
u	Air velocity	[m/s]
A	Cross Sectional Area of Particle	[m^2]
Re_D	Reynolds Number	[-]
D_p	Diameter of Particle	[m]
F_w	Weight of Particle	[N]
g	Gravitation Constant	[m/s^2]
V	Volume	[m^3]
r_p	Radius of particle	[m]
x_i	Mole Fraction of Species i	[-]
$X_{OX,eff}$	Effective Oxidizer Factor	[-]
a_i	Effective Oxidizer Strength Coefficient of product species i	[-]
T_{ign}	Ignition Temperature	[K]
F/O	Fuel-to-oxidizer ratio	[-]
P	Pressure	[Pa]
T	Temperature	[K]
R_i	Gas Constant of Species i	[-]
Yi	Mass Fraction of Species i	[-]
Pr	Prandtl Number	[-]
k	Thermal Conductivity of Gas	[W/m-k]
t_b	Combustion time	[s]
L_{streak}	Streak Length	[m]
u_{gas}	Particle Velocity	[m/s]
L	Length of Quartz Tube	[m]
Gr	Grasshof Number	[-]

Ra	Rayleigh Number	[-]
Nu	Nusselt Number	[-]
h	Heat Transfer Coefficient	[W/m^2-k]
r_o	Outer Diameter of Quartz Tube	[cm]
r_i	Inner Diameter of Quartz Tube	[cm]
$\dot{m}_i$	Mass Flow Rate	[kg/s]
$\dot{Q}_i$	Volumetric Flow Rate	[m^3/s]

GREEK SYMBOL	DESCRIPTION	UNITS
$\mu_{mixture}$	Dynamic viscosity averaged and weighted for the entire gas mixture	[Pa*s]
μ_i	Dynamic viscosity for species i	[Pa*s]
ρ_{gas}	Product gas density averaged and weighted for entire gas mixture	[kg/m^3]
ρ_{Al}	Aluminum density	[kg/m^3]
ϕ	Equivalence Ratio	[-]
ρ_i	Density of Species i	[kg/m^3]
α	Thermal Diffusivity	[m^2/s]
β	Gas Expansion Coefficient	[-]
ν	Kinematic Viscosity	[m^2/s]

SUBSCRIPTS	SUBSCRIPT MEANING	USAGE
in	Inner Quartz Tube Wall Temperature	T_{in}
out	Outer Quartz Tube Wall Temperature	T_{out}
o	Out Wall Radius	r_o
i	Innter Wall Radius	r_i
L	Nusselt Number of Overall Tube Length	Nu_L
film	Film Temperature	T_{film}

∞	Temperature at infinity	T_∞
i	Species i	
st	Stoichiometric Condition	$(O/F)_{ST}$
ox	oxidizer	$yi_{,ox}$, $\dot{m}_{ox}$
$fuel$	fuel	yi_{fuel}, $\dot{m}_{fuel}$
$mixutre$	Overall gas mixture	$\mu_{mixture}$
gas	Gas Density	ρ_{gas}
ign	Ignition	T_{ign}
OX,eff	Effecive Oxidizer Factor	$X_{ox,eff}$
p	Particle	D_p, r_p

ACKNOWLEDGEMENTS

The writer would like to begin by thanking Prof. Kenneth K. Kuo whose leadership and direction has helped me grow and learn more than I ever believed possible. It has been a great honor to work under him. His pursuit of excellence and perfection will, undoubtedly, have an impact on the rest of my life.

The author would also like to thank the support from Professor Alon Gany and Dr. Valery Rosenband of Technion in Israel. They provided the particles and valuable information that allowed for the completion of this study. Their generous help and assistance in greatly appreciated.

I would like to particularly thank Mr. Ryan Houim who has given insightful and thoughtful advice throughout the duration of this project. Also, I would like to thank Mr. Scott Blakeslee and Bao Qi Zhang who helped to fabricate some of the equipment that was used in this study. Finally, I would like to thank the immense and endless support I have received from my colleagues and friends, the current and former members at the High Pressure Combustion Lab; Dr. Eric Boyer, Mr. Pete Ferrara, Dr. Jeff Moore, Mr. Brian Evans, Mr. Andrew Cortopassi, Mr. Patrick Kutzler, Mr. Heath Martin, Mr. Timothy Wawiernia, Mr. Jonathan Essel, Mr. Alexander Colletti, Mr. Matt Degges. I truly feel privileged to have met and become friends with all of them.

Chapter 1

Introduction

1.1 Background

Aluminum particles have been used for a long period of time as an energetic additive in propellants and explosives. As can be seen in Figure **1.1** Al has a high volumetric heat of release when compared to other metallic additives and still performs fairly well on a mass basis without some of the other practical limitations, like toxicity or expense, of the other additives.[1] For these reasons aluminum is a very effective way to add a great deal of heat to a combustion system with the least amount of weight. Additionally, in rocket motor propulsion systems the Al particles act as an effective damping mechanism to suppress combustion instabilities. These reasons have resulted in the wide use of aluminum in propulsion applications.

However, the use of aluminum does not come without its share of significant drawbacks. Of particular problem is the high ignition temperature due to the protective oxide shell that forms on the outside of aluminum. When aluminum comes into contact with the oxygen found in ambient air it forms a protective oxide coating of Al_2O_3. The melting temperature of Al_2O_3 is 2327 K making the aluminum particle ignition temperature prohibitively high. This is of particular interest because aluminum is largely

used as a metallic fuel that is aerosolized in the post-detonation blast cloud of a thermobaric explosive (TBX) event. However, high ignition temperature of aluminum particles can be of particular concern in blast cloud environments of thermobaric explosives (TBX), where large quantities of aluminum particles need to be ignited rapidly for a subsequent sustained blast wave fueled by the metallic combustion process.

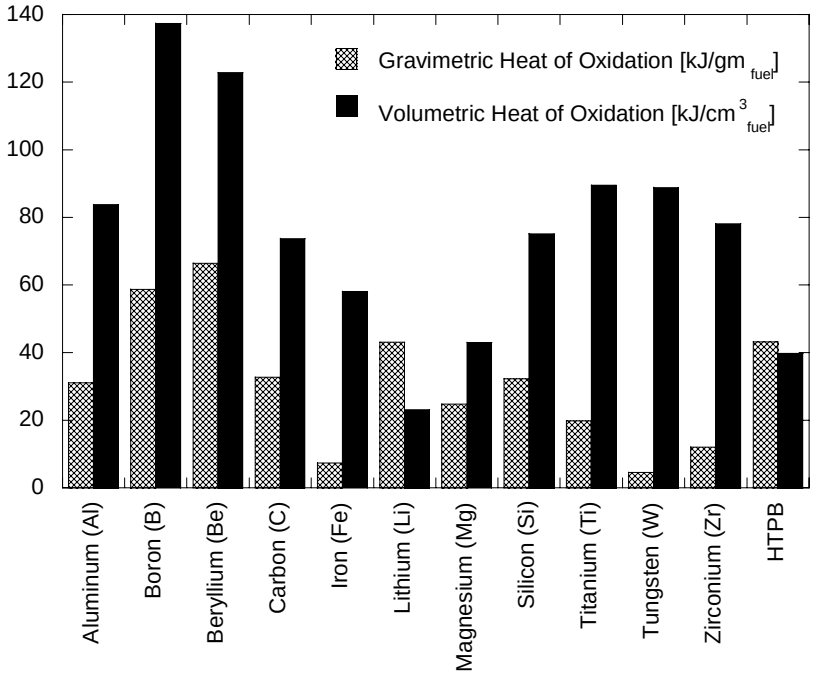

Figure **1.1**: Heats of combustion with oxygen (heat of oxidation) of several fuels[1]

The concept of thermobaric explosives, also known as volumetric explosive or vacuum bombs, is relatively simple. A bomb or shell is detonated to form an aerosolized cloud of combustible dust or mist. This cloud is ignited and subsequently burned to add more energy to the system and causing a sustained hydrodynamic over-pressurization wave that will extend in all directions. The effects are devastating with the primary destruction combing from the over-pressurization wave and fireball created by the initial

blast. This will extend in all directions, around corners, through corridors, and even through barricades[2].

These weapons have become more useful in the current US war on terror. The explosives are particularly useful in destroying cave dwellings and underground bunkers. Additionally the high heat release that is created by the blast wave makes it a desirable candidate for chemical and biological agent defeat. Conventional explosives and warheads use fragmentation as the primary means of killing targets. However, this tactic is not very useful in situations where enemy combatants can hide deep in caves or bunkers. Also, a conventional explosive do not burn hot enough or long enough to destroy chemical or biological weapons and in many cases the blast will only serve as a mechanism for dispersal. This is where a thermobaric bomb can become a particularly useful weapon. Using lessons from the explosions that would occur in coal mines when a cloud of fine coal particulate would began to combust, the US military began to develop a thermobaric weapon that when dropped in the mouth or opening of a cave an aerosol cloud would develop that travel down the cave when ignited it would cause a deadly over pressurization wave that can reach into the depths of the cave and even bounce off of walls and other features of the cave. Finally, the massive combusting cloud robs all of the oxygen from the air leaving any remaining entrenched targets to be neutralized by asphyxiation[2]. Additionally the fireball hot fireball created by these blasts in conjunction high energy blast wave creates a viable mechanism for destroying dispersed biological and chemical agents.

However while aluminum is an excellent choice of fuel for this application its high ignition temperature serves as a significant drawback. By decreasing the ignition

temperature of the aluminum particles, significantly fewer particles will be left unburned resulting in a stronger, more effective blast wave. The focus of this study is to investigate the effects of a thin coating of nickel around the surface of the aluminum particles. Nickel acts to reduce the ignition temperature of the Al particles in two ways, first it reduces the likelihood of aluminum particle to form into large agglomerations due to the lower melting temperature of nickel when compared to aluminum oxide. Additionally, the nickel and aluminum begin to react with each other causing exothermic intermetallic reactions, which serve to begin the Al-particle ignition and subsequent combustion process.

1.2 Research Motivation

The intent of this research is to determine if applying a thin layer of nickel to the surface of aluminum particles provides distinct advantageous properties to the particles. Untreated aluminum particles suffer the issue of having such a high ignition temperature meaning that in many cases the particle is either not igniting or igniting so late that it is not adding the full potential of heat to the system. There are multiple ways at attempting to solve this problem. One method is to alter the geometry of the particles by either shrinking the size or altering the aspect ratio. This could be advantageous in reducing the ignition temperature and burn time. However, this could also lead to practical problems such as the high sensitivity, high cost associated with nano-aluminum, and the packing density issues associated with aluminum flakes. Another method is to alter the inhibitive oxide coating of the aluminum particles. Simply removing the coating is not going to be

a viable solution for several reasons. First, bare aluminum particles would become pyrophoric meaning that they could auto-ignite in ambient air making them prohibitively dangerous. Secondly, if the aluminum were not to auto-ignite in the air they would simply develop an oxide coating unless they were stored in an inert atmosphere. These practical implications lead to another method that would reduce the ignition temperature without significantly changing geometry of the particle. Applying coatings that have a lower melting temperature than aluminum oxide would, in fact, drop the ignition temperature of the particles. The new coating would melt off at lower temperatures than aluminum oxide allowing the active aluminum to begin to react with the oxidizing atmosphere sooner than if left untreated. Taking this one-step further several coatings could have the ability to react with aluminum providing additional heat to the reaction. This is beneficial because the it would mean that the coating itself could begin the reaction at a lower temperature because the coating would be effectively adding heat to the system rather than just being an inert barrier to ambient oxygen adding nothing more than dead mass to the system. This is why nickel coatings on aluminum particles are of particular interest. Nickel has a lower melting temperature than alumina at 1728 K and it also reacts exothermically when alloyed with aluminum. This means that a nickel coating on aluminum particle will react exothermically, if this reaction releases sufficient heat it could begin the oxidation reaction of aluminum at a much lower temperature.

1.3 Research Goals

The goals of this research are to compare the ignition and combustion behavior of nickel-coated aluminum particles and uncoated aluminum particles. To complete these goals the following objectives are going to be carried out.

1. Test the ignition temperature of the Ni-coated against their uncoated counter parts in a multi-diffusion flat-flame burner to see if the nickel coating provides any advantageous effects.
2. Test the combustion behavior of the coated and uncoated aluminum particles. If there is a significant variance in the duration of the combustion this could mean several things. A short burn time could show that the particles are not burning completely and a long burn time could mean that the nickel is inhibiting oxidizer transport to the reacting aluminum. Each would indicate that there are potentially more complex processes that are occurring which would require a deeper understanding.
3. Compare the effect of particle size on the combustion behavior of the aluminum particles. Two different particle sizes will be used in this study, 9 μm and 32 μm-sized particles in nominal diameter. The purpose of selecting these sizes is that ignition and combustion of 32 μm particles should clearly be diffusion limited, while the ignition and combustion of 9 μm particles lies within the transition regime between diffusion dominated mechanisms and kinetically dominated mechanisms.

4. Compare the effects of the oxidizing atmospheres of O_2, H_2O, and CO_2 on the combustion of the coated and uncoated particles. The reactant and oxidizer compositions will be varied so that the oxidizing atmosphere of the particles can be adjusted. This means that post flame equilibrium calculations must be completed to find how the so the post combustion oxidizers can be effectively varied as a function of the inlet species.

Chapter 2

Literature Review

Aluminum combustion has a long history that extends over 50 years. It has been used in a wide variety of applications particularly as a fuel additive for both propellant systems and explosive applications. Because of the effectiveness of aluminum as not only an excellent additive to solid propellant systems but also serving as a damping mechanism is solid motors there is a large body of literature surrounding this area of combustion.

Price[4] investigated the molten metal accumulation on the burning surface of propellants before the particles are lifted in the combustion region of a rocket motor. Using the work of several other studies Price[4] described the distinct combustion zones of surrounding each of the burning aluminum particles. The convective stream in composed of several regions: a bright flame envelope, a dimmer convected flame smoke shroud, a convected Al_2O_3 smoke trail, and an attached oxide lobe on the surface of the particle. Additionally, he stated that many recovered burned particles formed into hollow oxide spheres. Prentice[5] investigated single particle combustion in hot gas environments and observed significant fragmentation along with jetting-and-spinning phenomena, which he attributed to the oxide lobe formation on the particle surface.

Beckstead[6] formed a comprehensive aluminum combustion summary from a wide range of sources. He found a common ignition temperature of about 2300 K, which is the melting temperature of the aluminum oxide shell the forms on the particle surface.

Additionally, he summarized that the ignition delay of the particles was dependant on the thickness of the oxide shell that has formed on the surface of the particle. He compiled data to find if the "D^2 law" was applicable, but instead found that the "D^n law" was more applicable for larger particle sizes due to the oxide layer formation with the n exponent being between 1.5 and 1.8. Additionally, he compiled several works that compared the relative oxidative effectiveness of oxygen, water, and carbon dioxide. He concluded that O_2 was the most effective oxidizer, H_2O was approximately 50 percent as effective, and CO_2 was about 20 percent as effective. However, in most explosive and rocket motor environments oxygen is not widely available in any significant quantities, in these cases H_2O and CO_2 are the considered to be the primary aluminum particle oxidizers. His correlation is widely regarded as the most effective means of modeling aluminum combustion behavior down to 10 μm.

Bazyn et al.[7] conducted a study on the combustion of 10 μm-sized aluminum particles in the reflected region of a shock tube and found that the CO_2 is slightly more effective than H_2O as an oxidizer. They found an opposite trend in the effectiveness of H_2O, CO_2 and O_2. They also found pressure exponents of −0.9, 0.2, and 0.3, for O_2, H_2O, and CO_2 respectively, $(i.e., t_b \propto p^n)$. Bayzn et al.[8] also used the reflected region of a shock tube to study the combustion of 80 nm aluminum particles. They found that with nano-aluminum the reaction times begin to decrease significantly with increasing ambient temperature, this data fits well in an Arrhenius form. They also found that the combustion duration of the aluminum particles is a strong function of pressure, with combustion time decreasing by a factor of 4 when the pressure of the oxidizing gases was increased from 8 to 32 atm. This means that when the aluminum particle sizes begin to

drop below the level of 10 μm there is strong evidence to support the fact that the combustion of the particles is beginning to be limited by kinetic mechanisms rather than species diffusion to the surface of the particle. These findings are of particular interest because the 9 μm particles that are going to be tested in this study are within the transition region between diffusion and kinetic limitations.

Using lessons learned from nano-aluminum combustion Houim et al[9] completed an experiment that studied the ignition and combustion of aluminum flakes, 16 μm diameter and 200 nm in thickness, in the post flame gases of a Hencken burner. Ignition temperatures as low as 1800 K were reported and with the lower ignition temperature attributed to the asymmetrical nature of the flakes that caused increase stresses in the protective oxide layer. Additionally, the aluminum flakes had the advantage of being relatively inexpensive and having combustion times that were similar to their 200 nm spherical counterparts. These results were very interesting and promising, but not without a drawback. The aluminum flakes, due to their unusual geometry, suffer from a very low packing density when loaded into propellants and explosives making them an undesirable alternative to bulk aluminum particles.

Another method that has been considered to reduce the ignition temperature and ignition delay time is to apply either a reactive or a protective coating to the outside surface of the aluminum particles. A reactive coating could ignite at a lower temperature and would be hot enough to begin the aluminum combustion process. However, this could be problematic if the reactive coating oxidized forming an additional protective boundary on the Al particles. Another option is to apply a protective coating that would melt at a lower temperature than aluminum oxide and effectively prevent ambient oxygen

from ever reaching the surface of the aluminum during storage. Then in the combustion event the coating would simply melt off at a lower temperature and expose active aluminum to an oxidizing atmosphere. One coating that was of particular interest a thin layer of nickel. Previous studies have shown that applying a nickel coating will reduce the ignition delay time and particle ignition temperature for several different particle sizes. A nickel coating is advantageous for multiple reasons. First the nickel coating prevents agglomerations from forming[10] due to the lower melting temperature of nickel (1723 K) as compared to aluminum oxide (2327 K). Additionally, the nickel and aluminum alloy together creating intermetallic reaction that is exothermic, which has enough heat release to begin the oxidation reaction of nickel. This means the nickel coating acts as both an energetic coating and a protective coating at the same time.

Babuk et. al.[10] completed an experimental study on the effect of applied coatings on agglomerate formation in propellant combustion. They found that nickel and fluorinated hydrocarbon coatings eliminated the largest agglomeration in high-pressure applications. However, in low-pressure applications, the effects on reducing the agglomerations were not as significant. Additionally it should be noted that while the large agglomerates were eliminated the agglomerations that did occur contained more metal content while less oxide content.

Brietner et. al.[11] also completed a study where they compared the effect of several different metallic coating in addition to alloyed particles in an attempt to reduce particle agglomerations. They coated particles with copper, nickel, and iron and also alloyed aluminum with both magnesium and copper. The purpose of the study was to find how metallic encapsulation prevents particle agglomerations that form on burning propellant

surfaces. Nickel performed particularly well due to its elevated melting temperature (1728 K) preventing the particles from forming into agglomerates at the gas phase layer of the propellant combustions. Additionally, it was noted, in this study that the coated particle burned more completely than the uncoated particles and formed less agglomerates than the alloyed particles.

Yagodnikov et. al.[12] completed a study on the effect of a nickel encapsulation on flame propagation in an aluminum particle aerosol. They theorized that the high melting temperature of the Ni would prevent agglomerations, but would still allow an ignition temperature considerable lower than an alumina coating. Experiments were carried out in a constant-volume at atmospheric pressure. A flame would progress from an open end of a vertically located tube to a closed end producing a laminar flame-propagation regime. They found that adding the nickel coating increased the flame speed of the aerosol by approximately 1.5-4 times the value of typical aluminum particles. This occurred without considerably reducing the combustion characteristics of aluminum particles. Additionally, it was found the ability of the particles to disperse was not affected by the particle coating.

Another area that warrants particular interest is the combustion synthesis of nickel-aluminides. Aluminum based intermetallic compounds have high potential for use at high temperatures due to their low density and increasing strength with temperature. Additionally, these materials have exceptional creep and corrosion resistance making them particularly useful for a large range of applications. In many cases, nickel-aluminides are formed by heating either coated aluminum particles with nickel or mixing aluminum or nickel particles with high quantities of Ni[13]. Many of these materials are

formed by slow heating in vacuum or inert environments meaning that the combustion synthesis is relying on an exothermic alloying reaction between the nickel and aluminum to initiate and complete the reaction to form NiAl compounds.

Hanyaloglu et. al.[13] performed a study on creating Ni_3Al intermetallic alloys using reactive sintering. They used fine (2μm) aluminum particles with a thick nickel coating that are three times the mass of the aluminum. One of the tests that were run is differential thermal analysis, DTA, to find and understand the exothermic and endothermic reactions that were occurring under slow heating. Referring to the binary phase diagram[14] in Figure **1.1** there is a eutectic near 640^{o}C corresponding to about 10 wt% of nickel. In the cases of the Ni-coated aluminum when the powder was slowly heated it became liquid at 640^{o}C and provided a means for rapid interdiffusion Al and Ni. Subsequently the compound formation generated a great deal of heat through exothermic reactions. This is important to note because intermetalic reactions may, in some instances, kick off the combustion reaction.

Thiers et. al.[15] performed a study where they pressed disks of 2 to 1, Al to Ni mixtures and heated them under a near vacuum to find when a thermal explosion would occur under varying heating rates from 200 K/min to 900 K/min. The tested 3 different mixtures, two were binary mixtures of separate Ni and Al particles. The other was a batch of Ni coated Al particles. The binary mixtures had ignition temperature near 1000 K that was independent of the heating rate. However, the Ni-coated Al particles had an ignition temperature of 1100 K at a slow heating rate of 200 K/min and a 900 K ignition temperature at a heating rate of 900 K/min. Additionally, the maximum temperature that

was attained was near the adiabatic flame temperature for these particles (~1900 K). The ignition temperature seemed to be related to the melting temperature of the eutectic that occurs at 910 K (see fig. 1.1) and the melting temperature of aluminum at 933 K. This result was confirmed with previous studies on Ni-Al reaction systems. Although, it is important to note that this study was unique in that it was the first to test a mixture where the aluminum is in a higher quantity and where the heating rate was high at 900 K/min. In addition, many past studies found that the heating rate's effect on the ignition temperature seem to be inconclusive. Other studies have shown a decrease in ignition temperature[16], no effect on the ignition temperature[17], or an increase in the ignition temperature[18].

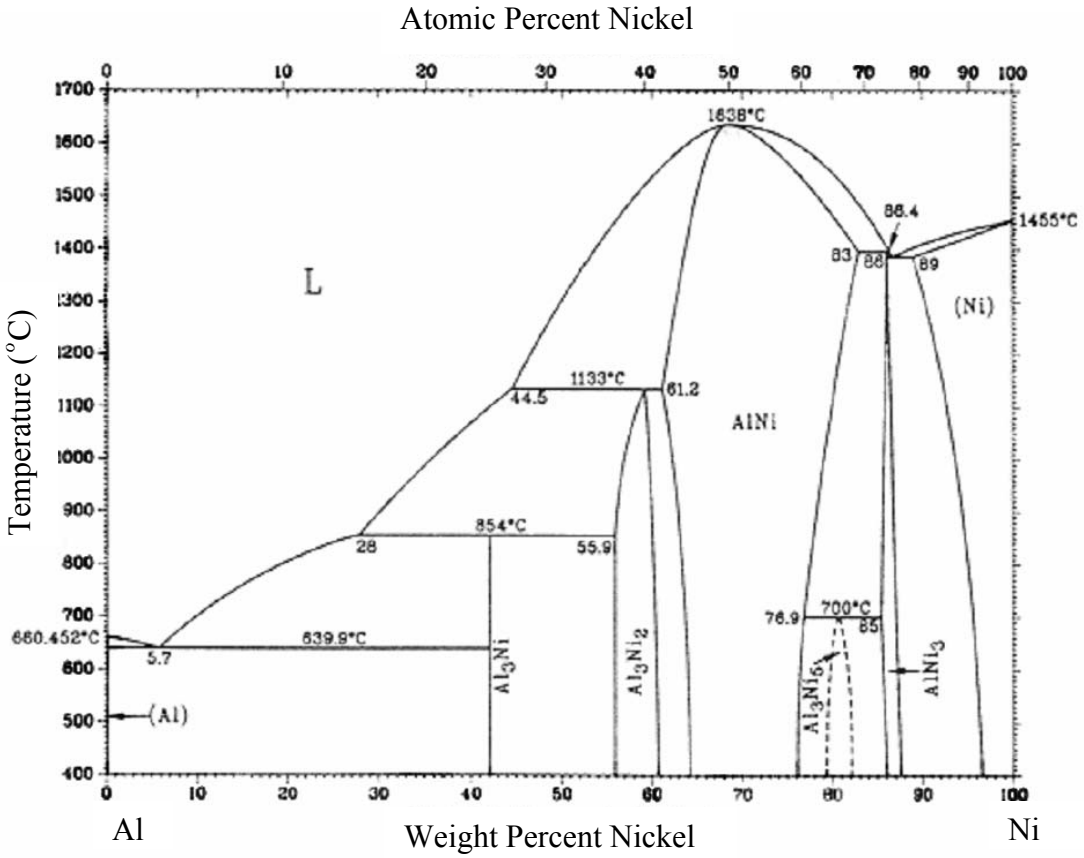

Figure **2.1**: Binary phase diagram for nickel and aluminum.[14]

Hahma et. al.[19] completed a full investigation on the effectiveness of various coatings on activated aluminum powders. They applied coatings of a complex fluorinated compound, cobalt, and nickel. These samples were then tested and compared against the uncoated counterparts using four different methods: microscopic imaging of the pre-ignition process, digital imaging of the combustion process in air, nitrogen, and carbon dioxide, TGA, and DSC. They found that the complex fluoride coating prevented agglomeration in all stages of burning, while the metallic, cobalt and nickel, coatings promoted aluminum oxide agglomeration while preventing agglomeration during the combustion reactions. Additionally, they found that the ignitability of the all of the materials was significantly improved, with the untreated particles showing the inability to ignite at all. All of the treated particles ignited and burned in atmospheres of carbon dioxide and air, while only aluminum particles with a nickel coating of 10 wt% were able to be ignited in a pure nitrogen environment. Even though the cobalt coating showed that they were able to ignite at the lowest temperature in these slow heating experiments it was the nickel-coated particles that showed the greatest ignitability.

The reactions of the nickel-coated particles in this study are of the most interest. Two types of nickel-coated particles were tested, one with a 1% Ni-coating and one with a 10% Ni-coating. It was found that the 1% Ni-coating was not sufficient in many cases to overcome the endotherm created by the melting aluminum within the particle and in many cases the particles with only 1% Ni-coating did not behave differently from the untreated particles. Exothermic reactions were believed to be occurring within the metallic compounds and it was found the nickel-coating prevented particle agglomerations prior to and during combustion. The burn rate also improved with the

nickel-coating and it was the most pronounced when the particles were combusted in air. The increase in the burn rate was attributed to the catalytic effects of the nickel coating, particularly that it increased the diffusive transport of oxygen and nitrogen through the oxide lobe of a burning particle. This increased the local temperature, thus increasing the diffusion even more significantly. These effects were so strong that the aluminum particle coated with 10 wt% Ni showed nitride formation even when combusted in air.

Rosenband et. al.[20] completed a study where activated aluminum particles were studied as an additive to energetic materials. They were attempting to shorten the ignition delay time and to enhance the combustive characteristics of energetic additives. Aluminum particles were activated by applying a coating of various oxidizers as well as a nickel coating to the surface of the particles. The portion of this study that is of most interest is the effect of the nickel coating on enhancing the combustion of the aluminum particles. They applied a thin coating of Ni (5 wt%) to aluminum particles that appeared as a series of bonded 100-200 nm spheres on the surface the aluminum particles. The primary objective was to study was to reduce the agglomeration of aluminum particles in propellant combustion. Tests were completed where two types of propellant were placed adjacent to one that contained 15% uncoated 6μm Al particles and the other with 15% 6μm Al particles that had 5 wt% coating of nickel. The propellants were then burned and photographed at 1000 frame per second. It was quite obvious from photographic evidence that the propellant with a nickel coated contained significantly smaller particle agglomeration. However, the pressure effects of the particles were not discussed.

Additionally, they completed several tests where they placed the Al particles on a small piece of electrically heated canthal tape and slowly heated in atmospheric air.

Their results were surprising, showing a significant reduction in the ignition temperature of the Al particles. It was found that the tape could not be heated to a high enough temperature to ignite the untreated aluminum particles, while nickel coated particles showed the ability to ignite. Referring to the phase diagram that is shown in figure 1 they theorized that a eutectoid reaction occurred at 640^{o}C forming an intermetallic phase on the surface of the particle of Ni/Al. As the particles continue to heat a peritectoid reaction occurs at 1100^{o}C creating an all liquid phase of liquid Al and NiAl. The liquid interface allows for ready diffusion of oxygen to the aluminum surfaces. Additionally, the exothermic heating of the intermetallic reaction between nickel and aluminum further speeds the diffusion of oxygen to the surface of the aluminum particle.

Bocanegra et. al.[21] carried out a study on using both a nickel coating and particle size reduction to reduce the ignition temperature of aluminum particles. Using an electro-dynamic levitator and laser heating the particle ignition delay time and combustion time at different nickel contents were studied. It was observed that the ignition delay time significantly decreases with increasing nickel mass fraction from 0-3%. The data obtained showed a clear distinction between two ignition delay times. Particles with a Ni coating between 3-14 wt% showed a much shorter ignition delay time. The combustion time did increase with increasing weight fraction if nickel up to 5 wt% then as the wt% increased from there the combustion time fell to baseline values. Particles were examined using SEM analysis and it was found that some particles were not completely covered with Ni. These particles would contain grains of Ni along the surface, but alumina would still be present. Despite the lack of homogeneity, the

partially coated particles still ignited at reduced temperatures from the uncoated particles. This seems to indicate that intermetallic reactions between the Ni and Al are causing the ignition delay time to reduce. The fact that the combustion time decreases as the particles coating become homogenous indicates that the cracking of the nickel shell after the aluminum has fully become molten leads to a more energetic reaction.

Andrzejak et. al.[22] studied the ignition mechanism of single nickel coated aluminum particles. The study conducted a series of tests using an electrodynamic levitator then laser heating the particles in argon and carbon dioxide atmospheres. The particles that were used in this study were quite large, approximately 2.5 mm. Three particle coating thicknesses were used containing a 6, 29, or 56 wt% coating of Ni. The experiments that were performed in Ar atmospheres showed that the particle containing 29, or 56 wt% Ni were able to react without oxidizer present. However, the coating of 6 wt% proved to be too thin of a coating to ignite the particles. It was found that the ignition temperature was 1325^{o}C independent of the atmosphere (Ar or CO_2) or the nickel content.

By quenching particle in different stages of combustion, they were able to examine the way that the nickel interacted with the aluminum. The following mechanism was proposed. As the aluminum melts at 660^{o}C a solid layer of $NiAl_3$ begins to form at the interface. Upon reaching the melting point of $NiAl_3$ at 854^{o}C, solid Ni_2Al_3 begins to form at the interface. At 1133^{o}C, the Ni_2Al_3 subsequently melts and begins to form NiAl, which penetrates deep into the outer Ni shell. The NiAl reaction is the most exothermic and with the increase in surface area as more NiAl is formed results in a self-

accelerating reaction. These particles are igniting several hundred degrees higher than in prior studies because the rapid heating does not allow the time for significant heat losses. It is theorized that the particles with a 6 wt% coating did not ignite because the of heat loss into the center of the large particles. This was not the case in other studies where particles with small percentage of nickel showed the ability to ignite. This indicates that different phenomena might be at causing smaller particles to ignite at lower temperatures.

Chapter 3

Experimental Methods

This experiment will test two different types of particles with and without a nickel coating. Additionally, two particle sizes will be examined to find how the size of the particle affects the ignition and combustion behavior of the particles. A modified Hencken burner is used to create hot, post-combustion products that will be used to study both the ignition temperature and combustion duration of the particles as they burn in various oxidizing atmospheres.

3.1 Particle Types

The particles that were studied in this investigation were supplied by Dr Valery Rosenband and Dr. Alon Gany from Technion in Israel. They are aluminum particles that were coated in a thin layer of nickel that accounted for approximately 5 wt% of the total particle. The coating technique is proprietary information so little is known about the actual process. The Al particles consisted of two sizes that were 9 μm and 32 μm. These sizes were used because 9 μm particles begin to exhibit some behavior or kinetically controlled particles while 32 μm particles have been well characterized as diffusion limited. Several SEM micrographs of the particles were collected by Dr. Bangzhi Liu of the Material Characterization Lab at Penn State University and are shown in Figures **3.1** throgh **3.3**.

Figure **3.1** is an image showing a large number of 9 μm particles spread across the entire slide to show the general shape and morphology of the many of the particles. Figure **3.2** is a close up image of the 32 μm particles to exemplify the surface of the particle. As can be seen from the images the particles are not necessarily spherical but have a round profile and some significant variation in size. Additionally the coating that was applied to the particles is a mostly uniform that appears as nano-sized spheres spread all over the surface of the particles. However, in some cases the particles were not completely coated and this resulted in a bare spots where the aluminum would show through the Nickel coating as in Figure **3.3**.

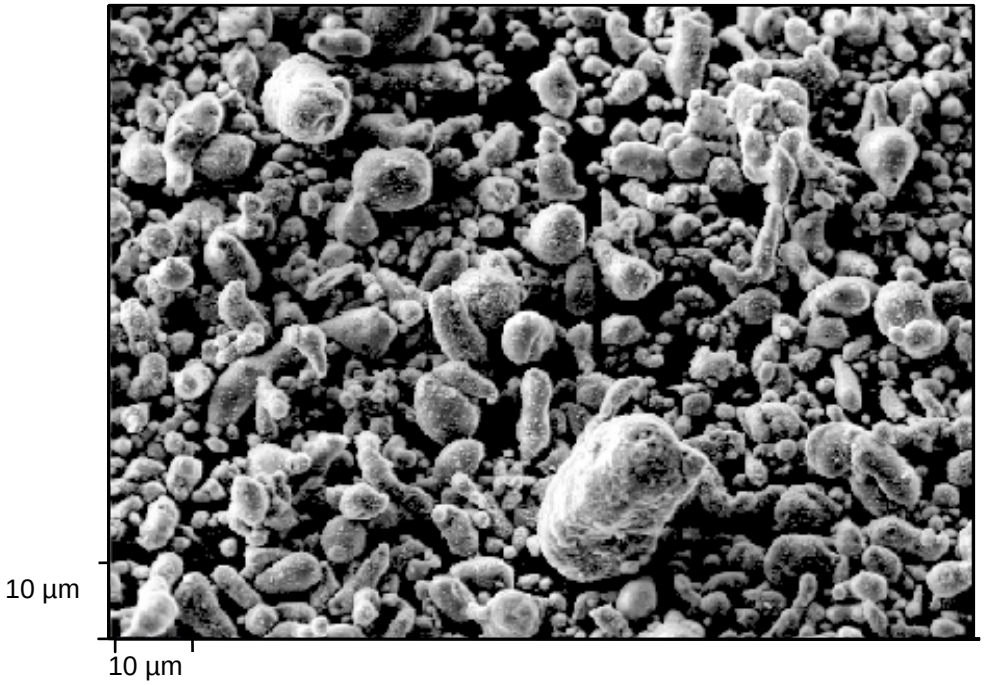

Figure **3.1**: SEM micrographs of the 9 μm Ni-coated Al particles. Note the large size distribution and variation of particle shapes.

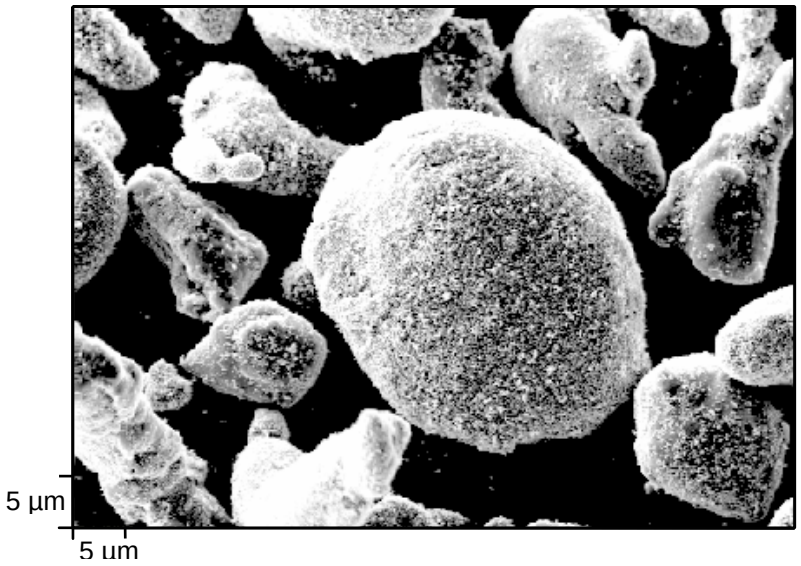

Figure **3.2**: SEM micrographs of the 32 µm Ni-coated Al particles to exemplify the particle surface.

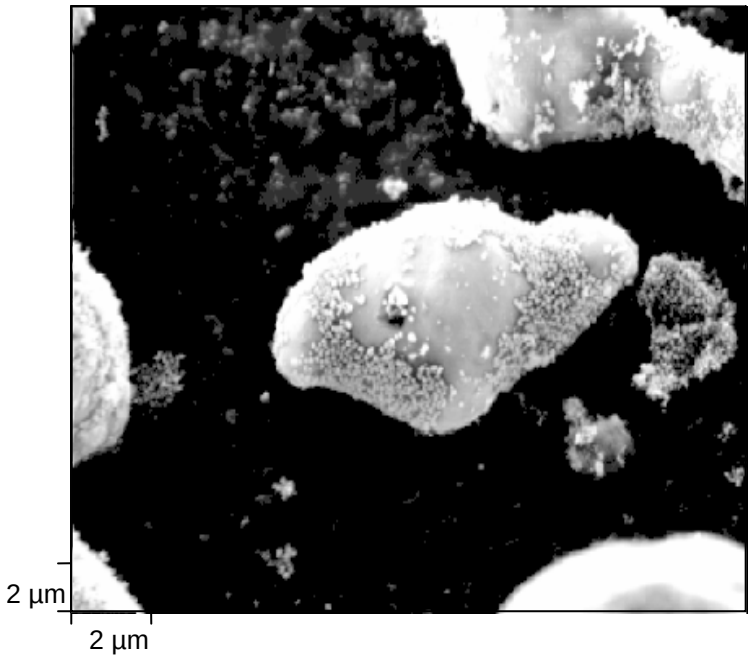

Figure **3.3**: SEM micrographs of a 32 µm Ni-coated Al particles to show the bare spots that occurred on some of the particle surfaces.

3.2 Experimental Apparatus

In this experimental study a modified multi-diffusion flat flame burner was used to ignite and study the combustion of the Al particles and the Ni-coated Al particles. The burner was used to study the ignition temperature by a 'go' or 'no go' test procedure and the burn time characterization with a photo-multiplier tube and video recording. The flat flame burner allowed for the systematic variation of reactant gases allowing for a characterization of oxidizing gases. By varying the burner fuel types and oxidizer content the oxidizing species could be varied between water (H_2O), carbon dioxide (CO_2), and molecular oxygen (O_2). These three gas types are considered the primary oxidizing species of Al particles in propellant and explosive environments. The specific concentrations of the product species was calculated by inputting the reactant species into an equilibrium calculation using CHEMKIN.

A similar burner was used in previous studies to study the combustion of Aluminum flakes. That burner had a core region of diffusion flamelets that simulate a single flat flame. An annular ring of nitrogen (N_2) flown around the flat flame was meant to prevent the ambient environment from mixing with the hot product gases and causing a combustion environment that could no long be characterized with equilibrium calculations. However, it was discovered that in certain circumstances the particles would continue to combust at high enough locations that a shielding gas ring was no longer sufficient. Additionally small fluctuations in the room air would affect the trajectory of the combusting aluminum particles. In an effort to continue to prevent the outside environment from mixing the hot post-flame gases a fourteen-inch-long quartz

tube was placed around the fuel and oxidizer allowing for a physical barrier to be placed between the flame and the outside environment. This proved to be advantageous for several reasons. First it allowed for usable boundary condition to be established around the core of the flow allowing for more complex heat-loss and combustion simulations. Additionally, it fully prevented any effects from the ambient atmosphere to the combustion environment of the particles. Quartz was selected due to its light transparency allowing for visual diagnostic methods in addition to its favorable thermal expansion characteristics that allowed for very steep variations in temperature without shattering the tube. Figure **3.4** is a flow diagram of the experimental setup that was used in this investigation showing the flow of both the main gases and the gases that were used in the fluidized bed feeder.

The fuels were selected to be a mixture of carbon monoxide and hydrogen, which were controlled by rotameters on a control panel adjacent burner. A photograph of the control panel used for the main burner is shown in Figure **3.5** with the various gases and purge valve indicated. Oxygen was used as the oxidizer and nitrogen was used as diluent, which was introduced into the same stream as O_2. The quantity of the oxygen was varied through a series of equivalence ratios so that the effects of oxygen in the hot gases can be studied. Additionally, the fuel mixture of the hydrogen and the carbon monoxide was adjusted so the product gases of water vapor and carbon monoxide could be systematically varied and the relative effects on the ignition and combustion could be studied.

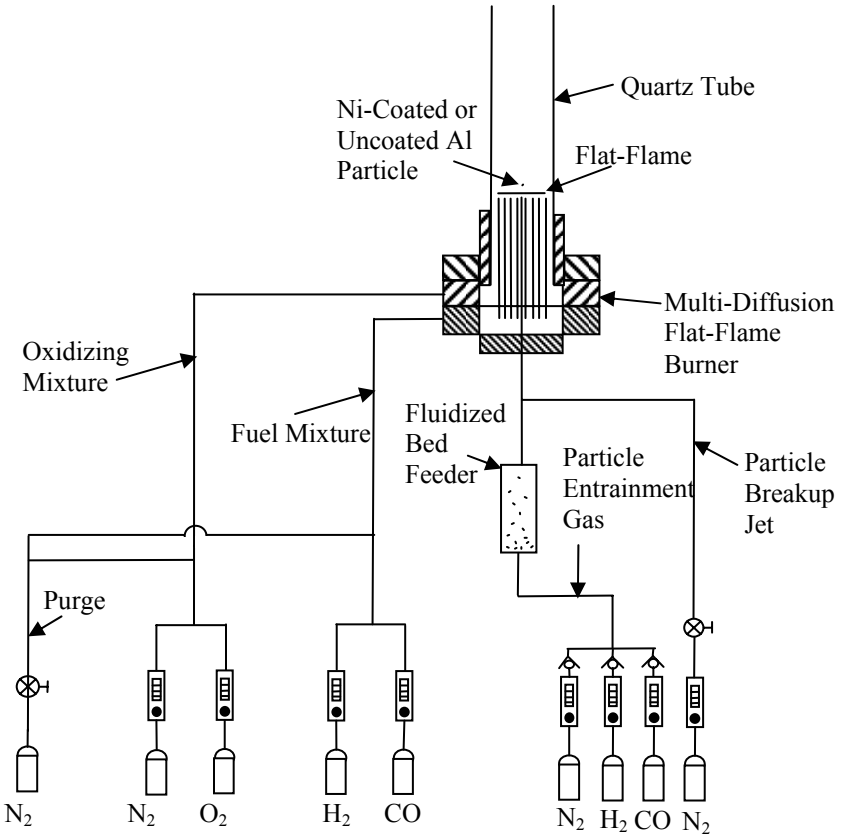

Figure **3.4**: A detailed flow diagram of the experimental test setup that details the burner and the fluidized bed particle feeder.

Figure **3.5**: A photograph of the control panel used in this project. It should be noted that the panel was adapted from a previous project leaving several meters unused.

The modified flat-flame burner simulated a flat flame by creating a series of 84 small diffusion flamelets that are close enough to nearly merge into one simulated flat flame. Figure **3.6** is a cutaway side view of the burner. Fuel flows into the bottom ring, colored red, of the burner where it is evenly injected into the lower chamber with an injection ring. From here the fuel flows to the surface of the burner through a series of thin stainless steel tubes. The oxidizer mixture was injected similarly into the upper ring, colored green, of the burner where it was equalized in a reservoir before rising through a steel honeycomb flow straightener to the surface. The oxidizer chamber and fuel chamber are separated with by a series of O-rings to prevent premixing. The particles are injected into the center port, colored orange, so that the flame and the boundary conditions are axisymmetric about it. Note that the full length of the quartz tube is not shown, so that the burner can be viewed in more detail. Figure **3.7** shows a diagram of the burner surface with the fuel ports and the oxidizer ports pointed out. Additionally the center injection port can is marked in red. Figure **3.8** is an example of a particle burning in the post-combustion zone. The pictured flame is at an equivalence ratio of 0.5 and a fuel mixture of 100% hydrogen. Figure **3-9** is a closer view of a particle streak. In this image of the particle combustion streak it is possible to see where the particles are igniting and subsequently extinguishing.

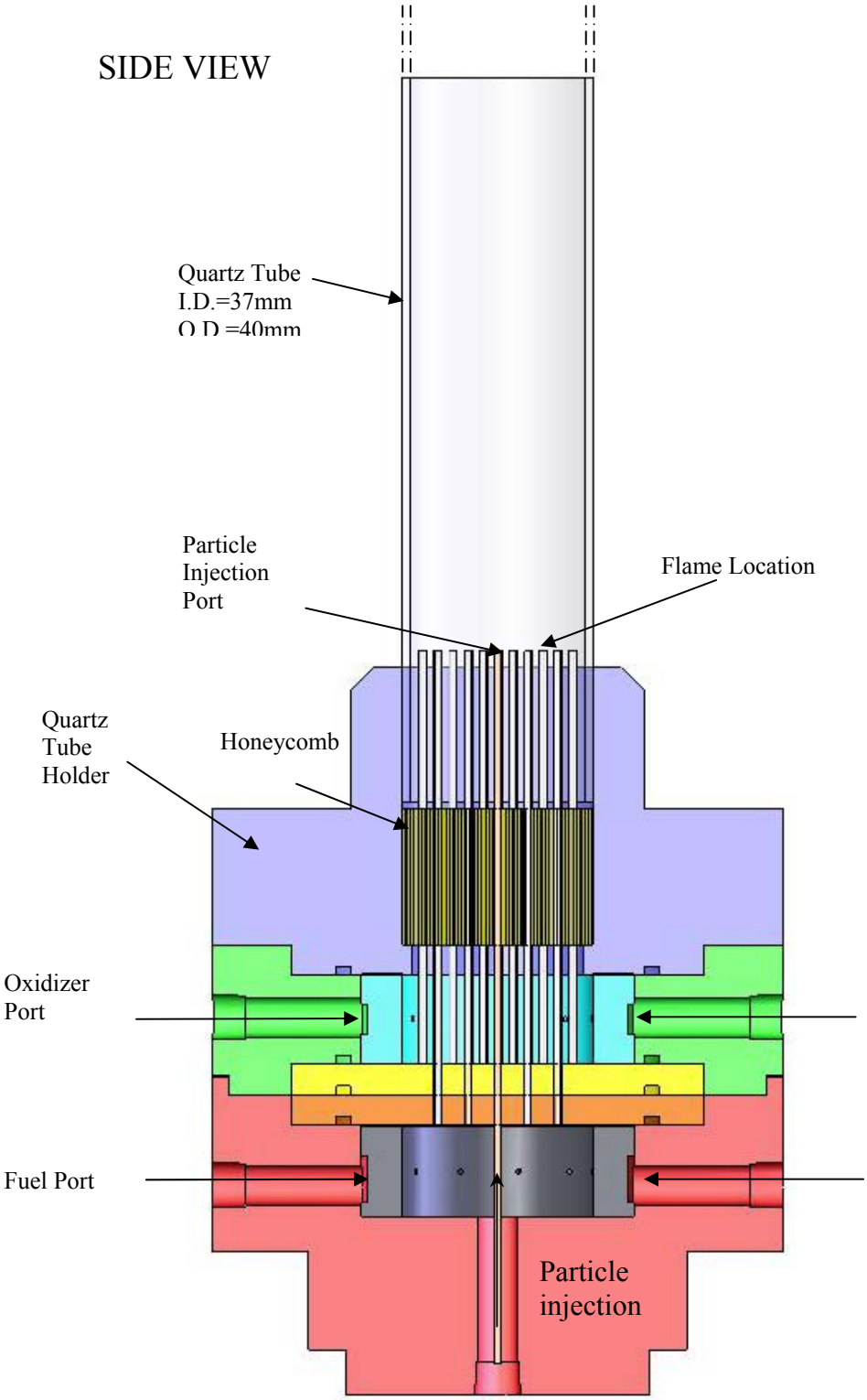

Figure **3.6**: A cut-away side view of a modified flat-flame Hencken burner.

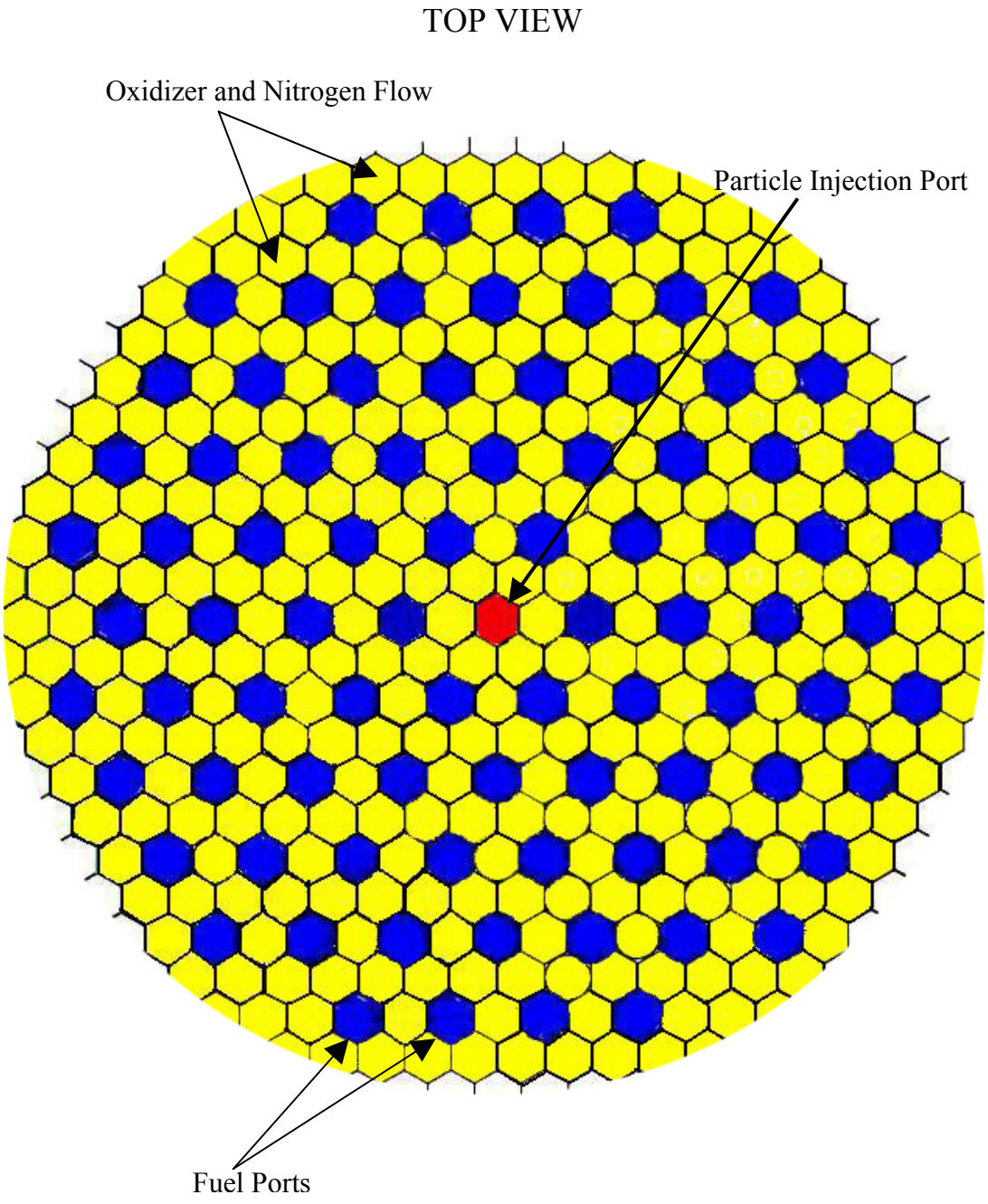

Figure **3.7**: A top view schematic of the burner surface.

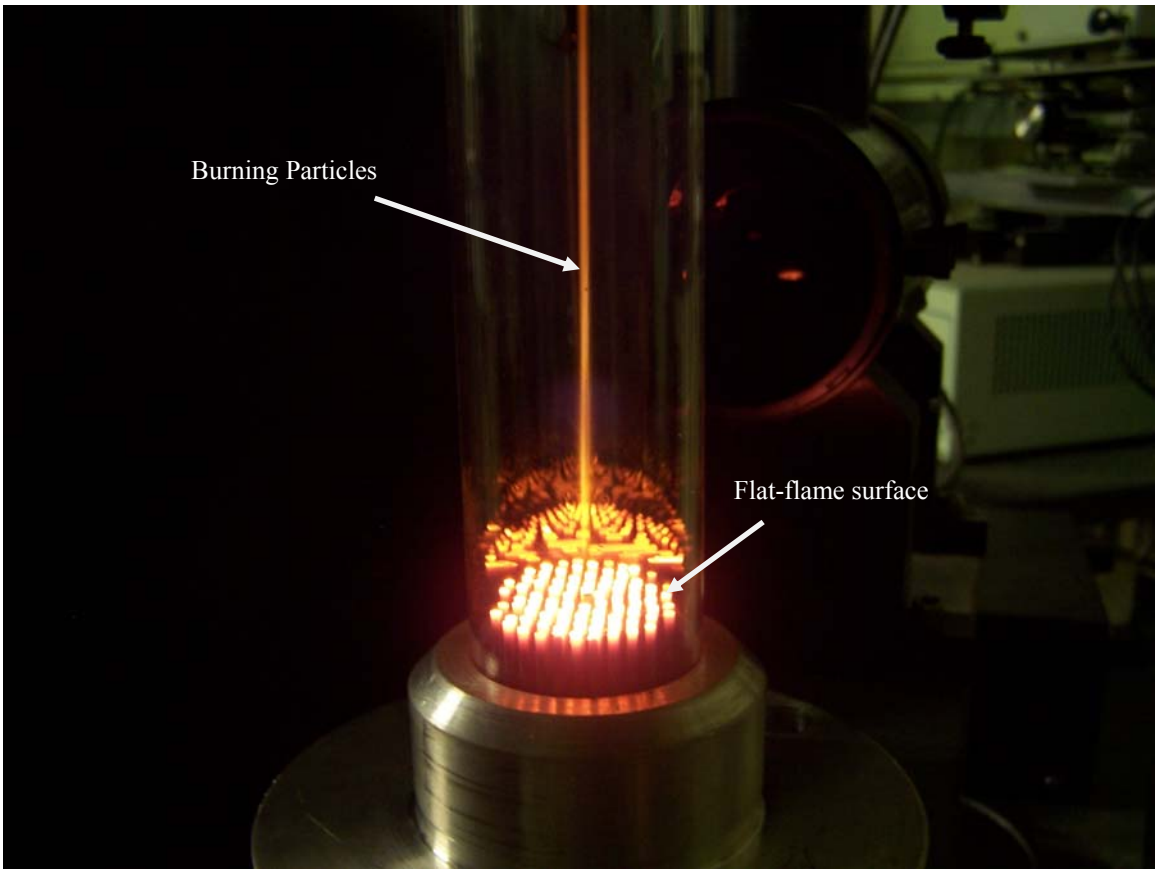

Figure **3.8**: Image of the burner while operating with the flame and a particle streak readily apparent. This test condition is 100% H_2 as the fuel mixture and ϕ=0.5.

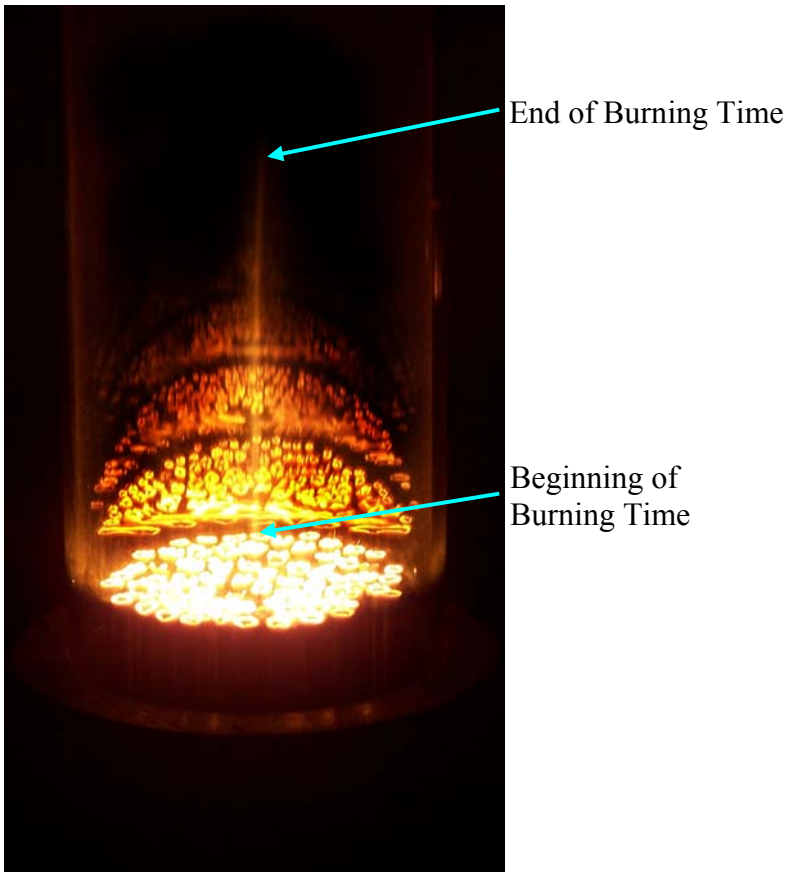

Figure **3-9**: Particle combustion streak where the beginning and end of the combustion event shown. This test condition is 100% H_2 as the fuel mixture and ϕ=0.5

The particles were entrained into the flow using a fluidized bed feeder. Photographs of the fluidized bed feeder broken down (left) and assembled (right) are shown in Figure **3.10**. The gas enters through the tubing manifold below the particle bed feeder through the 1/8" compression-to-NPT fitting causing the particles to form a cloud. The particles are then lifted through a long thin tube and injected into the center of the burner. Approximately 5 grams of Al or Ni-coated Al particles was mixed with 20 grams of 160-mesh glass beads, for breaking up the particle agglomerations, and are added to the particle bed feeder. Also, several 2 mm glass spheres were added to prevent the

particles from clumping at the walls. Additionally, a small amount of desiccant was added to the mixture to prevent moisture from accumulating and causing the particles to agglomerate. A gas jet enters from the bottom of the fluidized bed feeder where it pass through a diffuser to ensure that the particles are entrained casing a floating cloud of particles in the fluidized bed feeder. These particles will then be lifted into the flow of the gas and eventually injected into the surface of the burner where it is fully entrained into the flow. At the exit of the feeder, a converging gas nozzle was present to prevent recirculation zones and to hold a filter in place. This filter is a 400-mesh screen with ~37 μm openings was placed in the as the exit of the feeder for the 9 μm particles. This ensured the particles were undergoing combustion were single particles and not agglomerates. Agglomerated particles were found to not occur in any significant number for the larger 32 μm particles however the screen was also utilized with 100 μm holes punched into it with a needle. A diagram of the detailed flow field is shown in Figure **3.11** with streamlines shown along with glass breakup beads.

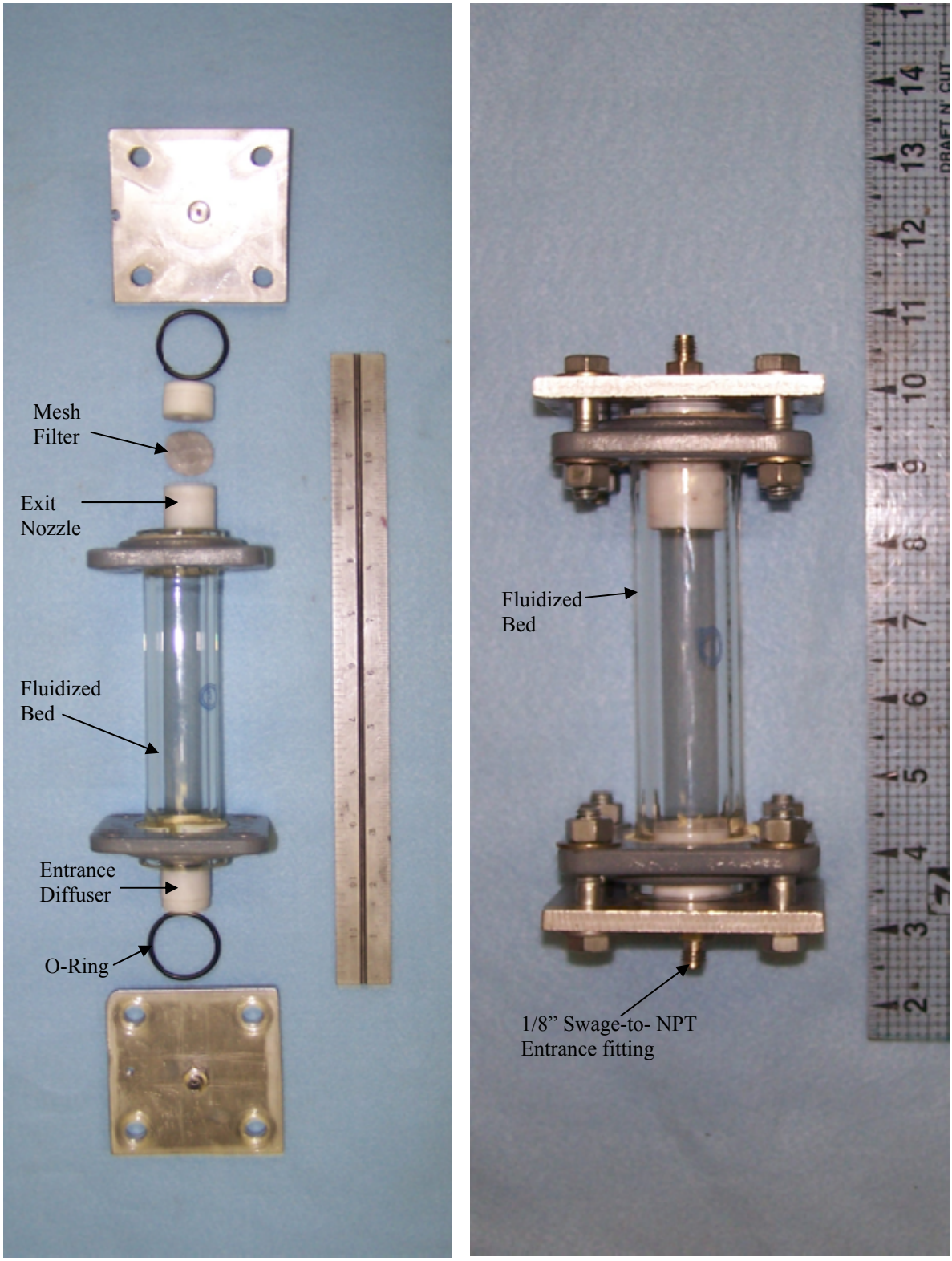

Figure **3.10**: A photograph of the fluidized bed particle feeder taken apart (left) for visualization purposes and assembled as it would be installed (right).

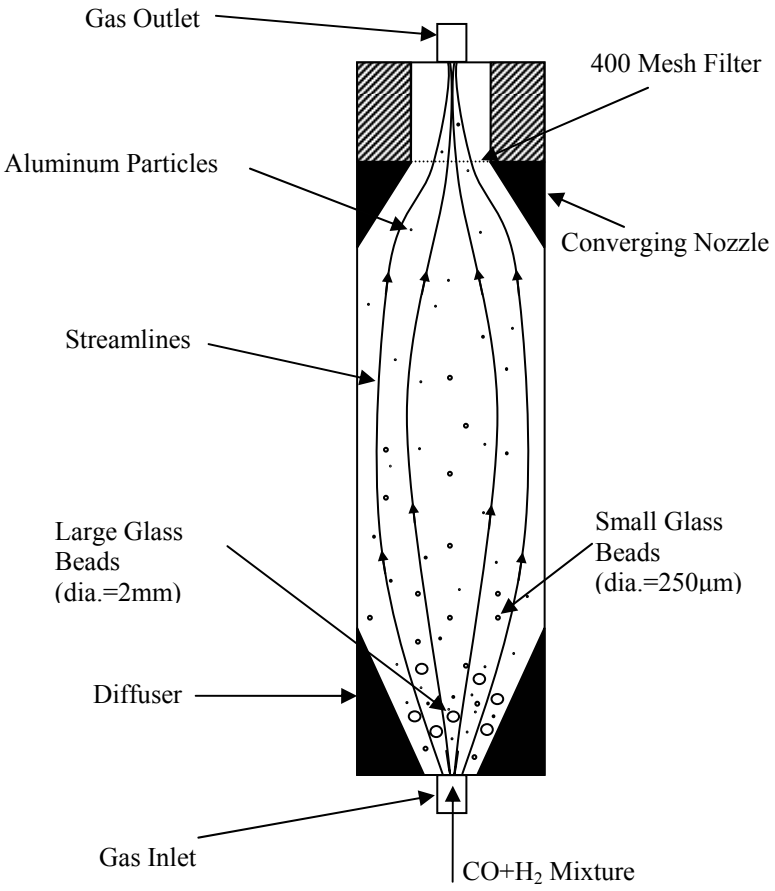

Figure **3.11**: Diagram of the flow-field within the particle bed feeder.

3.3 Diagnostic Setup

To measure the particle ignition temperature a visualization technique was used in conjunction with equilibrium flame temperature measurements. The combustion times were found in two different ways. The duration of a photo-multiplier tube's voltage rise was used to collect and measure the burn times. Additionally, the burn times were found using a video graphic technique where the particles would be recorded on video and from the streak length and a calculated gas velocity the combustion duration could calculated. To calculate the gas velocity within the quartz tube a CHEMKIN model was utilized.

3.3.1 Measurement Diagnostics

The particle ignition temperatures were developed using a "go or no go" criteria. The diluent portion of oxidizer stream was slowly increased until the particles would no longer ignite. This gas composition was then calculated at an equilibrium flame temperature to determine the lowest gas temperature at which the particles would ignite. Using video graphic evidence the particles were determined to be undergoing combustion when they were emitting visible light. Initially it was of concern that the particles would simply heat up and there would one could no discern the difference between heated particles emitting radiation and particles igniting and subsequently burning. However, the particle bed feeder was loaded with a variety of aluminum oxide particle sizes ranging from quite small (~10 μm) to large (~200 μm) in size to determine if the particles would

be would discernable when captured on video. However, this was found not to be the case and there was never any evidence of radiative emission from the particle simply heating up in the gas stream. So it is assumed if a particle is detected on video then the particle has ignited.

The ignition temperature was initially going to be found by locating where the particle is ignited and then using CHEMKIN simulation to find the exact temperature where that particle ignited. However, in all of cases, the particle would ignite at or very close to the surface of the burner before the flow was able to cool significantly. Also, the particle still passed through the high temperature of the flame zone and that temperature might have been necessary to initiate the reaction. This means that the equilibrium flame temperature was used as the best approximation ignition temperature of the particle and was used as such in this study.

The one potential drawback of this method is that in finding the particle ignition temperature a lower concentration of oxidizer will be present at particle surface when the ignition initiates. However, this fact is taken into account as the ignition temperature is plotted against an effective oxidizer concentration that uses the true concentration of the oxidizing species. This means that two conditions with the same fuel composition and oxidizer ratio may not directly compare to one another because there will be a large concentration of N_2 in the flow with the particle that has the lower ignition temperature. However, as can be seen in the ignition temperature results Chapter 4 it is still possible to directly compare the results of the particle ignition temperatures as a function of an effective oxidizer. Due to the wide variation in oxidizing species and in the product

stream there were enough test conditions to adequately study the how the ignition temperature is affected by the effective oxidizers in the product gases.

Although the primary objective of this study was to find if a nickel coating brought about a reduction of temperature it was important to also collect the combustion times of the particles. It would be highly undesirable if applying the nickel coating caused a significant increase or decrease in the combustion time of the particles. This is important to note because if a coating impeded the oxidizer from reacting with the bare aluminum it could in cause a longer combustion duration that would characteristically undesirable. Conversely, a significant reduction in the combustion time would be an indicator that the coating might be causing the particle artificially to quench and not completely, combust the metallic fuel that is available. As a result, it was necessary to study the combustion duration of the coated and uncoated aluminum particles. If the combustion duration of the two types of particles were relatively close to one another this would be one indication that the coating did not significantly inhibit the combustion characteristics of the Al particles. A diagram and detailed photograph of the diagnostic system around the burner are shown in Figure **3.12** and Figure **3.13** respectively.

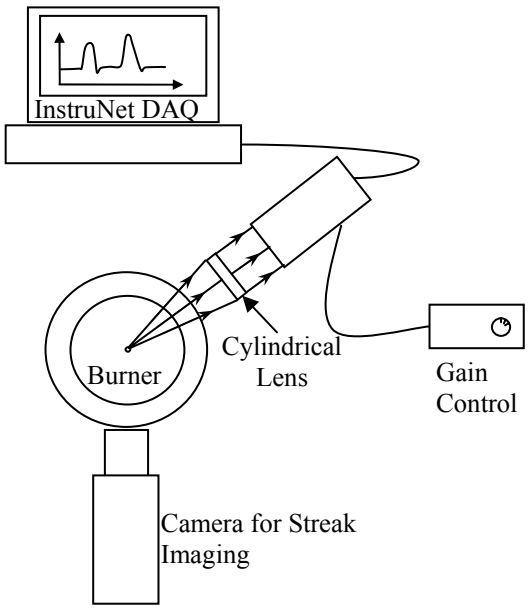

Figure **3.12**: Schematic of the PMT and Camera diagnostic systems for measuring the burning times of the aluminum particles.

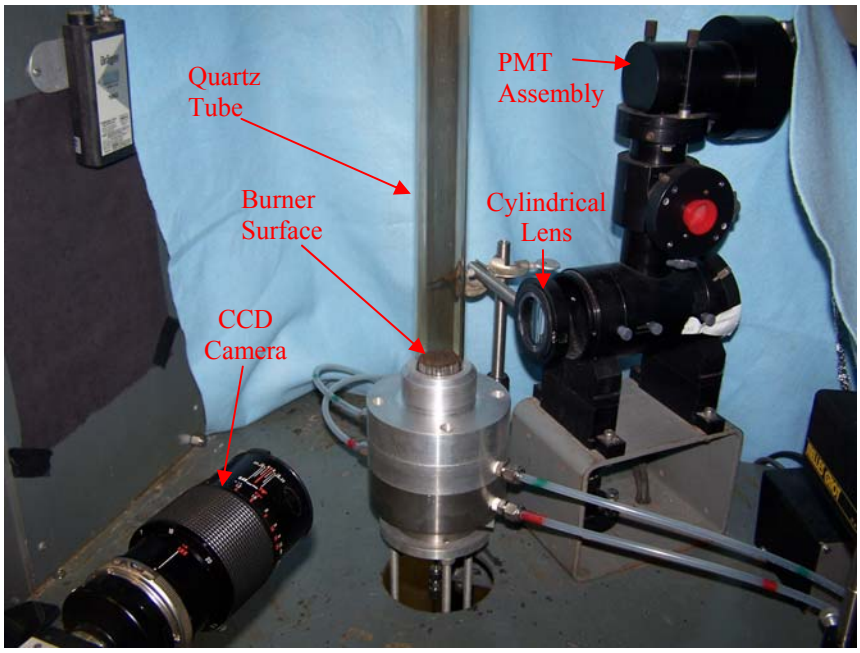

Figure **3.13**: Experimental setup of the multi-diffusion flame burner with the optical diagnostic systems present.

The combustion times were measured in one of two ways. An RCA Model 4526 photomultiplier tube (PMT) housed in a TSI model 9160 system was used to collect light from emitting from the burning particles. The PMT was designed to view light in the visible range from 300 to 800 nm with a peak quantum efficiency of 22% at 380 nm. The TSI housing was a control circuit with a low noise preamplifier built in meant to give good signal amplitude even at low levels. The light was collected along the axial centerline of the burner using a cylindrical lens, which focused the light from a line to a collimated source. The collimated light was then focused on the PMT aperture using a focusing lens within a color separator (TSI model 9144) that had the PMT housing circuit mounted on the top of the separator. The color separating optics were removed to collect the maximum amount of light meaning the system was only used due to its preset optical lengths that were optimized for the PMT. A diagram of the light path from the burner to the PMT is shown in Figure **3.14**. However, the cylindrical lens was only 2" in total diameter and many particles would have a streak length that was longer than this viewing width meaning they are still combusting after leaving the viewing area of the lens system.

Therefore, a video-graphic technique was used to record the particles through the combustion process. The velocity at any given time was known from a CHEMKIN simulation that will be described in section 3.3.2 and the length of time that it took for the particle to combust was found by measuring the length of the combustion streak. The burn time (t_b) could be found using equation Eq. **(3.1)**. L_{streak} is the length of the particle streak and u_{gas} is the calculated centerline velocity of the gas mixture, which corresponds to the particle velocity that was found with the CHEMKIN simulations.

$$t_b = \frac{L_{streak}}{u_{gas}} \qquad \textbf{(3.1)}$$

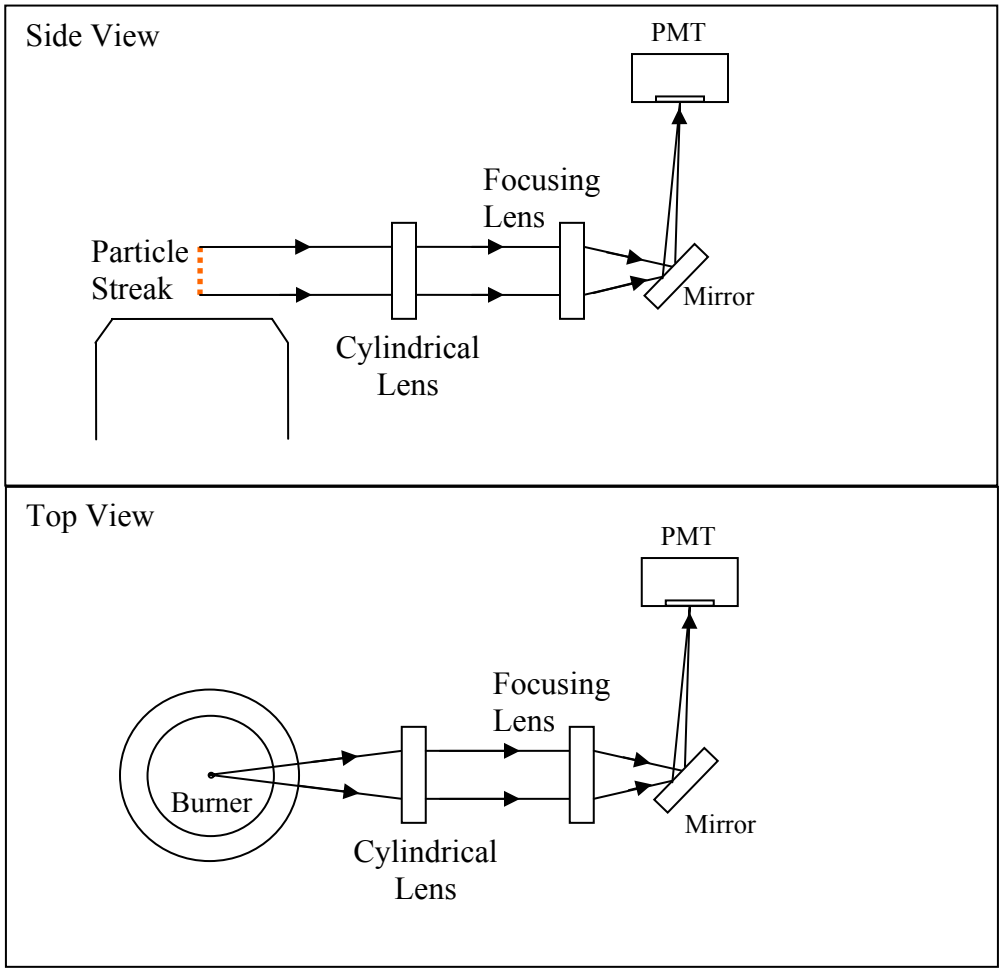

Figure **3.14**: A diagram of the light path from the particle streak at the centerline of the burner to the detector on the PMT.

The intensity peaks were plotted and the combustion time was determined to be the length of time from the intensity causing the voltage to rapidly rise to when it dropped off to the same level it began rising. A plot of a typical intensity peak is shown in Figure **4.6** where there are two separate peaks of particles burned at different

temperatures. When ignition begins, the light output rises very rapidly, then begins slowly to drop off as it continues to burn, and subsequently extinguishes. Intensities were not always the same, some were much higher than others, but the particles were considered combusting if the rise was large enough to discern it from the baseline noise.

3.3.2 CHEMKIN Model

A CHEMKIN simulation was prepared that was necessary to find the gas velocities within the quartz tube. Simply calculating the velocity based on the volumetric flow rate would be insufficient due to the buoyancy effects from the hot post-combustion gases and boundary layer effects that caused centerline of the flow to accelerate while the gas velocities at the walls was zero. The model was developed in two parts with fuel and oxidizer entering into a perfectly stirred reactor to determine the combustion temperature and products from the combustion reaction. The output of that is then directed to the input of a cylindrical sheer flow reactor. A diagram view of the simulation can be seen in Figure **3.15**.

For the perfectly stirred reactor it is necessary to calculate and then input the mass flow rate oxidizers and the fuel. It is also necessary to calculate the mass fraction of the oxidizers constituents as well as the fuel constituents. To calculate the mass flow rates it was first necessary to develop calibration curves for the rotameters so the volumetric flow rates could be calculated. Omega provided flow data for the meters and a curve fit was developed from this. Figure **3.16** shows and example where the O_2 flow rate was

found using a curve fit in Microsoft Excel the remainder of these flow calibrations can be found in Appendix 2.

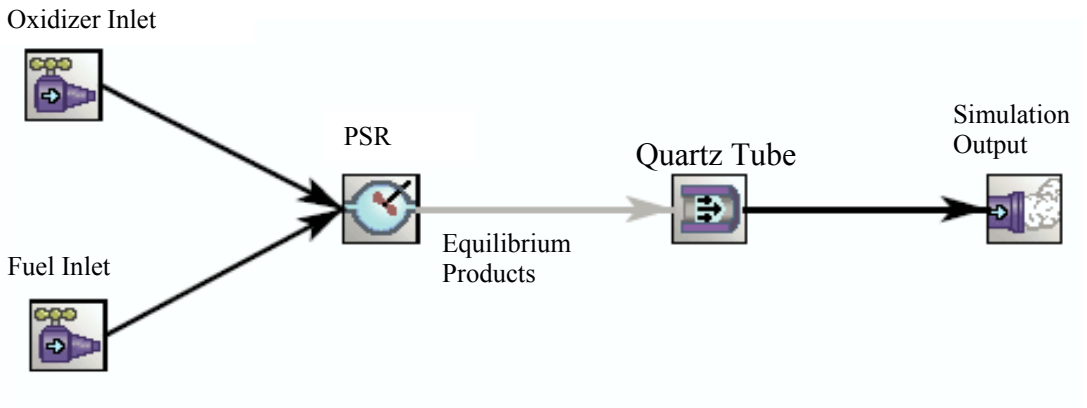

Place Figure Here

Figure **3.15**: Diagram view of CHEMKIN model for simulating the axial velocity and temperature profiles inside the quartz tube.

O_2	
Reading	Flow (ml/min)
10	1046.606174
20	2412.655749
30	3680.634929
40	4898.475461
50	6099.123197
60	7239.501568
70	8467.34671
80	9673.396095
90	10814.19483
100	11843.4821
110	13068.95219
120	14203.16176
130	15404.14578
140	16563.72418
150	17588.65019

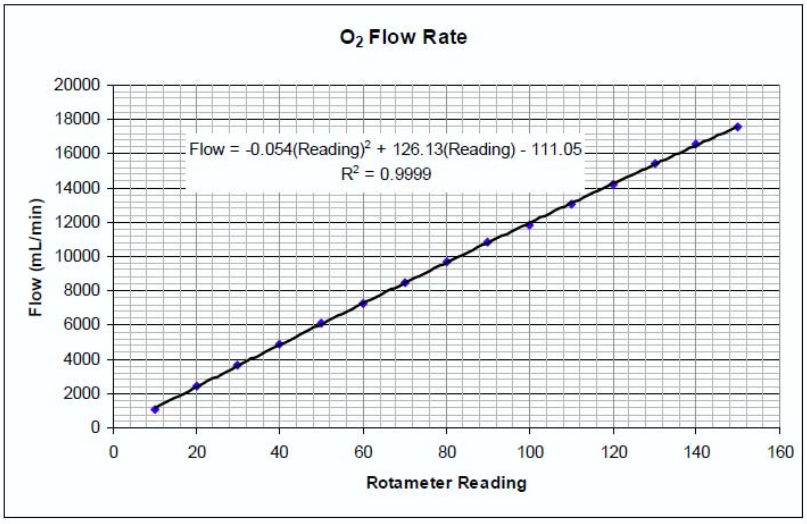

Figure **3.16**: Calibration of the oxygen flow-meter reading to find the volumetric flow rate of the gas.

The mass flow rate was calculated with Eq. **(3.2)**, where *i* is representative of the species that the mass flow rate is being calculated Q_i is the volumetric flow rate, ρ_i is the density of the gas, and m_i is the mass flow rate of the species.

$$\dot{m}_i = \dot{Q}_i \rho_i \tag{3.2}$$

The density is calculated with the ideal gas law as shown in Eq. **(3.3)** where P is the pressure, T is the temperature, and R_i is the gas constant of species i.

$$\rho_i = \frac{P}{R_i T} \tag{3.3}$$

Then the oxidizer and fuel mass flows are then calculated as shown in Eq. **(3.4)** and Eq. **(3.5)**.

$$\dot{m}_{ox} = \dot{m}_{O_2} + \dot{m}_{N_2} \tag{3.4}$$

$$\dot{m}_{Fuel} = \dot{m}_{H_2} + \dot{m}_{CO} \tag{3.5}$$

The mass fractions are calculated in Eq. **(3.6)** with y_i being the mass fractions of the oxidizer or the fuel.

$$Y_{i,fuel} = \frac{\dot{m}_i}{\dot{m}_{fuel}} \quad \text{and} \quad Y_{i,ox} = \frac{\dot{m}_i}{\dot{m}_{ox}} \tag{3.6}$$

For the shear flow reactor it was necessary to develop a temperature profile of the inside of the quartz tube. To do this a duplicate 14” quartz tube was instrumented with 4, 125 μm S-type thermocouples (TC) at the wall of the tube and one at the center of the exit port. A detailed diagram of the TC-instrumented quartz tube is shown in Figure **3.18**

and a photograph of the quartz tube that was used in the experiments is shown in figure Figure **3.17**. This tube was instrumented such that it could closely simulate the temperatures that were being experienced by the clear quartz tube that was used for the ignition temperature tests and the combustion time measurements. From the outer wall temperature measurements, it was then necessary to calculate the corresponding temperatures at the inner wall. The outer wall temperature profile was curve fit so that air properties could be found from the following correlations. The Prandtl number, *Pr*, was correlated as a function of temperature in Eq. **(3.7)** with *T* being the temperature. Thermal diffusivity, α, was calculated in Eq. **(3.8)** as a function of temperature. Additionally, the thermal conductivity, k, of the gas was calculated in Eq. **(3.9)** as a function of temperature. Finally, the kinematic viscosity, *v*, was correlated in Eq. **(3.10)** as a function of temperature.

$$\mathrm{Pr}(T) = \left(4.7739*10^{-6}\right)T^2 - \left(0.00050892\right)T + 0.81832 \qquad \textbf{(3.7)}$$

$$\alpha(T) = \left(1.1082*10^{-10}\right)T^2 + \left(7.832*10^{-8}\right)T - 1.0482*10^{-5} \qquad \textbf{(3.8)}$$

$$k(T) = \left(-3.2914*10^{-8}\right)T^2 + \left(9.8277*10^{-5}\right)T - 2.4853*10^{-4} \qquad \textbf{(3.9)}$$

$$v(T) = \left(8.7193*10^{-11}\right)T^2 + \left(4.3291*10^{-8}\right)T - 4.7722*10^{-6} \qquad \textbf{(3.10)}$$

Next, it is necessary to define the average temperature over the length of the tube. The temperature that is integrated is from the temperature profile developed from the four measured temperatures on the outer tube wall as shown in Eq. **(3.11)**. In this case, *L* is the length of the tube while *x* is a specified location, and T is the provided curve fit from measured temperatures.

$$T_{film} = \frac{1}{L}\int_0^L T(x)\,dx \qquad \textbf{(3.11)}$$

From this the temperature is used to develop the Grasshof number in Eq. **(3.12)** where g is gravity, L is tube length, v is the viscosity and β is the expansion coefficient defined as Eq. **(3.13)**.

$$Gr = \frac{\mathrm{g} * \beta * \left(T_{film} - T_{\infty}\right) * L^3}{\nu^2} \tag{3.12}$$

$$\beta = \frac{1}{\left(\frac{T_{film} - T_{\infty}}{2}\right)} \tag{3.13}$$

The viscosity for Eq. **(3.13)** and Eq. **(3.12)** was evaluated at Eq. **(3.14)**.

$$v = v\left(\frac{T_{film} - T_{\infty}}{2}\right) \tag{3.14}$$

From this the Rayleigh number is calculated with Eq. **(3.15)** where Pr is evaluated at Eq. **(3.16)**.

$$Ra = Gr * \mathrm{Pr} \tag{3.15}$$

$$\mathrm{Pr} = \mathrm{Pr}\left(\frac{T_{film} - T_{\infty}}{2}\right) \tag{3.16}$$

The Grashof and Rayleigh numbers were then used to in the Nusselt number correlation in Eq. **(3.17)** that was found in Incropera and Dewitt.[23]

$$\overline{\mathrm{Nu}_{\mathrm{L}}} = 0.68 + \frac{0.67 * Ra_{L}^{1/4}}{\left[1 + \left(\frac{0.492}{\mathrm{Pr}}\right)^{9/16}\right]^{4/9}} \tag{3.17}$$

Then the average heat-transfer coefficient is calculated as Eq. **(3.18)**.

$$\overline{h(x)} = \frac{k * \overline{Nu_L}}{L} \qquad \textbf{(3.18)}$$

This means that the local heat transfer coefficient can be calculated in Eq. **(3.19)** where x is the axial location along the tube wall.

$$h(x) = \overline{h(x)} + x * \overline{h'(x)} \qquad \textbf{(3.19)}$$

Finally from this the inner wall temperature can be profiled in Eq. **(3.20)**.

$$T_{in}(x) = T_{out}(x) + \frac{r_o}{k_{Quartz}} * Log\left(\frac{r_o}{r_i}\right) * h(x) * \left(T_{out}(x) - T_{\infty}\right) \qquad \textbf{(3.20)}$$

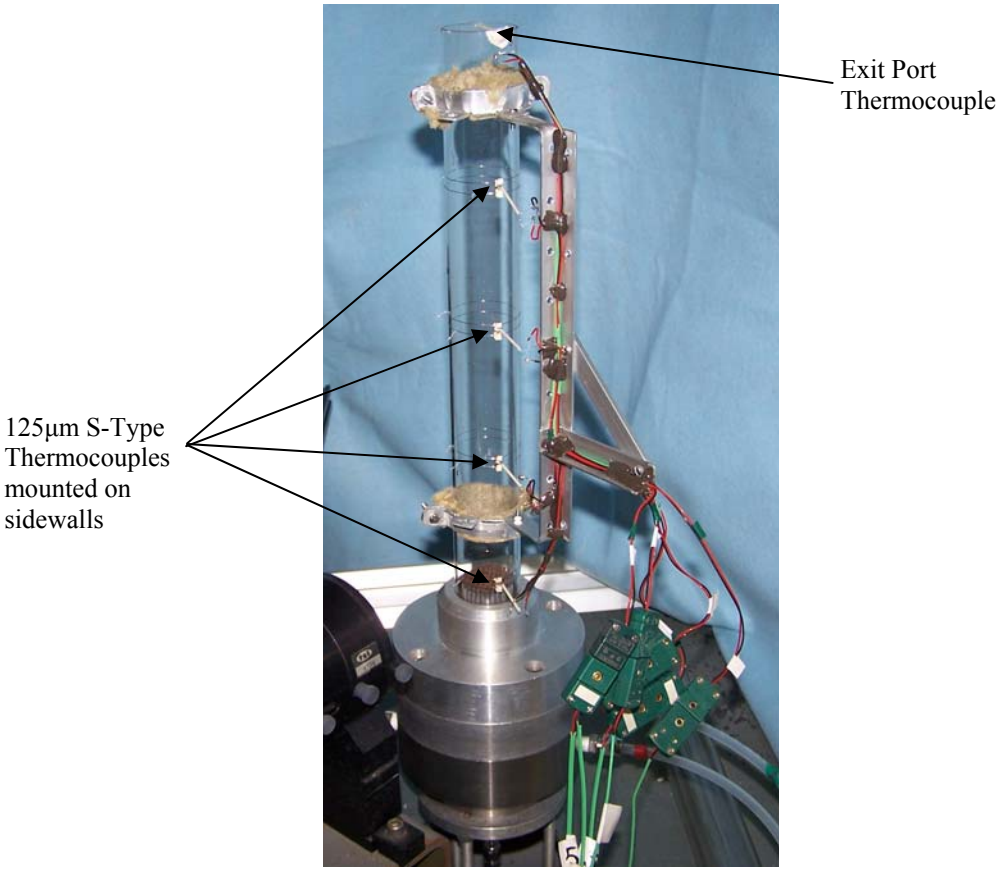

Figure **3.17**: A photograph of the quartz tube that was used in the temperature measurements with the thermocouples mounted to the sidewalls.

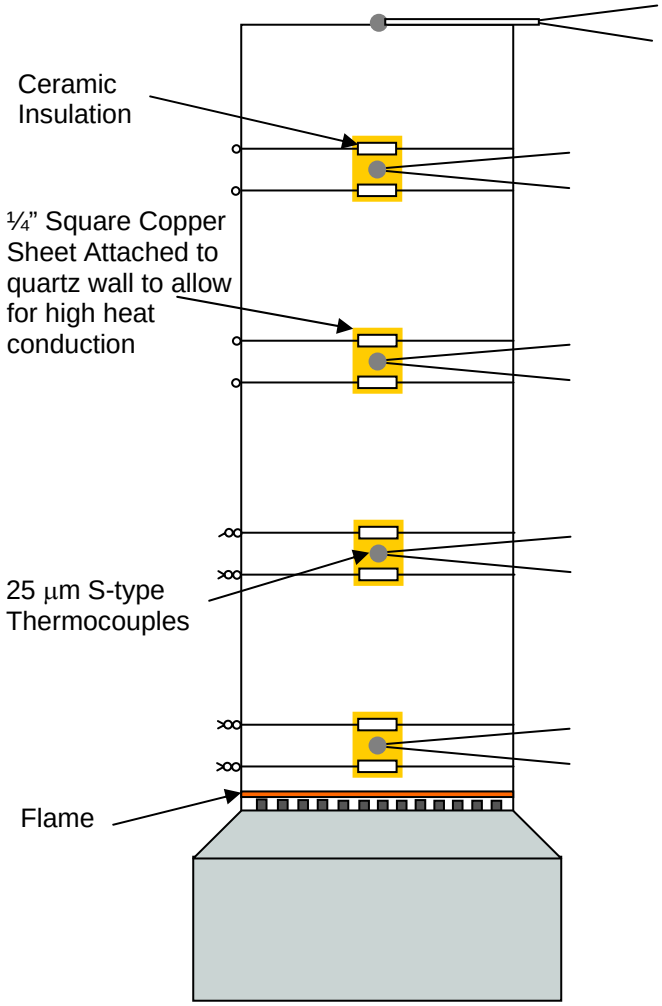

Figure **3.18**: A diagram of the TC instrumented quartz tube with 4 s-type thermocouples (125 μm bead) mounted on the walls of the tube and on thermocouple at the center of tube exit plane.

3.4 Test Matrix

3.4.1 Ignition Temperature Test Matrix

Table **3.1** shows a detailed table of the ignition test matrix that was used in present study. The matrix was repeated for 4 different scenarios. The ignition temperatures were compiled for the 9 μm and 32 μm Ni-coated and uncoated aluminum particles accounting for all potential ignition test scenarios. The tests were selected to find how the primary oxidizers of O_2, H_2O, and CO_2 affect the ignition properties of the coated and uncoated particles. To vary the level of O_2 the equivalence ratio was varied from 0.25 to 1.5. The equivalence ratio is defined in Eq. **(3.21)**, where O is the oxygen concentration and F is the fuel concentration.

$$\phi = \frac{\left(F/O\right)}{\left(F/O\right)_{st}} \tag{3.21}$$

This means that an equivalence ratio less than 1.0 is going to have an excess amount of oxygen in the post-combustion the products. While an equivalence ratio, greater than one will be fuel-rich with almost no oxygen in remaining and only reacted H_2O and CO_2 acting as particle oxidizers in the products. For each of test case equilibrium calculations were completed so that a good characterization of the oxidizing species would be present in the post-combustion products. Figures **3.19, 3.20, 3.21,** and **3.22** show plots of the results from the equilibrium calculations. It should be noted that the y-axis is the relative product mole fraction. This means that these are not true mole fractions rather they are the relative ratios of the species as the oxidizers of the aluminum particles. They are

simply provided to show why the specific test conditions were chosen. It can be seen for that for all cases the carbon dioxide decreases with decreasing levels of CO and the water vapor increase increases with increasing hydrogen content in the fuel stream. For the equivalence ratios of 0.25 and 0.5 the CO_2 and H_2O levels nearly intersect at a fuel composition of 50% H_2 and 50% CO. However, for when the equivalence ratio is equal to 1.0 and 1.5 the H_2O and CO_2 levels cross at or near a fuel mixture of 40% H_2 and 60% CO as can seen in figures **3.21,** and Figure **3.22**. It is also important to note that it was not possible to use CO as the only reactant in a fuel mixture. This is because the carbon monoxide reaction requires the hydroxyl radical to be present to attack the CO feeding the oxidation step. A small presence H_2 allows for a stable flame where blowout preventing from becoming a significant issue.

Table **3.1**: The ignition test matrix that was complete for all 4-test trials.

Composition of Fuel	**Equivalence Ratio**			
	0.25	0.5	1.0	1.5
H_2=100% CO=0%	Test 1	Test 2	Test 3	Test 4
H_2=75% CO=25%	Test 5	Test 6	Test 7	Test 8
H_2=50% CO=50%	Test 9	Test 10	-	-
H_2=40% CO=60%	-	-	Test 11	Test 12
H_2=25% CO=75%	Test 13	Test 14	Test 15	Test 16
H_2=5% CO=95%	Test 17	Test 18	Test 19	Test 20

3.4.2 Combustion Time Measurement Test Matrix

The combustion times were collected for both the 9 μm and 32 μm Ni-coated and uncoated aluminum particles accounting for the remainder of the test scenarios. This test matrix was reduced in size to save in the costs of gas reactants and particles as well as time. The tests with an equivalence ratio of 1.5 were eliminated because of issues with flame stability at high CO concentrations and the potential dangers associated with a blowout and subsequent re-ignition. Also when the equivalence ratio is 1.5 little addition information is provided. The test matrix for the combustion times is shown in Table **3.2**.

Table **3.2**: The combustion test matrix that was complete for all 4-test trials.

Composition of in Fuel	**Equivalence Ratio**		
	0.25	0.5	1
H_2=100% CO=0%	Test 1	Test 2	Test 3
H_2=50% CO=50%	Test 4	Test 5	-
H_2=40% CO=60%	-	-	Test 6
H_2=5% CO=95%	Test 7	Test 8	Test 9

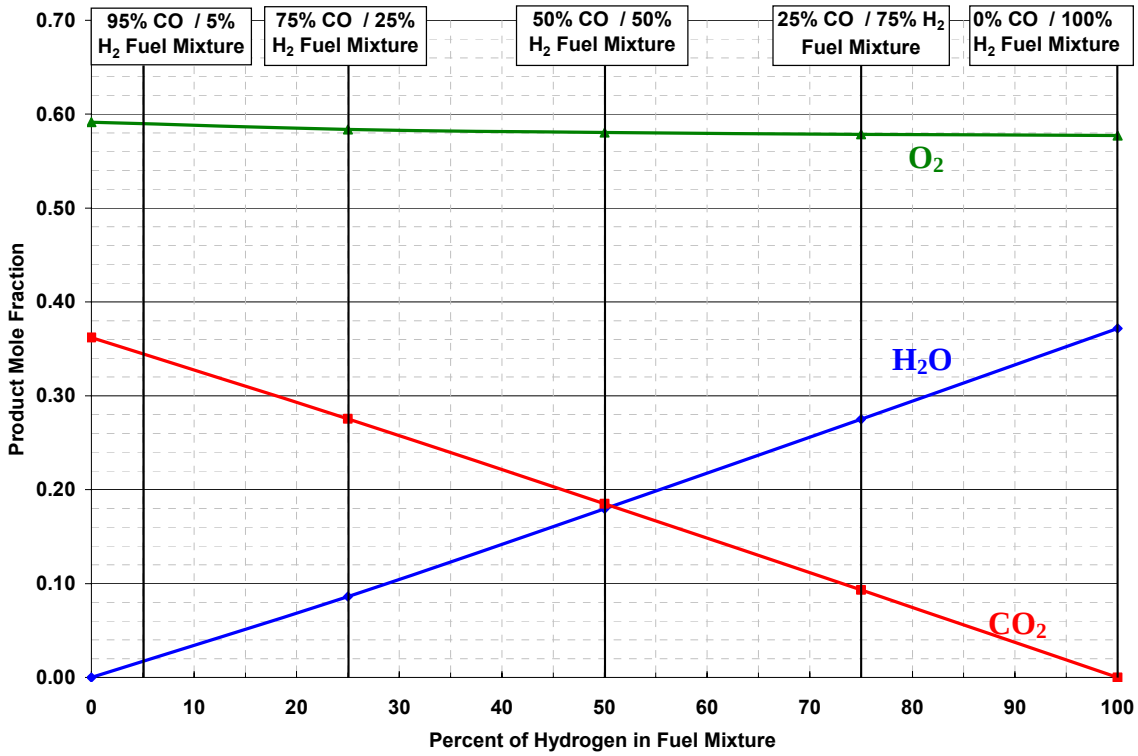

Figure **3.19**: Oxidizer species mole fractions in combustion products that are available for reaction with the Al particle. (ϕ=0.25)

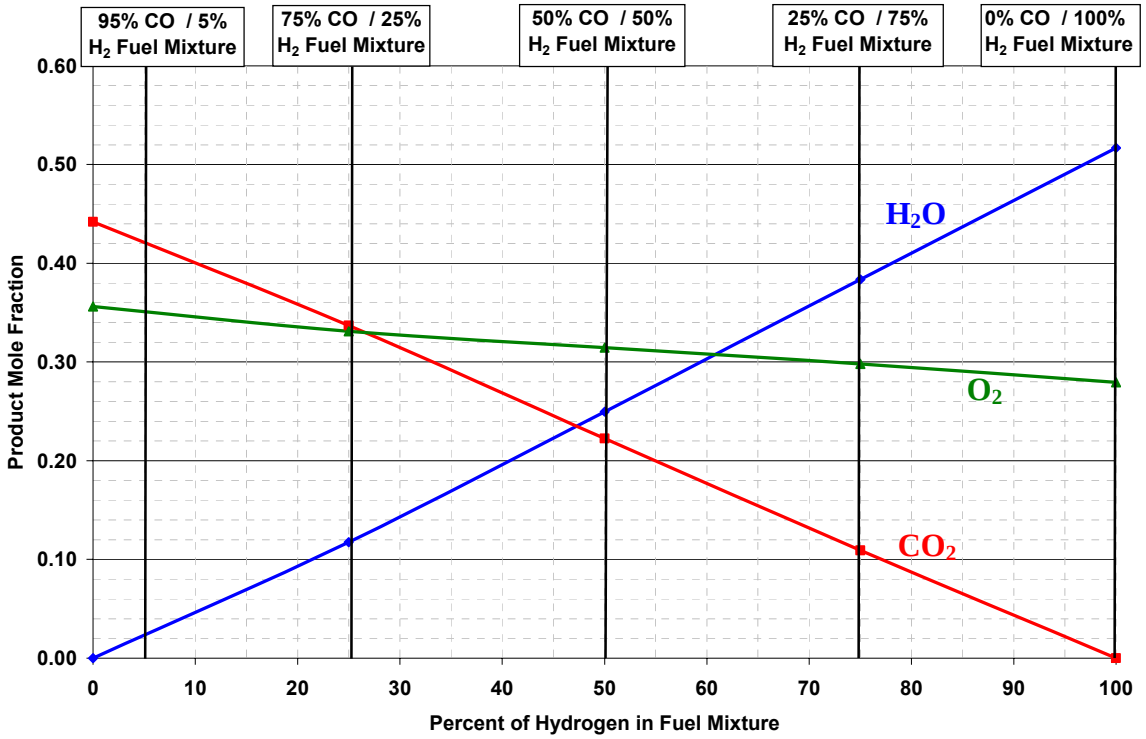

Figure **3.20**: Oxidizer species mole fractions in combustion products that are available for reaction with the Al particle. (ϕ=0.50)

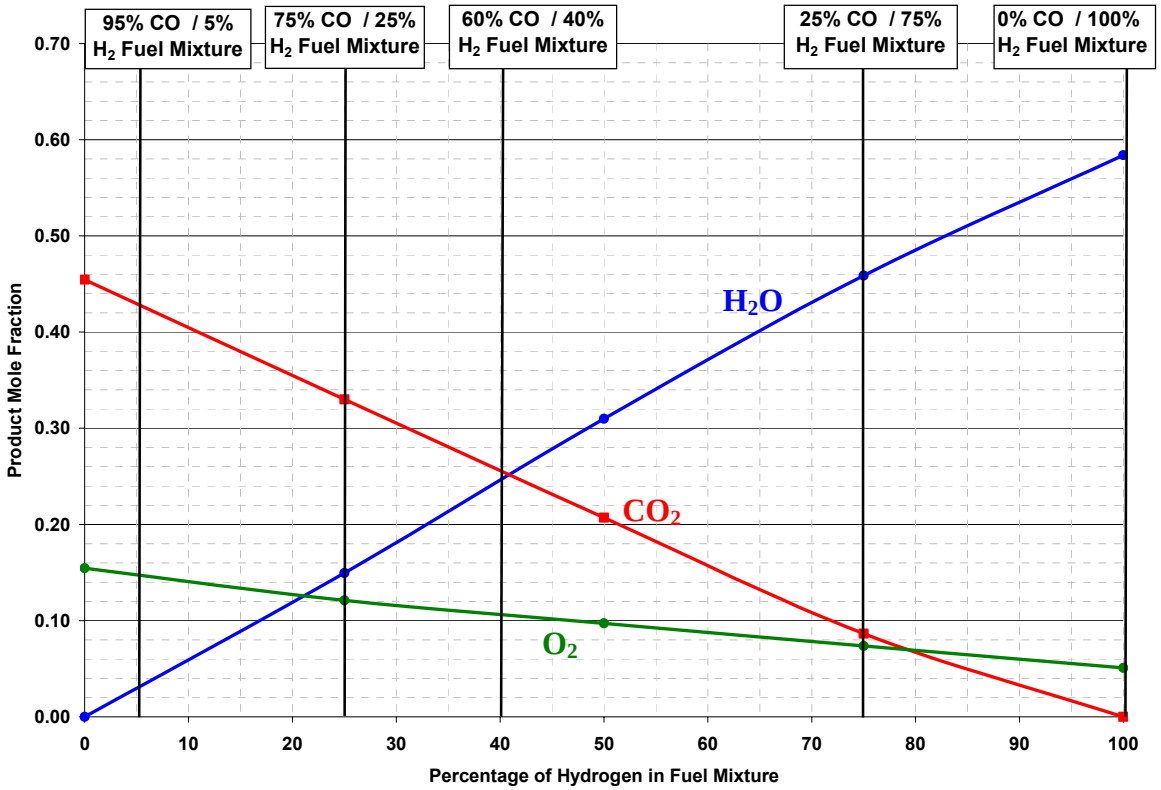

Figure **3.21**: Oxidizer species mole fractions in combustion products that are available for reaction with the Al particle. (ϕ=1.0)

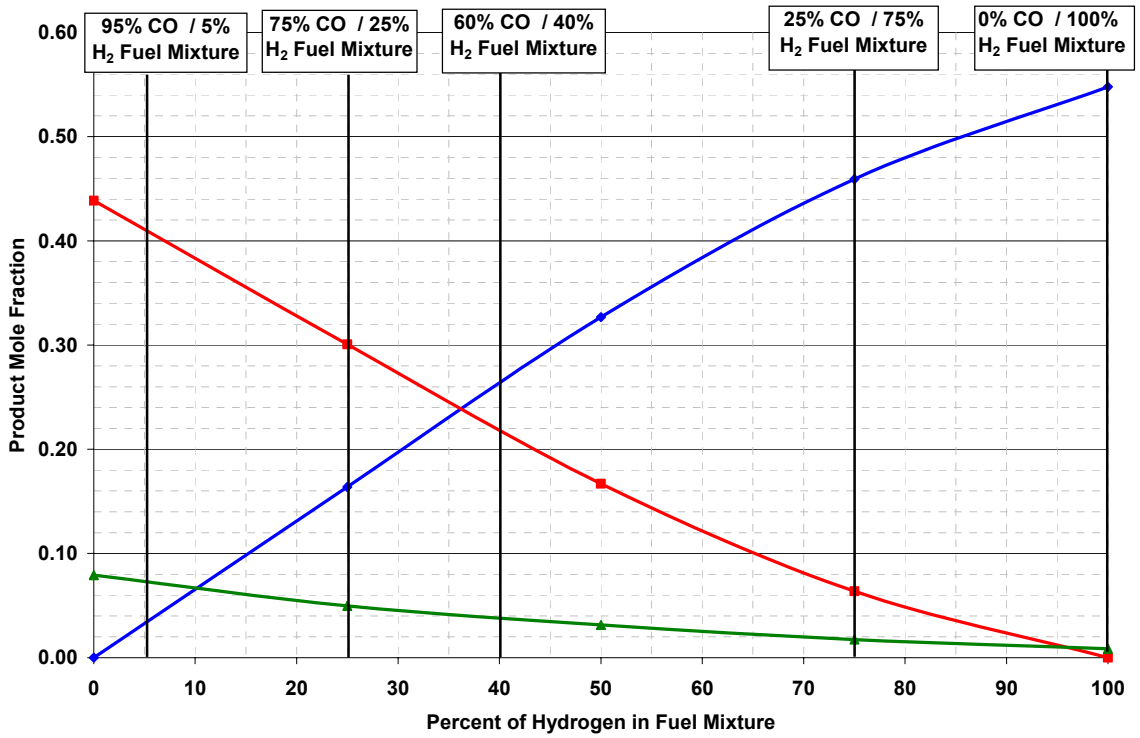

Figure **3.22**: Oxidizer species mole fractions in combustion products that are available for reaction with the Al particle. (ϕ=1.5).

Chapter 4

Results and Discussion

4.1 Combustion Time Results

The combustion times of the particles were found and plotted as a function of equivalence ratio in Figure **4.1** and Figure **4.2**. Each line corresponds to a specific fuel mixture of varying H_2 and CO as the fuel composition. In the plot the blue colored data points and corresponding lines are representative of the Ni-coated particles, while the red and orange colored lines are representative of the uncoated aluminum particles. Error bars correspond to one standard deviation above and below the burn time of the particles. Each point is a mean value of twenty data points, with 10 being collected using the photo multiplier tube and 10 being collected using the video-graphic captures of the particles streaks.

The results for the 32 μm particle match reasonably well with the correlation developed by Beckstead[6] as can be seen in Figure **4.3**. However, the smaller 9 μm particles do indeed seem to have combustion times that are larger than those predicted by Beckstead's correlation. This goes back to the studies that were carried out by Bazyn[7] where the particle combustion time is in the transition regime between kinetically-controlled and diffusion-controlled mechanisms. The particle combustion time is not going to drop continuously shown in Beckstead's plot. The assumption is that the controlling factor in the combustion process is that rate that the oxidizers diffuse to the

reacting surface of the aluminum particle. However, at small particle sizes the mechanism that controls the combustion process is the surface kinetics of the oxidizing reaction. In the kinetically controlled regime, the oxidizer is being delivered to the surface at a faster rate that the reactions are occurring so there combustion reaction is limited. The 9 μm particles are likely in the transition regime where both the surface kinetic reaction rates are important along with the diffusion rates of the oxidizer to the surface of the particles. Additionally it is important to note that the combustion rates are going to be more sensitive to temperature and pressure for this particle size, but are still going to be strongly influenced by the oxidizing species that are present within the flow.

It is difficult to pick out trends and to develop a correlation for the particle burn times that were found in this study. The error bars are quite large so a correlation will not be developed mostly because it would not be of much value in a different application. The potential reasons for such a large error will be discussed later in the chapter. However, if one looks at the mean values a trend can be drawn out from these particular results. It can be seen that with increasing oxygen concentrations (ϕ increases) the particles burn times consistently decreased. Additionally, it can be seen that with increasing carbon dioxide concentration in product flow seemed to cause the particle burn times to increase. These trends allude to the fact that the oxygen is likely the most effective oxidizer of the aluminum particles with water vapor being less effective and the carbon dioxide being the least for both particle sizes.

Despite the inability to produce a useful correlation these result did, in fact, answer the question that tests set out to answer. This is whether the nickel significantly affects the combustion time of the particles. The greatest concern in applying a coating

to aluminum particles is that somehow, the coating could inhibit the combustion event. The combustion time for the coated and uncoated particle are almost on top of one another for both particle sizes. This indicates that the thin Ni-coating does not impede the combustion process. This is a very important finding because if the combustion time was much longer this could indicate that the nickel is influencing either the transport of the oxygen to the surface or the kinetic reaction rates at the surface of the particle. Additionally, if the combustion times would have been significantly less this could also be problematic because it could indicate that the particles are not burning to completion. Other factors could cause the particles to combust at a faster rate making these particles beneficial in certain applications. However, these concerns are not important in this investigation because while the error bars are very large the mean values of the combustion times for the particles are almost identical. It could certainly be said that, even with the experimental error experienced in this study, the particle combustion rate is not changed due to the applied coating of the nickel.

If more financial support were to become available it would be very interesting to study the particle in post-combustion conditions or quenched partially through the combustion process using either an Auger spectroscopy or a technique known as electron probe-microanalysis. Both of these techniques allow for elemental mapping through the particle. This could give valuable information about the combustion event that is occurring with the particles particularly if they are completely oxidized by seeing if there is oxygen throughout the entire particle. However, funding restrictions and the prohibitively high cost of these methods did not allow for these studies to be carried out in this work.

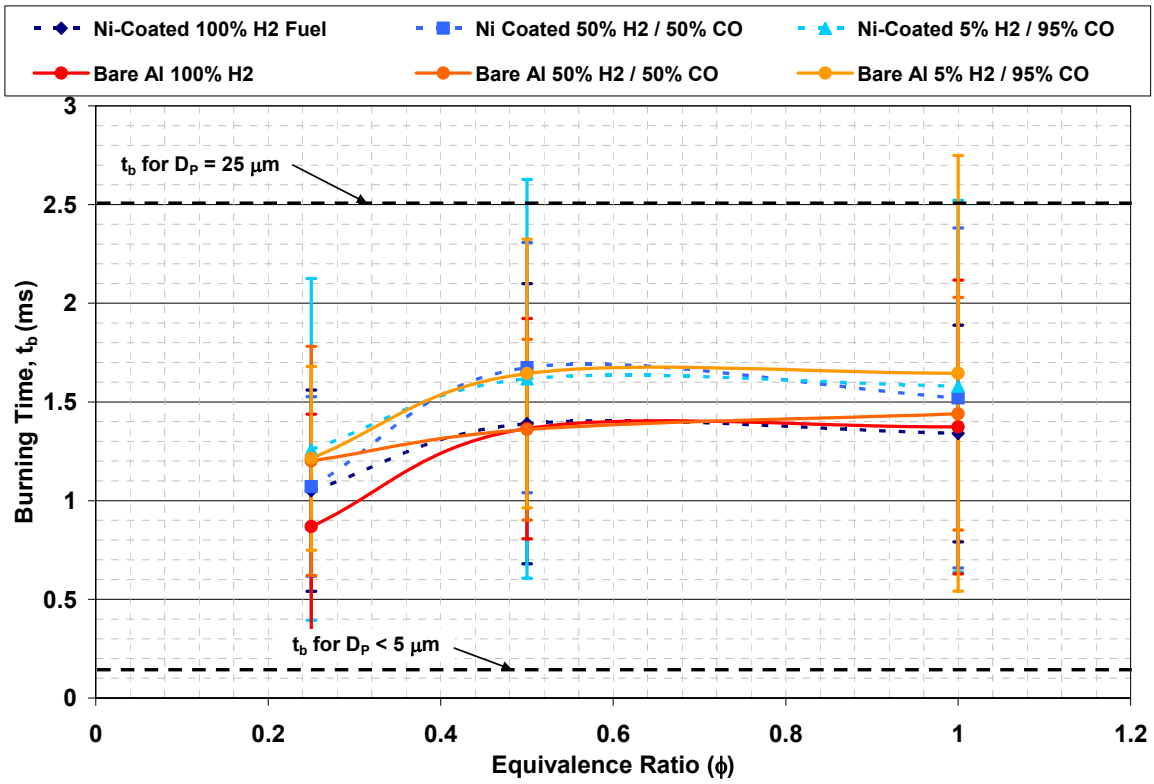

Figure **4.1**: Measured burning times of 9 μm nickel-coated and un-coated aluminum particles with comparison to burning times for particles one standard deviation below (D_p< 5 μm) and one standard deviation above (D_p = 25 μm) the mean particle size.

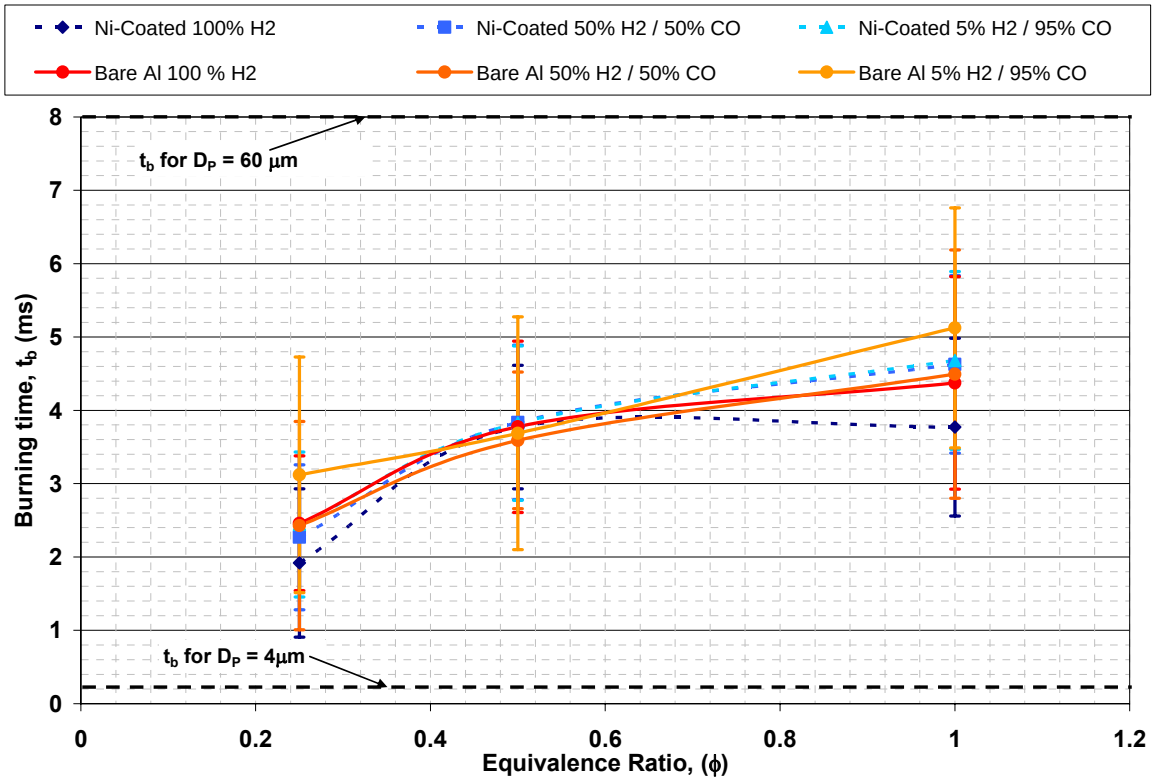

Figure **4.2**: Measured burning times of 32 μm nickel-coated and un-coated aluminum particles with comparison to burning times for particles one standard deviation below (D_p= 4 μm) and one standard deviation above (D_p = 60 μm) the mean particle size.

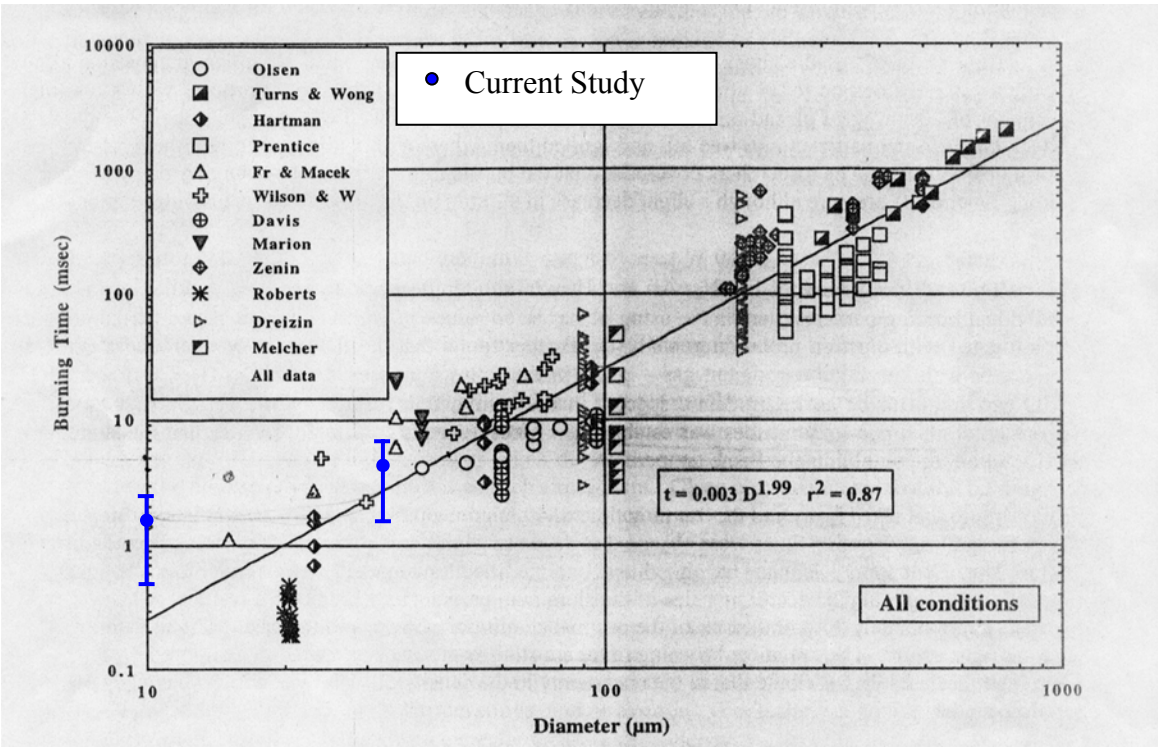

Figure **4.3**: Correlation of many sources of experimental burning time data developed by Beckstead[6].

The large error that was found to be a part of the combustion times can be linked to several factors. The most notable was the large distribution in particle sizes associated with the particles that were provided. The particle size distributions are shown in Figure **4.4** and Figure **4.5**. Only distributions of the nickel-coated particles are shown, but since nickel is significantly denser than aluminum, a 5-wt% coating only consists of a very thin layer. Typical measured values of this coating only consisted of thicknesses in the nano-meter range. The larger 32 μm particles had a standard deviation of 29 μm in size and the smaller particles 9 μm particles had had a standard deviation of 16 μm. Additionally, aluminum combustion is a topic that has typically generated a lot of scatter

in the data. Considering that plot that was developed by Beckstead in Figure **4.3**, by looking at the scatter of the data at ~35 μm there is almost a decade worth of scatter. One reason for this variability is determination of the burn times by various researchers. Much of the aluminum particle is burned in the very early stages of combustion, so as after the combustion event ends the oxide shell is going to continue to emit light for a finite amount of time. The definition of when the particle completes the combustion process and the variability in the methods of testing are going to lead to scatter in the collected data from the various researchers.

For comparison the combustion durations for particles sized at one standard deviation above and one standard deviation below the mean particle size were pulled off of the correlation provided by Beckstead. These burn times are marked out with heavy black lines on the above and below the collected data in Figure **4.1** and Figure **4.2**. As it can be seen the data scatter is actually less than what is expected based on the scatter of the particles sizes. This is likely because extremely small particles will not have a visible combustion streak when compared to particles an order of magnitude larger. Conversely, very large particles will not have enough residence time in the hot-flame zone to begin the ignition process of the particle.

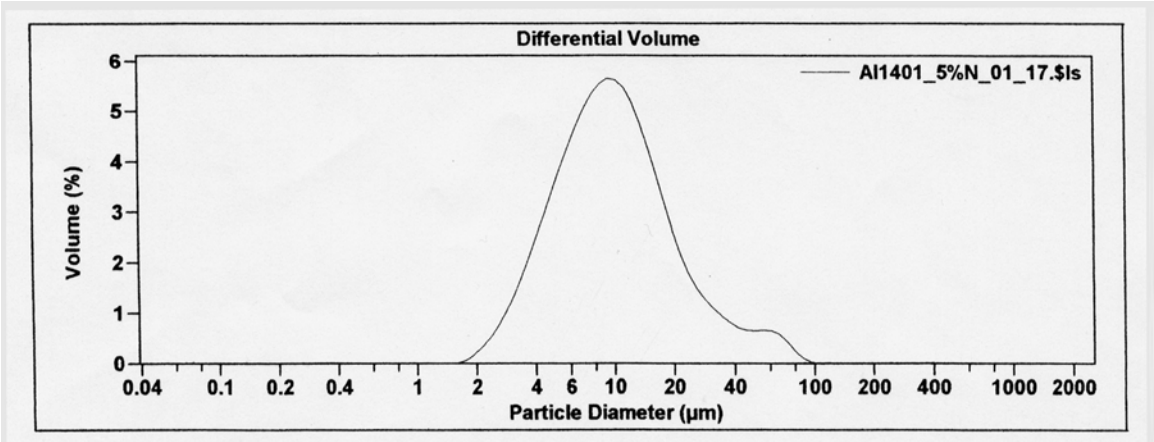

Figure **4.4**: Particle size distribution for a mean size of 9 µm and a standard deviation of 16 µm.

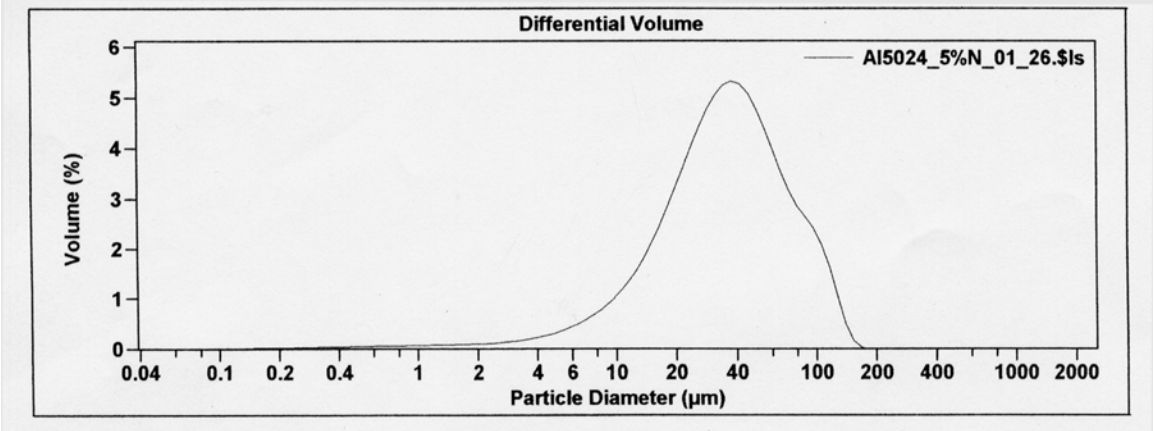

Figure **4.5**: Particle size distribution for a mean size of 32 µm and a standard deviation of 29 µm.

4.1.1 Results from PMT voltage rise tests.

The results that came about from the PMT voltage rise were easily attained by loading the in the plotting tool in MATLAB the combustion times were simply read off as a length of time it took from when significant light was being captured to when light was no longer being emitted. A plot showing a typical voltage spike that was collected can be viewed in Figure **4.6**. Two different particle combustion times are shown along with the temperatures that can be viewed on the plot. The intensity is arbitrary units because certain particles resulted in very intense combustion while other particles did not show as strong of a voltage spike. A spike was considered to be a burn time if the amplitude was larger than that of the baseline noise.

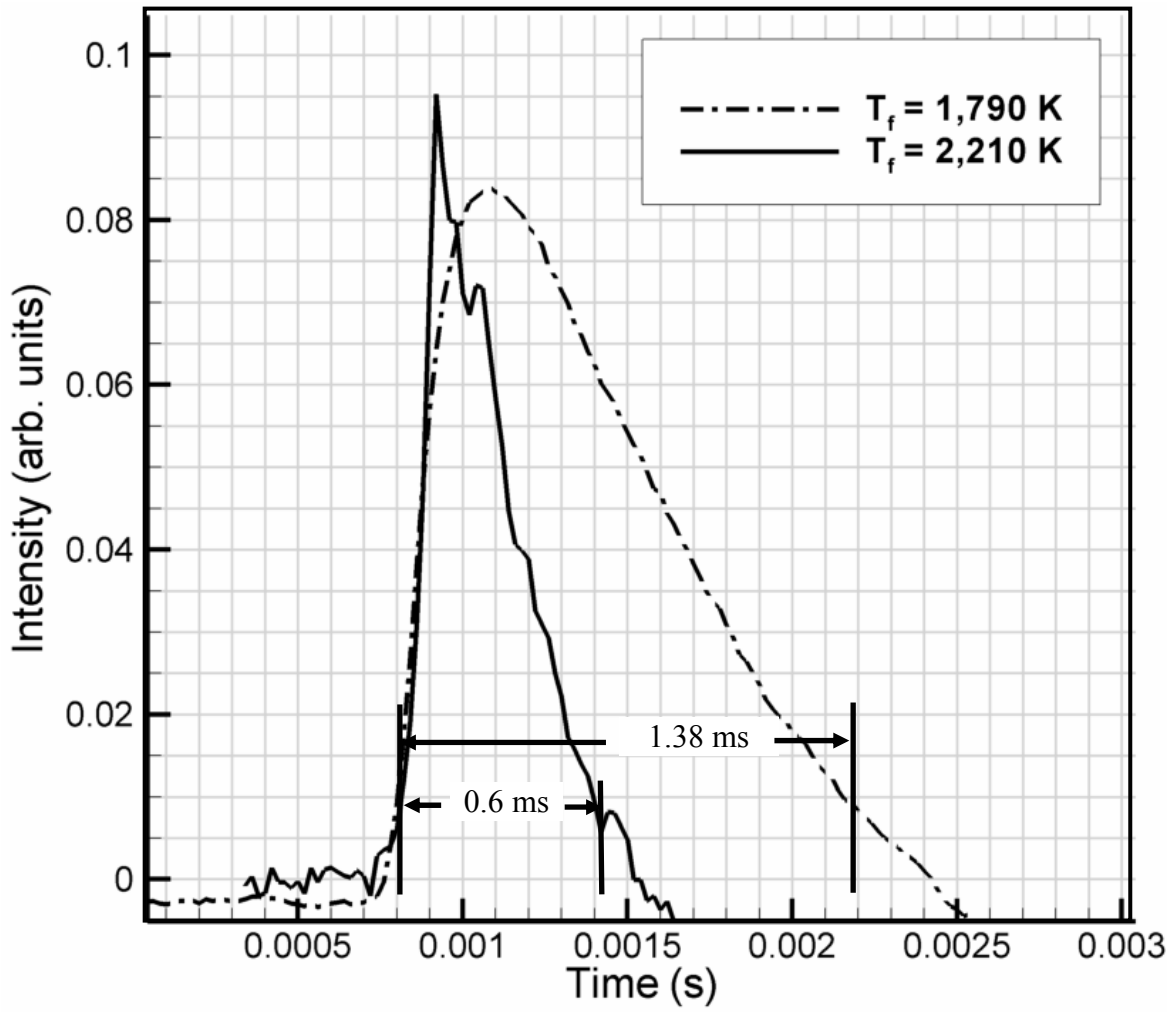

Figure **4.6**: Examples of two typical intensity peaks, which were used to determine the burning time of particles in different hot gas environments.

4.1.2 Results from Video-graphic captures

For each test condition a CHEMKIN simulation was completed to find the axial velocity along the centerline. The length of the combustion streak that is recorded with a video camera is then divided by the velocity to find the combustion duration. The particle velocity is assumed equal to the gas velocity. It is possible that the combustion

event is ending and the particles are simply emitting light radiation that is being captured. However, as a check out a wide range of aluminum particle sizes were run through the flat flame burner at with a high flame temperature around 2500 K and there were not visible particles from visible radiation emissions observed in any case. Therefore, it is assumed that the particles that are being seen are only particles undergoing combustion and if there is light being emitted it is likely very brief after the particle has completed combustion.

4.1.2.1 Entrainment of the particles

One potential problem is how to measure the particle velocity related to the gas velocity. If the particle is not fully entrained then measuring the gas velocity will not necessarily correlate to the particle velocity. To ensure that the particle and the gas velocity can be assumed nearly the same value a force balance was performed on the particle. The only force that was acting in the positive y-direction was a drag force created by the moving gas and the only force acting in the negative y-direction is gravity. So if the drag force is sufficiently large enough when compared to the gravity force then it can be concluded that the particles are fully entrained and are moving at the same speed as the product gases. The drag force is defined in Eq. **(4.1)** where F_d is the drag force, C_d is the drag coefficient, ρ_{gas} is the gas density, u is the gas velocity from the CHEMKIN simulation, and A is the cross-sectional area of a spherical particle.

$$F_D = C_d \rho_{gas} \frac{u^2}{2} A \qquad \textbf{(4.1)}$$

Where the drag coefficient is calculated in Eq. **(4.2)**.[24]

$$C_d = \frac{24}{\mathrm{Re}_D} \tag{4.2}$$

The Re_D is defined in Eq. **(4.3)** where D_p is the particle diameter, u is the gas velocity, ρ_{gas} is the product gas density, and $\mu_{mixture}$ is the mixture viscosity as defined in Eq. **(4.4)**. In this case the viscosity is found by calculating the equilibrium mole fractions of the product species and multiplying that against the corresponding viscosity found in the NIST chemistry webbook at 2000 K to find a mixture viscosity[25].

$$\mathrm{Re}_D = \frac{\rho_{gas} u D_p}{\overline{\mu_{mixture}}} \tag{4.3}$$

$$\overline{\mu_{mixture}} = \sum x_i \mu_i \tag{4.4}$$

The cross sectional area of the particle can be calculated as shown in Eq. **(4.5)**.

$$A = \frac{\pi}{4} {D_p}^2 \tag{4.5}$$

By substituting these equation into one anther the result is shown in Eq. **(4.6)**

$$F_D = \frac{24}{\left(\frac{\rho_{gas} u D_p}{\mu}\right)} \rho_{gas} \frac{u^2}{2} \frac{\pi}{4} {D_p}^2 = 8 \overline{\mu_{mixture}} u \pi D_p \tag{4.6}$$

By comparison the weight of the particles are calculated using Eq. **(4.7)** where F_w is the force from gravity, g is the gravitation constant 9.81 m/s^2, ρ_{AL} is the density of the solid particle, 2700 kg/m^3 for aluminum, and V is the volume of a spherical shaped particle.

$$F_w = \rho_{AL} V g \tag{4.7}$$

Where the volume of the sphere is defined in Eq. **(4.8).**

$$V = 4/3\,\pi r_p^{\,3} \qquad \textbf{(4.8)}$$

By completing a few sample calculations it was shown that drag force that was acting on the particles was at least an order of magnitude larger than the weight of the particle. In Table **4.1** are some sample numbers for the case where the fuel was equal to 50% H_2, 50% CO and an equivalence ratio of 0.5. For this test condition it can be seen that the drag forces were much larger than the weight forces meaning that the particles could be assumed as fully entrained. For small particles that drag coefficient C_d is very large which is why the drag forces are so much larger than the weight forces.

Table **4.1**: Sample drag verses weight calculation for the conditions of 50% H_2, 50% CO and ϕ=0.5

Particle Size	9 μm	32μm
Drag (N)	6.23E-09	2.21E-08
Weight (N)	1.13E-11	5.07E-10
Drag / Weight	552.6	43.7

4.1.2.2 CHEMKIN gas velocity results.

In all nine flow simulations were performed using the instrumented quartz tube along with the CHEMKIN model. These simulations resulted in velocity measurements that could then be taken and viewed along the centerline axis. In all of the cases, the velocity at the beginning of the flow was equal to that of the volumetric flow rate divided by the area. However, along the centerline axis of the tube the flow velocity would

gradually increase. The acceleration of the flow can be explained as a result of two phenomena that are occurring with in the tube. First the buoyancy effects from the hot post-combustion gases are going to cause the flow to accelerate in the lower portions of the tube. Secondly and probably more importantly, the flow is assumed to have a top have a top hat profile when it enters the quartz tube. However, since the flow is laminar as it travels axially through the tube it will begin to develop a parabolic shape. This means that the average velocity through the tube remains fairly constant, or may even slightly decrease due to pressure losses, but the centerline velocity is going to increase while the gas velocity near the wall slows a diagram of this can been seen in Figure **4.7** . The simulations showed a centerline velocity that could increase up to 50 percent higher than the initial value. However, in almost all cases the particle ignited and burned in the first 10 cm meaning that the velocity change was on the order of 20 to 30 percent in most cases.

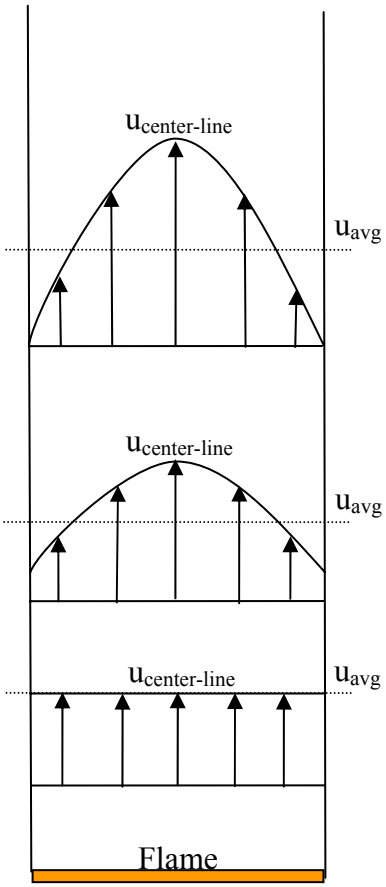

Figure **4.7**: Diagram of the flow seen within the quartz tube to explain why the centerline gas velocity is increasing with height while the average velocity remains unchanged.

Figure **4.8** is a result from one of the CHEMKIN simulations to find the axial velocity in the core flow region. As a check out the centerline, temperature is measured and compared with the result from Figure **4.9**. In these simulations, the centerline is shown as 0 cm on the cross-flow coordinate axis and the burner surface is shown as 0 cm in the axial-coordinate axis. Only half of the calculation is solved to save on computation times.

In this case, the measured gas temperature is 876 K as compared with the simulated gas temperature of 940 K. The other cases saw similarly close measured temperatures to calculated gas temperatures with the largest error being about 150 K, but most others being significantly less. This error is associated with the radiative heat loss of the bead and conductive heat-loss through the wires. The thermocouple is simply measuring the convective heat transfer to the bead, but the wire leading to the bead and the radiation away from the bead could lead to false readings. Additionally, if the flow is not uniform at the exit of the tube this will result in a low reading from the thermocouple. The gas temperature drops almost 700 K in some cases from the centerline of the tube to the outer-wall of the quartz tube so any flow irregularities at the exit will result in a significant difference in the exit temperature. The remainder of the solutions for the axial velocity measurements can be found in Appendix A.

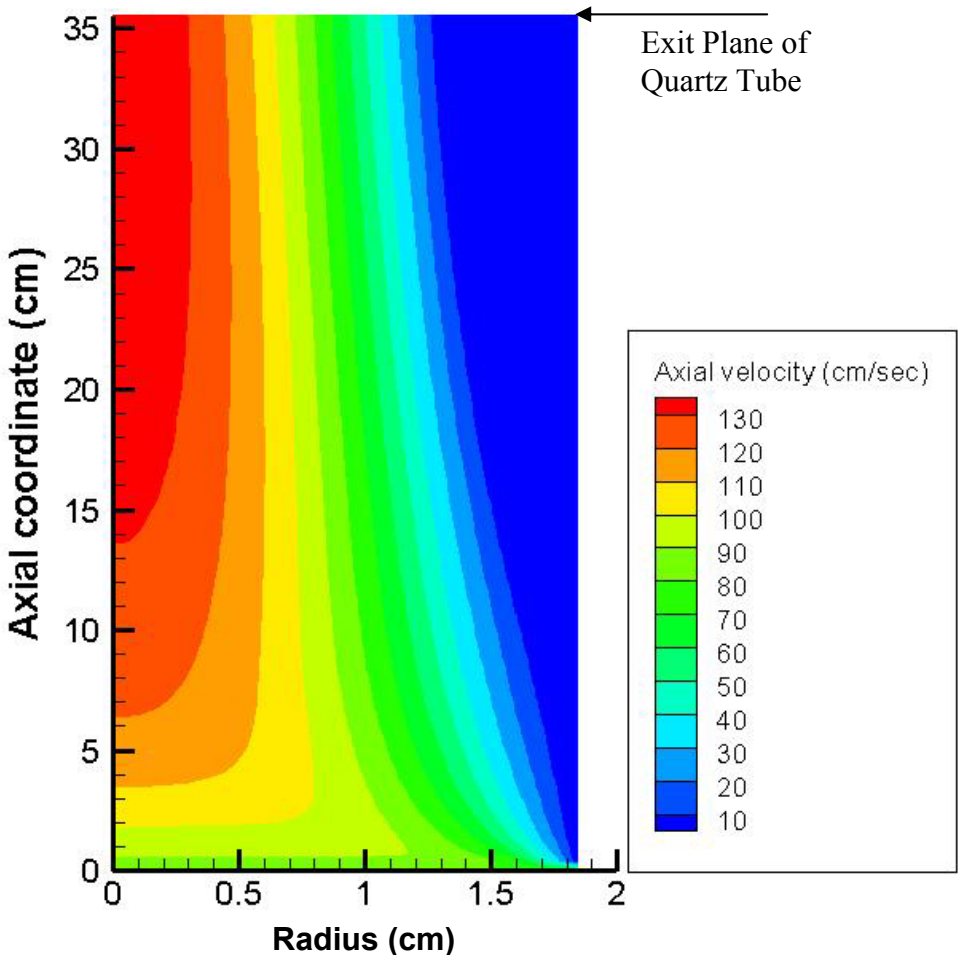

Figure **4.8**: Calculated gas velocity distribution in the quartz tube with the fuel mixture being 100% H_2 with 0% CO and ϕ=1.0.

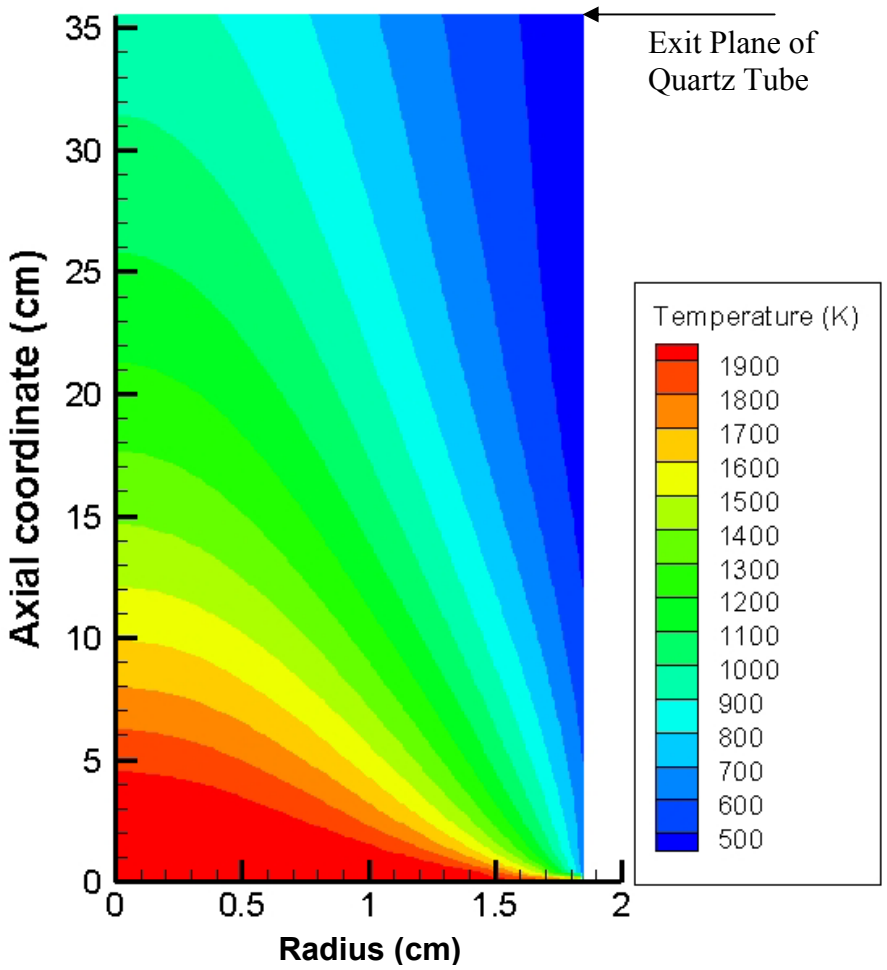

Figure **4.9**: Calculated gas temperature distribution in the quartz tube with the fuel mixture being 100% H_2 with 0% CO and ϕ=1.0.

4.1.3 Comparison of Combustion Time Measure Methods

The two methods were compared against one another to see if there was significant disparity between the two different measurement techniques. This would indicate that either one or both of the methods were potentially flawed in the measurement of the combustion times. However, this proved to not be the case. When

plotting the results of the two techniques against each other as can be seen in Figure **4.10** it can be observed that the mean combustion times lay very close to one another, certainly within the bounds of the experimental error that was experienced in this study. For this particular plot only the times of the Ni-coated 32μm particles were plotted. Plotting all of the results at the same time resulted plots that were very difficult to decipher. The comparison of the other particle types showed similarly close results.

These results are very important because one of the weaknesses of using a cylindrical lens that is focused onto a line of particles is that if the particle jets and spins it will quickly leave the viewing range of the PMT and register an artificially short combustion time. This is not an issue for the video-graphic technique because the images that are collected are directly observed. Any images that were observed to be jetting and spinning were discarded because a true trajectory could not be established. The fact that similar combustion times were measured using video images and PMT voltage rises indicates that both methods are valid techniques in measuring particle combustion time in the flat-flame burner.

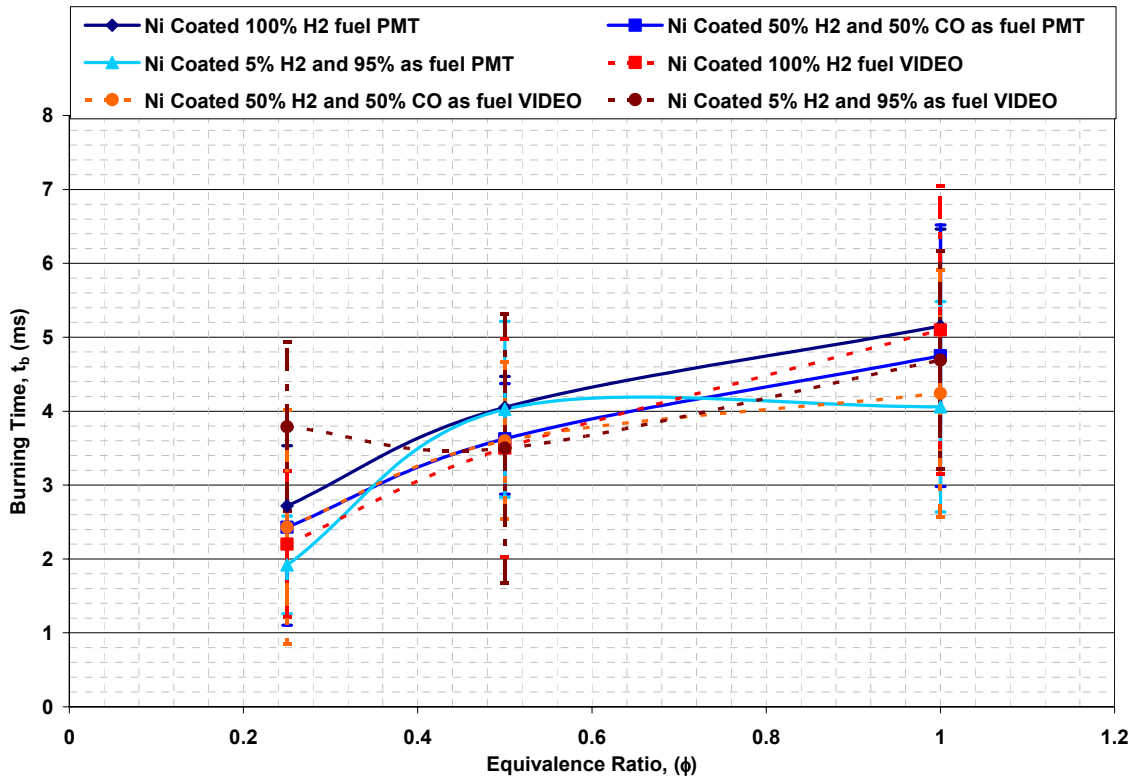

Figure **4.10**: Comparison of measured burning times using both PMT and video camera techniques to show similar results within the experimental error.

4.2 Ignition Temperature Results

4.2.1 Results of the Particle Ignition Times

The ignition temperatures were also going to be measured using the CHEMKIN simulation. However, in all cases that were tested it was found that the particles were igniting and combusting before the gas temperature began to significantly cool. In all cases, the particles began to ignite and begin to combust at or less than 5 cm, while the product gas would not begin to experience significant heat losses until at least 5-10 cm.

This became even more apparent as the mass flow rate of the reactants increased for two reasons. The high flow rates would result in cooler flames and product gases resulting in a lower heat flux with the ambient environment. Additionally, a high mass flow rate resulted in a shorter residence time within the quartz tube meaning that the gas had less time to lose heat to the ambient environment. This made the simulations unnecessary and, because of they were very time consuming, they were not run to find the ignition temperature. Since the particles were igniting in the hottest temperature of the burner, the equilibrium flame temperature was used to find the ignition temperature of the particles. Additionally, since the particles were passed through the flame zone of the burner it cannot be definitively stated that the particle would ignite if this high temperature region was not present. The high temperature zone might be necessary to begin the reaction or at the very least it might be necessary to overcome the melting of the aluminum.

Because the temperature of the flame was slowly decreased until the particles no longer ignited, it was concluded that the temperature of the gas in that particular case was equal to the minimum ignition threshold. The other factor that might influence the ignition temperature is going to be the partial pressure of the oxidizer in the gas stream. As the nitrogen flow is gradually increased, the concentration of the nitrogen is going to increase, taking the place of the other primary oxidizing species. However, this will have a much more significant effect on the combustion duration of the particles. The ignition temperatures that are reported are the minimum ignition temperature that are present in these particular conditions. It is possible that more favorable conditions or more complex

environments, like those seen in the post-detonation zone of a TBX blast, could result in lower or higher ignition temperatures.

In finding the ignition temperature of the particles, two things were varied amongst the tests, both the fuel mixture and the oxidizer concentration. The reactants were varied so that the primary oxidizer effect on the ignition temperature could be studied. Oxygen, water vapor, and carbon dioxide are the primary molecules that are the oxidizing species in aluminum combustion reactions. This means that the fuel and oxidizer reactants were varied so that after the combustion event they would create hot products with known mole fractions of O_2, H_2O, and CO_2. However, it was necessary to develop a way to plot the variation of temperature against the three primary oxidizing species. It has been well documented that the oxidizing species vary in their level of effectiveness in oxidizing the aluminum particles. Initially, the combustion times were going to be used to develop a correlation between the oxidizer concentration and the duration of the combustion event of the aluminum particle. However, as can be seen in Figures **4.1** and **4.2** that due to the data scatter a meaningful correlation could not be developed. Therefore, upon reviewing the literature it was found that Beckstead[6] compiled a summary of multiple sources of aluminum combustion data. They found that effect of the oxidizers could be weighted against each other to develop a way to correlate the combustion times more with much less data scatter as shown in Eq. **(4.9)**. Oxygen is the most effective oxidizer of aluminum particle with water vapor being half as effective and carbon dioxide being about 22 percent as effective. Beckstead found that the coefficient oxygen is 1 while the coefficient of the water vapor is 0.5 and the coefficient of carbon dioxide is 0.22 meaning that the final equation is shown in Eq. **(4.10)**.

$$X_{OX,eff} = x_{O_2} + a_{H_2O}x_{H_2O} + a_{CO_2}x_{CO_2} \quad \textbf{(4.9)}$$

$$X_{OX,eff} = x_{O_2} + 0.5x_{H_2O} + 0.22x_{CO_2} \quad \textbf{(4.10)}$$

The ignition temperature was plotted against the effective oxidizer concentration, $X_{OX,eff}$ in Figure **4.11** for the 9 μm particles and in Figure **4.12** for the 32 μm particles. The plots both show a very important result, the ignition temperature is significantly reduced due to the application of the nickel coating.

In both figures, it seems that the data for coated particles is more to the left of the plot where the effective oxidizer is small. This is because as the nitrogen levels are increased the concentrations of the oxidizers in the product stream are going to be reduced as a result. Initially, the relative concentrations of the oxidizers were going to be used in the effective oxidizers ordinate. However, this does not take into account how the partial pressure of the oxidizer affects the combustion of the particles. As more nitrogen is introduced in the reactant stream, the oxygen, water vapor, and carbon dioxide are going to become more diluted and less available to react with the particles. This means that is important to use true concentrations of the oxidizing species as they relate to the total product stream. Therefore, the concentrations of the oxidizers were found using equilibrium calculations at each of the ignition conditions. Due to the weighted strengths of the oxidizing species, the plots still able provide meaningful results.

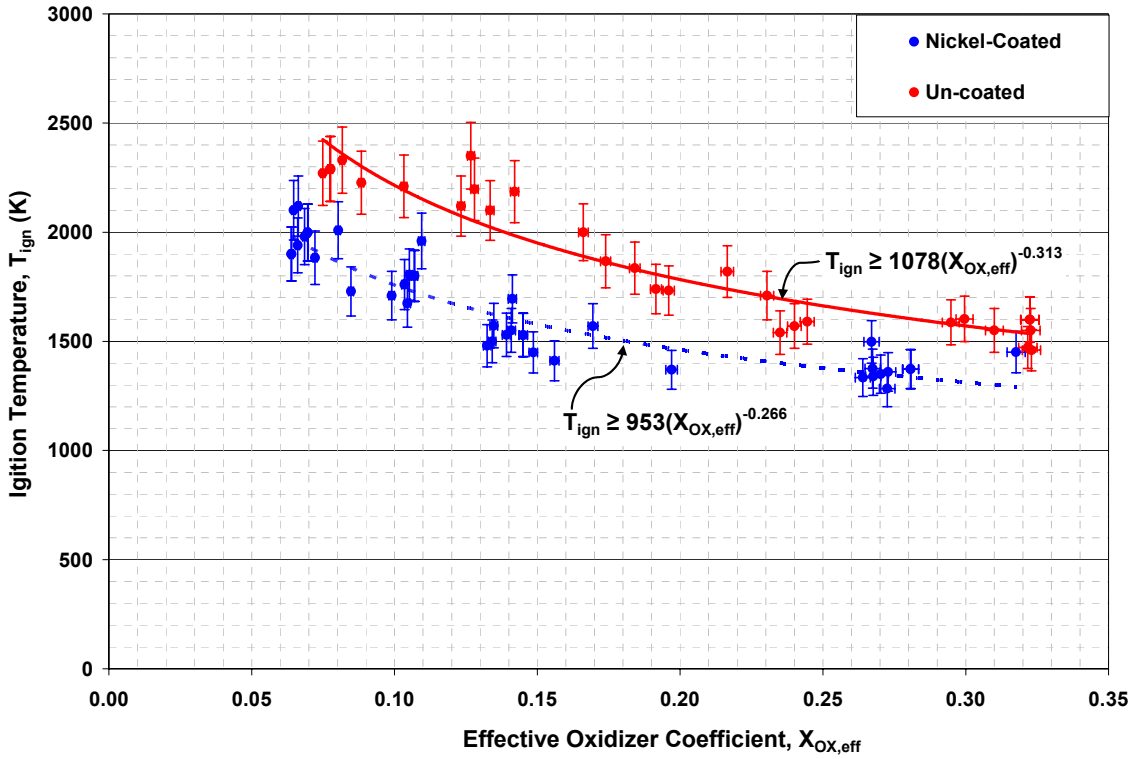

Figure **4.11**: Measured ignition temperature of 9 μm Ni-coated and uncoated aluminum particles as a function of the effective oxidizer coefficient, $X_{OX,eff}$.

These results are very promising showing a significant reduction in the ignition temperature of the particles. By fitting the data with curve fits ignition thresholds can be developed. This means that that all temperatures above the threshold will result in ignition while all of the temperatures below the threshold will likely not result in ignition. For the 9 μm Ni-coated particles the ignition threshold is shown in Eq. **(4.11)** while the threshold for the 9 μm uncoated particles can be seen in Eq. **(4.12)**.

$$T_{ign} \geq 953\left(x_{O_2} + 0.5x_{H_2O} + 0.22x_{CO_2}\right)^{-0.266} \quad \textbf{(4.11)}$$

$$T_{ign} \geq 1078\left(x_{O_2} + 0.5x_{H_2O} + 0.22x_{CO_2}\right)^{-0.313} \quad \textbf{(4.12)}$$

Similarly power-law curve fits were applied to the ignition temperature results for the 32 μm particles with the ignition threshold for the 32 μm Ni-coated particles shown in Eq. **(4.13)** and the ignition threshold for the 32 μm un-coated particles shown in Eq. **(4.14)**.

$$T_{ign} \geq 969\left(x_{O_2} + 0.5x_{H_2O} + 0.22x_{CO_2}\right)^{-0.190} \quad \textbf{(4.13)}$$

$$T_{ign} \geq 1868\left(x_{O_2} + 0.5x_{H_2O} + 0.22x_{CO_2}\right)^{-0.104} \quad \textbf{(4.14)}$$

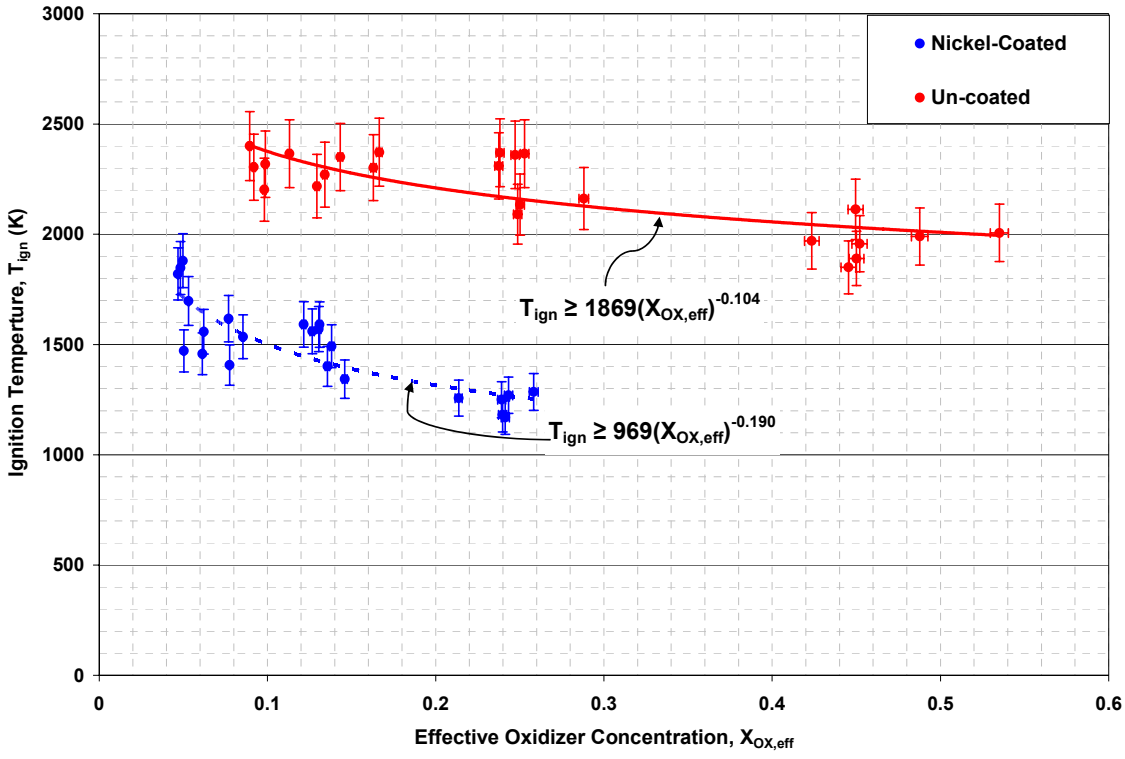

Figure **4.12**: Measured ignition temperature of 32 μm Ni-coated and uncoated aluminum particles as a function of the effective oxidizer coefficient, $X_{OX,eff}$.

From the results it can be seen that the ignition temperature dropped more significantly for the larger particle sizes. In both particles sizes the ignition temperature was lower for the Ni-coated aluminum particles. However, the 32 μm showed a more significant reduction in temperature when compared to its uncoated counterpart having a reduction of ignition temperature that averaged ~750 K. As opposed to the 9 μm particles that showed a reduction that averaged ~300 K. It did seem for the Ni-coated larger and smaller particles there was a similarly low ignition threshold. However, for the 9 μm uncoated aluminum particles the ignition temperature was considerably lower than the larger uncoated particles. This is likely due to the size that effects because as aluminum particle sizes drop below 20 μm the ignition temperature is typically reduced. Other researchers[26] have observed lower ignition temperatures for small particle sizes, particularly for nano-sized particles.

From review the previous literature on this topic it can be conclude that two mechanisms are potentially responsible for the reduction in the ignition temperature of the nickel coated aluminum particles. Since the nickel melts at a lower temperature than aluminum oxide it has been theorized that nickel will provide for a lower ignition temperature because it will melt off exposing active aluminum to a reactive flow. However, it was observed that in when there was sufficient effective oxidizer in the flow the particles would ignite at lower temperature than the melting point of nickel. Also nickel is a ductile material and, dissimilar to a brittle material like aluminum oxide, it is unlikely to crack or shatter from thermal stresses. Additionally, it can be seen from the SEM images that are shown in Figures **3-9** through Figure **3.3** that many of the particles

were not completely coated with a layer of Nickel. There a many instances on the particle surfaces where there are bare spots of aluminum present. From the method of testing it is possible that these particles were simply not ignited while the uniformly coated particles were ignited or it is more likely that there are other mechanisms at work that are allowing these particles to ignite more readily.

It is more likely that the primary mechanism for the significant reduction in the ignition temperature is an exothermic inter-metallic reaction between the aluminum and the nickel coating. According to Andrzejak[1] as the particle passes through the hot flame zone of the Hencken burner it the aluminum within the core is going to melt and form $NiAl_3$. When the melting point of $NiAl_3$ is exceeded at 1100 K Ni_2Al_3 will form and begin to release heat. As the temperature passes 1400 K NiAl will begin to form releasing more heat. However, in a previous study it was shown that with a 6 wt% coating of Ni all of the Ni coating was consumed prior to 1400 K. They did not observe ignition in these particles in inert atmospheres. It was postulated that the large particle size caused quenching of the reaction due to heat losses within the particle. That is not going to be the case with smaller particles that were used it this study. There will not be enough heat loss into the particles to quench the reaction and the hot post-combustion gases are just going to continue to add heat to the particles.

Secondly the intermetallic reactions add heat to the particle the layers of nickel and aluminum compounds are going to become molten allow for oxidizers to be transported to the particle surface. This is going begin a chain reaction where more heat is release thus further increasing the rate of oxidizer diffusion to the surface. This is likely why in instances where the effective oxidizer is very low the particle have higher

ignition temperatures. In these instances more heat is required from the hot gases to ignite the particle because less oxidizer is present in the gas stream to diffuse to the aluminum. It should be noted that while other studies have proved that Ni-coated aluminum will burn in an inert atmospheres, like Ar, all of those studies were conducted with much higher content of nickel. The coating thickness on these particles in this study has proven to be thick enough to cause a significant reduction in the ignition temperature, but it is still necessary to have an oxidizer present to ignite the particles.

The error bars that are associated with the plots in Figure **4.11** and Figure **4.12** are from the potential human error that is involved in reading the flow-meter settings. While great care is taken to make sure that each test is at the specified condition it is nearly impossible to locate a reading within 2 marks on the reading scale. Also it is possible that as the gases are flown for a while the regulators begin to cool allowing different flow rates of the gas causing the rotameters to slowly drift unnoticed over time. With this in mind equilibrium calculations were carried out to find the extremes for various cases. If all of the conditions were at the low and high points of their error it corresponded to a 6.5 percent error. In changing the reactants to find the error that would be imparted at onto the temperature of the gas this will also have an effect on the effective oxidizer factor. If the oxygen in slightly raised or lowered this will result in slightly more or less oxygen in the flow. The error that would be associated with this was also applied to the effective oxidizer factor giving x-error bars to the data points. However, this error was very low, on-the-order of 1 percent.

4.2.2 Correlation Uncertainty

The correlations were plotted with the ignition temperature on the y-axis and the correlated temperature on the x-axis. This showed how the data fit within ±10% of the correlation. All of the ignition temperature data is plotted for the 9 μm particles in Figures **4.13** and **4.14** this and it can be seen that all of the data points, or at least their error bars, are with the 10% uncertainty bounds and the correlation. The same can be seen in Figures **4.15** and **4.16** where the ignition temperatures of 32 μm coated and uncoated Al particles are plotted against the correlation. All of the data point, or their error bounds, fall in between the ±10% uncertainty that is shown for the correlated ignition boundary. This shows that while there is some scatter in the data it is still fitting reasonably well to within calculated ignition thresholds. Note that the origins on the plots are not at zero. This is show how the collected data corresponds to the correlations more effectively.

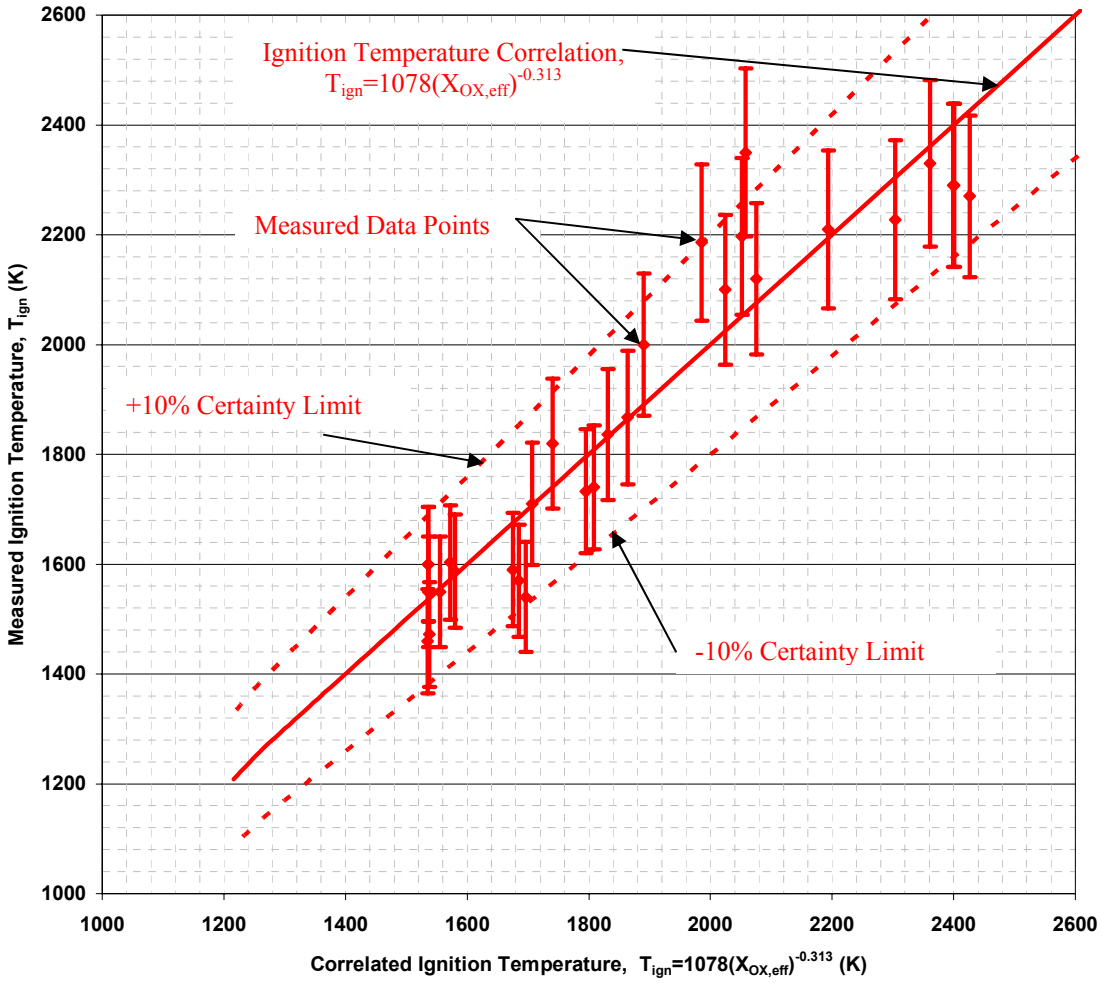

Figure **4.13**: The correlated ignition temperature verses the measured ignition temperature for the 9 μm uncoated Al particles shown ±10% uncertainty bounds of the correlation.

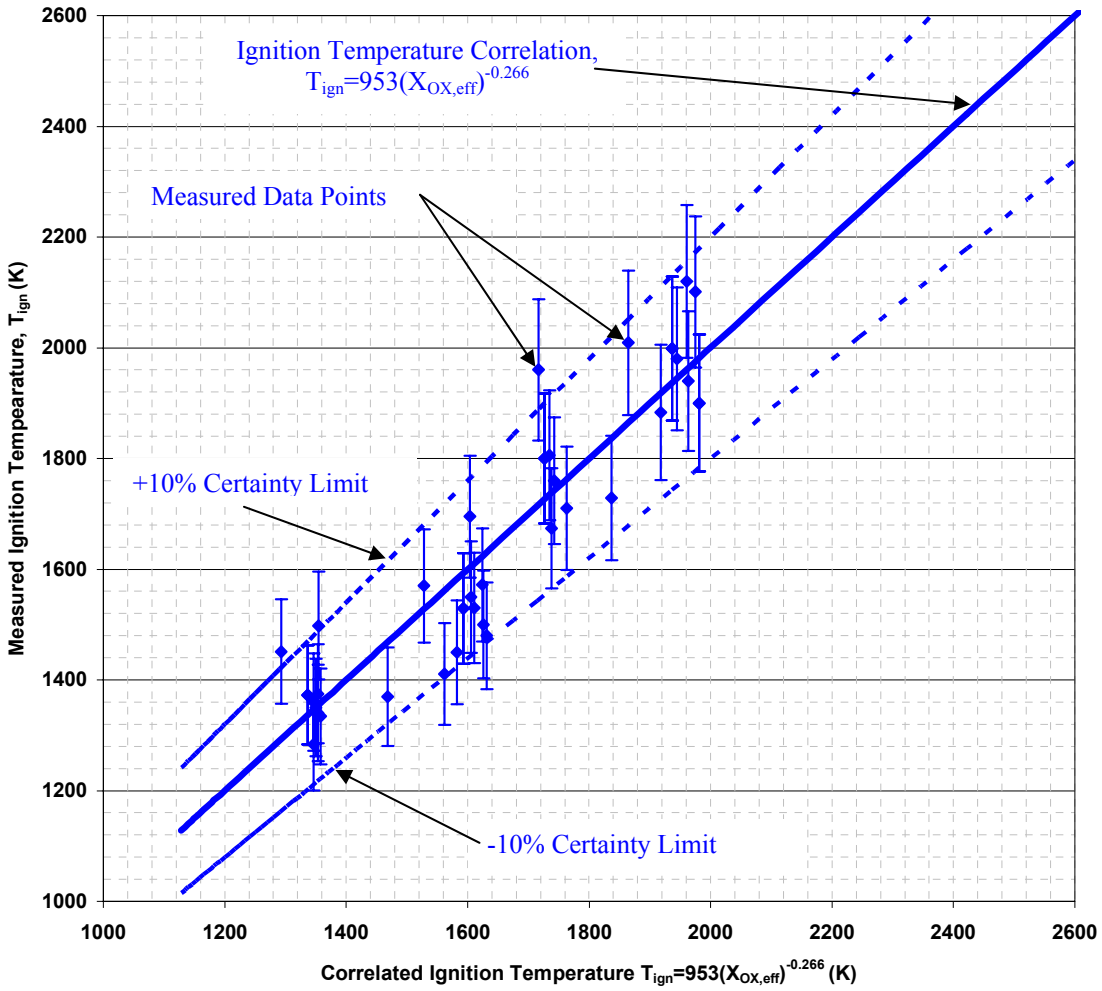

Figure **4.14**: The correlated ignition temperature verses the measured ignition temperature for the 9 μm Ni-coated Al particles shown ±10% uncertainty bounds of the correlation.

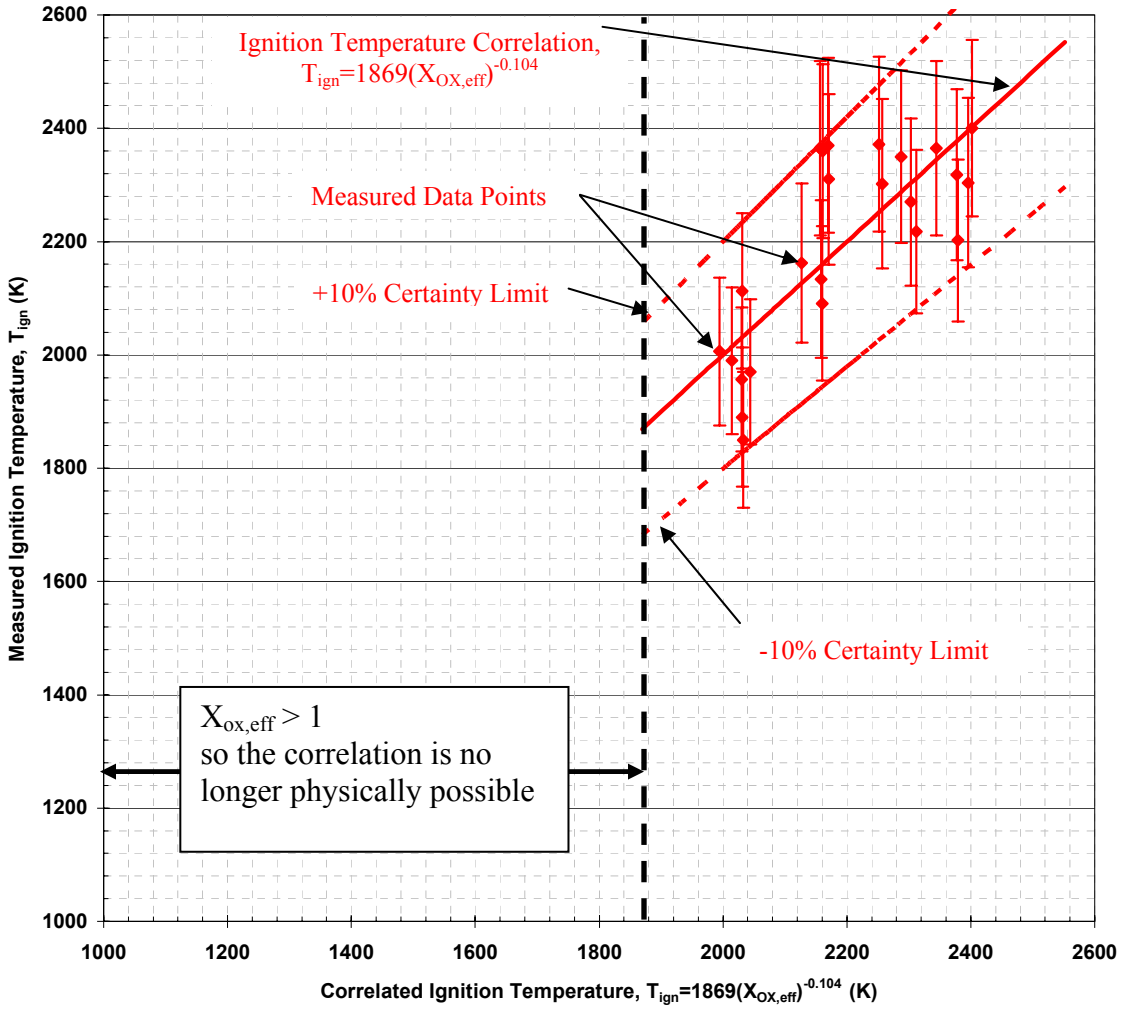

Figure **4.15**: The correlated ignition temperature verses the measured ignition temperature for the 32 µm uncoated Al particles shown ±10% uncertainty bounds of the correlation.

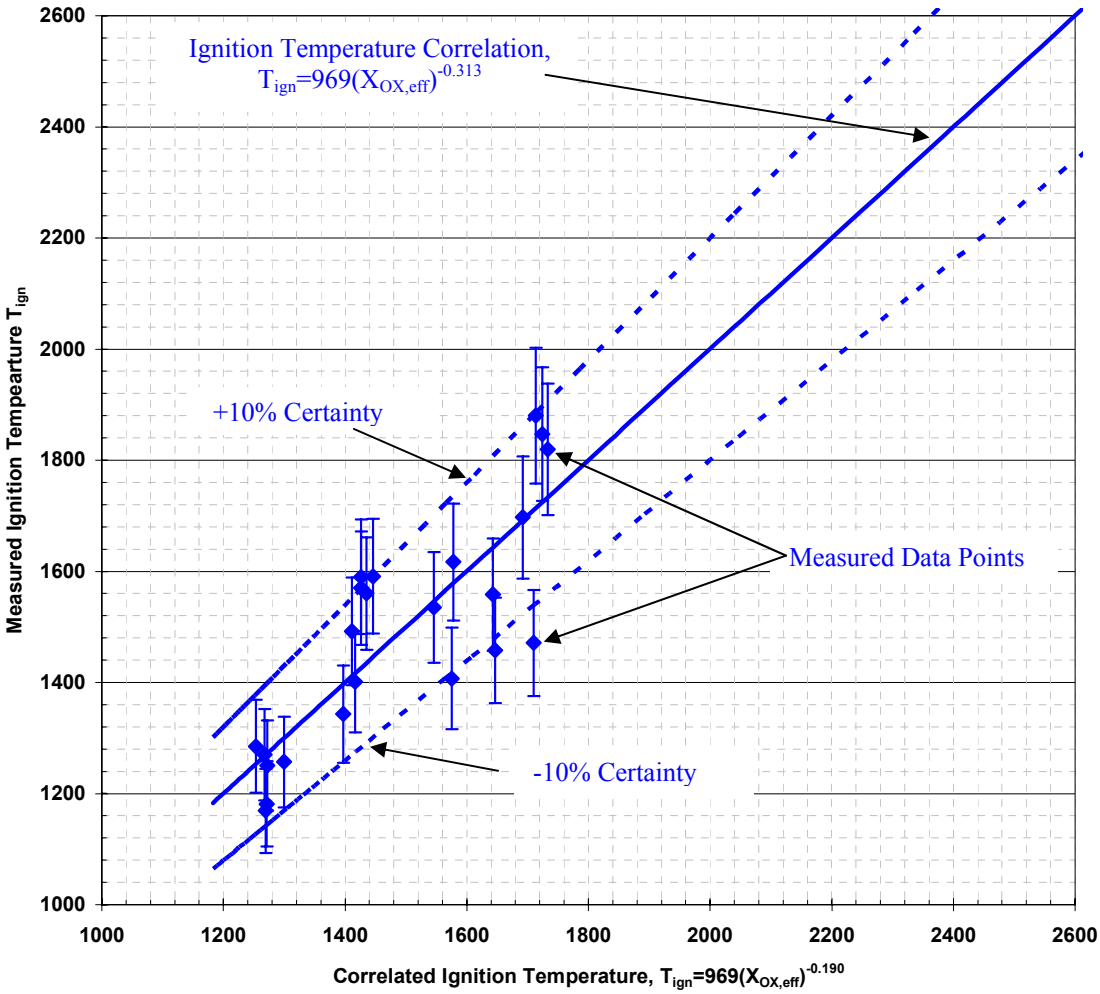

Figure **4.16**: The correlated ignition temperature verses the measured ignition temperature for the 32 μm Ni-coated Al particles shown ±10% uncertainty bounds of the correlation.

Chapter 5

Conclusions

5.1 Conclusions from this work

1. The nickel coating on the aluminum particle made it possible for an ignition temperature drop of ~750 K on average for the lager (~32μm) particles. The smaller particles did not experience such a significant drop, but there was still a notable reduction in ignition temperature of ~300 K. Ignition thresholds were developed and are shown in Chapter 4.
2. The lower ignition temperature is attributed to both inter-metallic reactions that occur between the nickel and the aluminum in combination with the oxidizers diffusing through the molten NiAl compounds to the aluminum core causing the Ni-coated Al particles to ignite at reduced temperatures.
3. Additional tests were carried out that the ignition temperature data is reproducible while using the Hencken burner.
4. The mean combustion times for the particles were almost identical with or without a nickel coating.
5. The mean combustion times that were collected match reasonably well with collected data from other previous experiments that tested aluminum particles of similar size.

6. The considerable data scatter for the combustion time can be attributed to the large particle size distribution. The primary controlling factor for aluminum combustion is the size of the particles. A large size distribution of particles is going to result in a combustion time results.

5.2 Future Work

If more funding were to become available there are several different aspects should be studied to add more to the knowledge scientific community about the effectiveness of the nickel coating on aluminum particles.

1. Tests where the particle is captured post combustion and then studied using Auger spectroscopy or electron probe microanalysis. Either of these techniques will definitively answer the question as to whether the aluminum particle is completely combusting. These techniques allow for elemental mapping of the through the surface of the particle. If there is oxygen content throughout the particle that means that the entire particle is oxidizing.
2. Other testing techniques should be used to study the effects of pressure and number density of the particles. Additionally, complex shock wave interactions information would be invaluable for TBX type weapons. Also, directly matching the TBX-post combustion products would be valuable information.
3. Using these particles as additive in different rocket fuel and propellants would give a lot of information about how it affects the burning rate in rocket type of environments.

Bibliography

1. G.A. Risha, B.J. Evans, E. Boyer, and K.K. Kuo, "Metals, Other Energetic Additives, and Special Binders used in Solid Fuels for Hybrid Rocket Applications", *Fundamentals of Hybrid Combustion and Propulsion*, Chapter 10

2. "Thermobaric Explosives." GlobalSecurity.org. 25 November 2005. <http://www.globalsecurity.org/military/systems/munitions/thermobaric.htm>.

3. Marcus, Jonathan. "Analysis: How thermobaric bombs work." BBC News. 20 Sep 2006, <http://news.bbc.co.uk/1/hi/world/south_asia/1854371.stm>.

4. Price, E. (1983) "Combustion of Metalized Propellants", Chapter 9, Fundamentals of Solid Propellant Combustion, Kuo, K. K., Summerfield, M. (ed.), *Progress in Astronautics and Aeronautics*, Vol. 90, AIAA, New York, NY. 479-513.

5. Prentice, J. (1973) "Combustion of Aluminum Droplets in Various Coidizing Gases Including CO2 and Water Vapor", Proceedings of the 10th JANNAF Combustion Meeting. Vol. III, Chemical Propulsion Information Agency, CPIA Pub. 243.

6. Beckstead M.W., Newman B.R., and Waroquet C., "A Summary of Aluminum Combustion." *50th JANNAF Propulsion Meeting. July 13th*, 2001.

7. Bayzn, T., Krier, H., and Glumac, N. (2005) Oxidizer and Pressure Effects on the Combustion of 10-μm Aluminum Particles, *Journal of Propulsion and Power*, 21: 577-582.

8. Bayzn, T., Krier, H., and Glumac, N. (2006) Combustion of Nanoaluminum at Elevated Pressure and Temperature Behind Reflected Shock Waves, *Combustion and Flame*, 145: 703-713.

9. Houim, R. W., Boyd, E. R, Kuo, K. K., "Combustion of Aluminum Flakes in the Post-Flame Zone of a Henken Burner," presented at the Seventh International Symposium on Special Topics in Chemical Propulsion (7-ISICP), Kyoto , Japan , September 17-21, 2007.

10. Babuk, V. A., Vassiliev, V. A. and Sviridov, V. V. (2001)"Propellant Formulation Factors and Metal Agglomeration in Combustion of Aluminized Solid Rocket Propellant", *Combustion Science and Technology*, 163:1, 261 — 289

11. A.L. Breiter, V.M. Mal'tsev, E.I. Popov, "Means of Modifying Metallic Fuel in Condensed Systems", *Combust. Explos. Shock Waves* 26 (1) (1988) 86–92.o

12. D.A. Yagodnikov, A.V. Voronetskii, "Experimental and Theoretical Study of the Ignition and Combustion of and Aerosol of Encapsulated Aluminum Particles", *Combust. Explos. Shock Waves* 33 (1) (1997) 49–55.

13. S.C. Hanyaloglu, B. Aksakal, I.J. McColm, "Reactive Sintering of Electroless Nickel-Plated Aluminum Powders." *Materials Characterization* **47** (1997) 9–16..

14. T.B. Massalski (Ed.), Binary Alloy Phase Diagrams, second ed., ASM, Materials Park, OH, 1990.

15. L. Theirs, A.S. Mukasyan, A. Varma, "Thermal explosion in Ni-Al system: influence of reaction medium microstructure" *Combustion and Flame* **131** (1–2) (2002) 198–209.

16. P. Zhu, J.C.M. Li and C.T. Liu, "Combustion reaction in multilayered nickel and aluminum foils", *Mater. Sci. Eng* A239–240 (1997), p. 532.

17. L. Plazanet and F. Nardou, "Reaction Process During Relative Sintering of NiAl" *J. Mater Sci* **33** (1998), p. 2129.

18. K.A. Philpot, Z.A. Munir and J.B. Holt, "An Investigation of the Synthesis of Nickel Aluminides Through Gasless Combustion", *J. Mater. Sci*. **22** (1987), p. 159

19. A. Hahma, A. Gany, K. Palovuori. "Combustion of Activated Aluminum." *Combustion and Flame* **145** (2006): 446-480.

20. V. Rosenband, A. Gany, "Activated Metal Powders as Potential Energetic Materials" presented at the Seventh International Symposium on Special Topics in Chemical Propulsion (7-ISICP), Kyoto , Japan , September 17-21, 2007.

21. P. Escot Bocanegra, C. Chauveau, I. Gökalp, "Experimental Studies on the Burning of Coated and Uncoated Micro- and Nano-Sized Aluminum Particles", *Aerospace Science and Technology* **11** (2007) 33–38.

22. T. A. Andrzejak, E. Shafirovich, A. Varma, "Ignition Mchanism of Nckel-Cated Auminum particles" *Combustion and Flame* 150, 2007, 60-70.

23. F.P Incropera, D.P. DeWitt, "Fundamentals of Heat and Mass Transfer", *John Wiley and sons*, Eq. (9.27) on p. 546.

24. J. Happel, *Low Reynolds Number Hydrodynamics,* Prentice Hall, Englewood Cliffs, NJ, 1965.

25. "NIST Chemistry Web book", January 22, 2009, <http://webbook.nist.gov/chemistry/#Documentation>.

26. Parr, T., Johnson, C., Hanson-Parr, D., Higa, K., and Wilson, K. "Evaluation of Advanced Fuels for Underwater Propulsion", *39th JANNAF Combustion Subcommittee Meeting.* (2003)

Appendix A

Results from CHEMKIN simulations

Figures A-1 through A-9 are the results of the CHEMKIN simulations to find the centerline gas velocities in the quartz tube that the particles experienced. In the cross flow coordinate 0 cm is the center-line of the burner at the center port where the particles are injected. In the axial coordinate 0 cm is the surface of the burner where the flame is located. These images indicate the axial velocity of the products gases as they travel vertically up the quartz tube. The important velocities are at center of the burner and it can be seen that the flow accelerated as it travels through the quartz tube. This is due to buoyancy effects and the core of the flow accelerating as the boundary layers along the wall decelerate the flow.

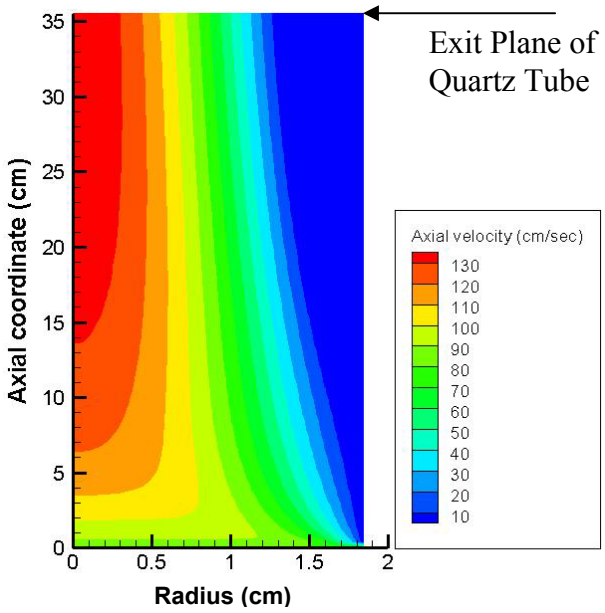

Figure **A.1**: Calculated gas velocity distribution in the quartz tube with the fuel mixture being 100% H_2 with 0% CO and ϕ=.25.

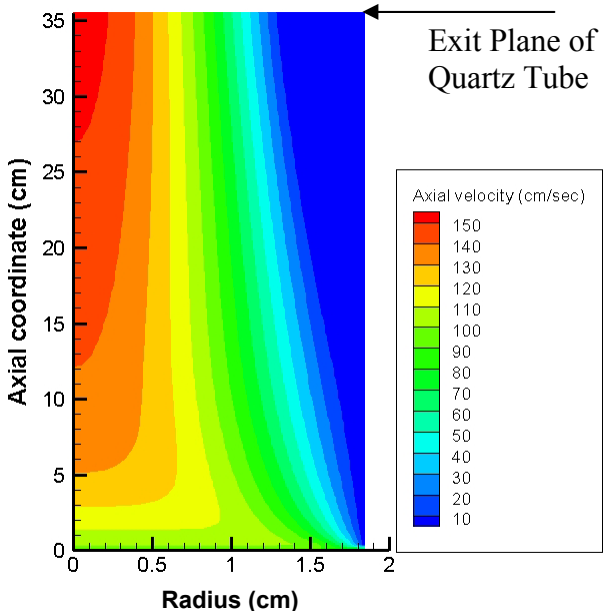

Figure **A.2**: Calculated gas velocity distribution in the quartz tube with the fuel mixture being 50% H_2 with 50% CO and ϕ=.25.

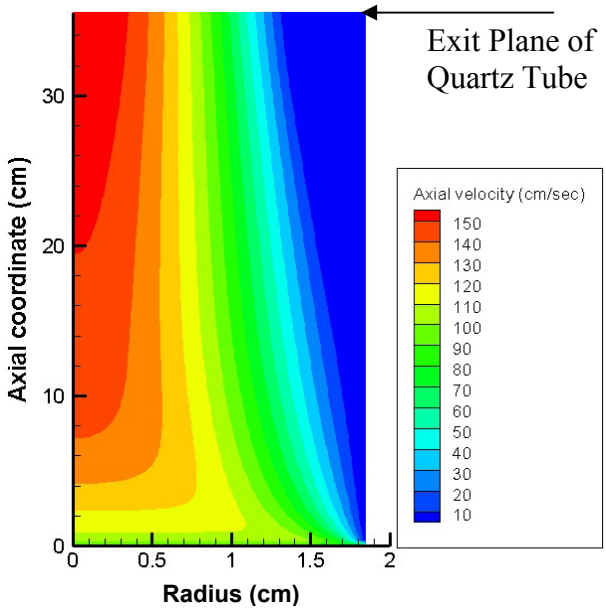

Figure **A.3**: Calculated gas velocity distribution in the quartz tube with the fuel mixture being 5% H_2 with 95% CO and ϕ=.25.

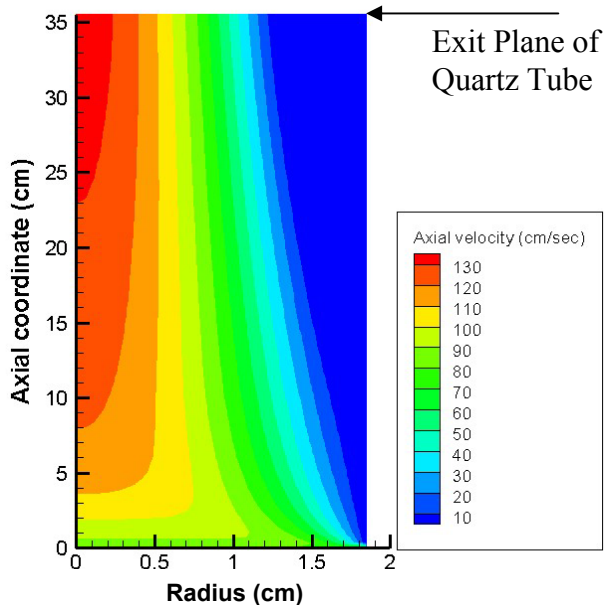

Figure **A.4**: Calculated gas velocity distribution in the quartz tube with the fuel mixture being 100% H_2 with 0% CO and ϕ=.5.

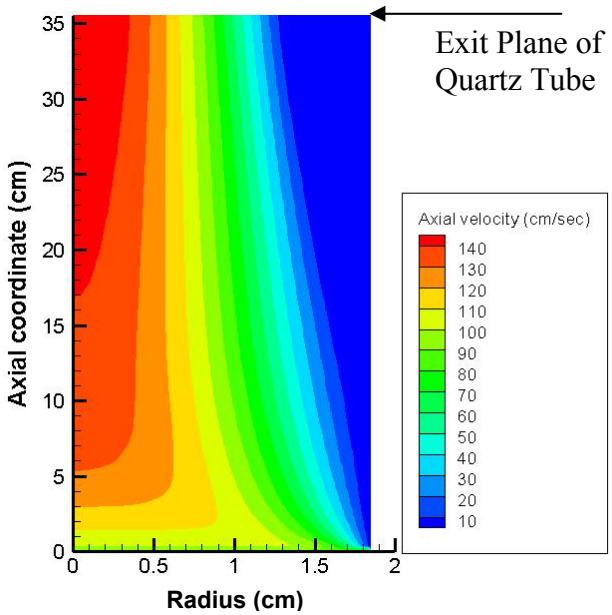

Figure **A.5**: Calculated gas velocity distribution in the quartz tube with the fuel mixture being 50% H_2 with 50% CO and ϕ=0.5.

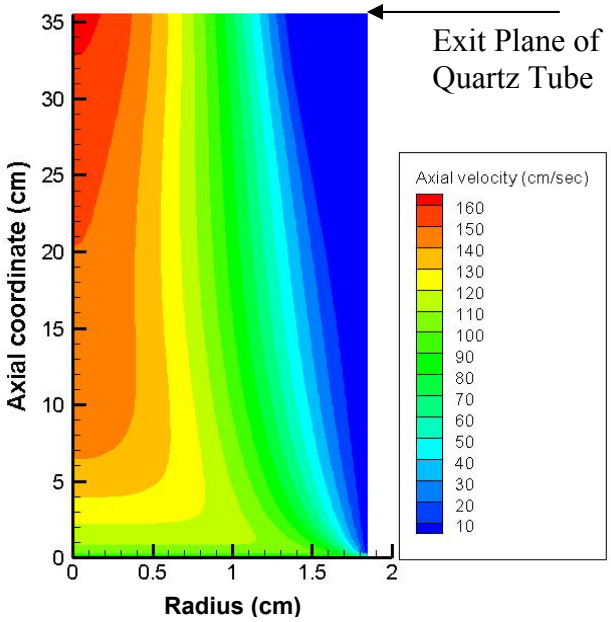

Figure **A.6**: Calculated gas velocity distribution in the quartz tube with the fuel mixture being 5% H_2 with 95% CO and ϕ=0.5.

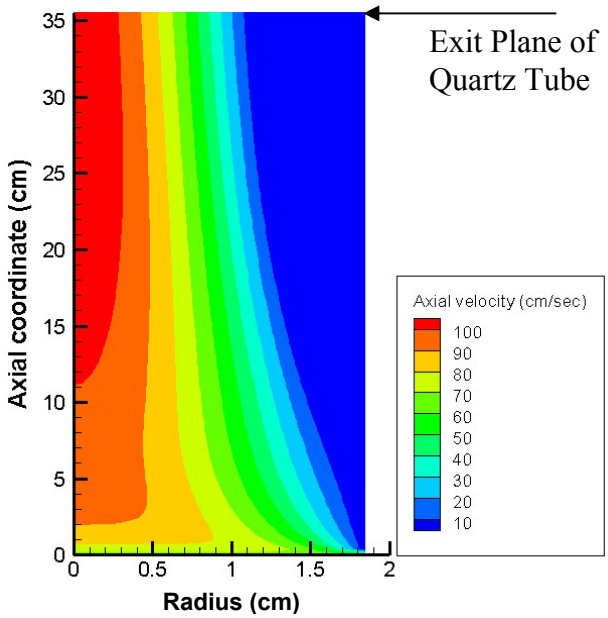

Figure **A.7**: Calculated gas velocity distribution in the quartz tube with the fuel mixture being 100% H_2 with 0% CO and ϕ=1.0.

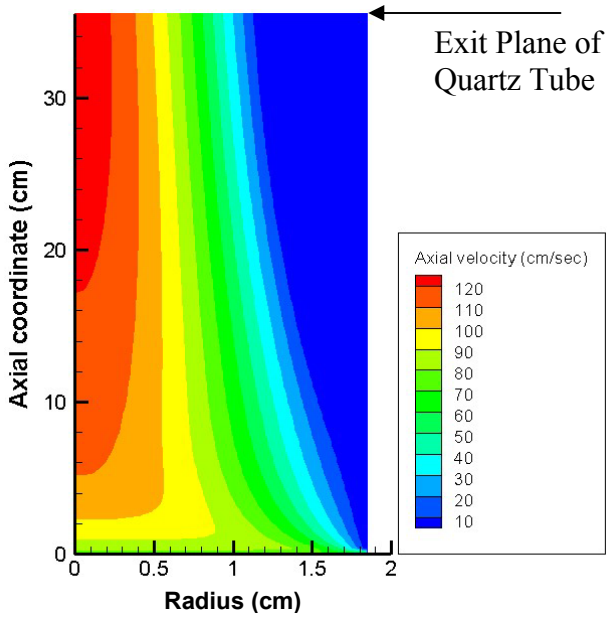

Figure **A.8**: Calculated gas velocity distribution in the quartz tube with the fuel mixture being 50% H_2 with 50% CO and ϕ=1.0.

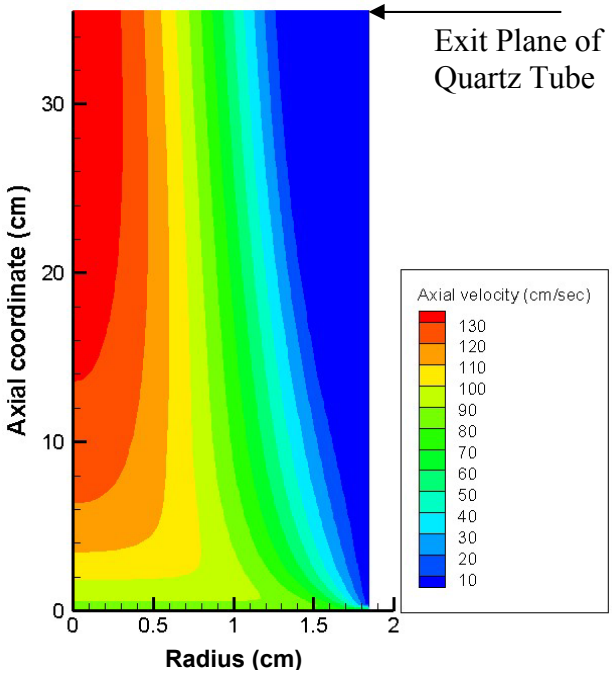

Figure **A.9**: Calculated gas velocity distribution in the quartz tube with the fuel mixture being 5% H_2 with 95% CO and ϕ=1.0.

Appendix B

Flow-Meter Calibrations

These are the calibration curves that are necessary to convert the flow-meter readings into actual flow rates. The raw data was provided for the individual gases by Omega, the manufacturer of the flow-meters. Figures **B.1, B.2, B.3, B.4, B.5,** and **B.6** are the curve fits from the data that are necessary to develop test conditions to simulate product species concentrations.

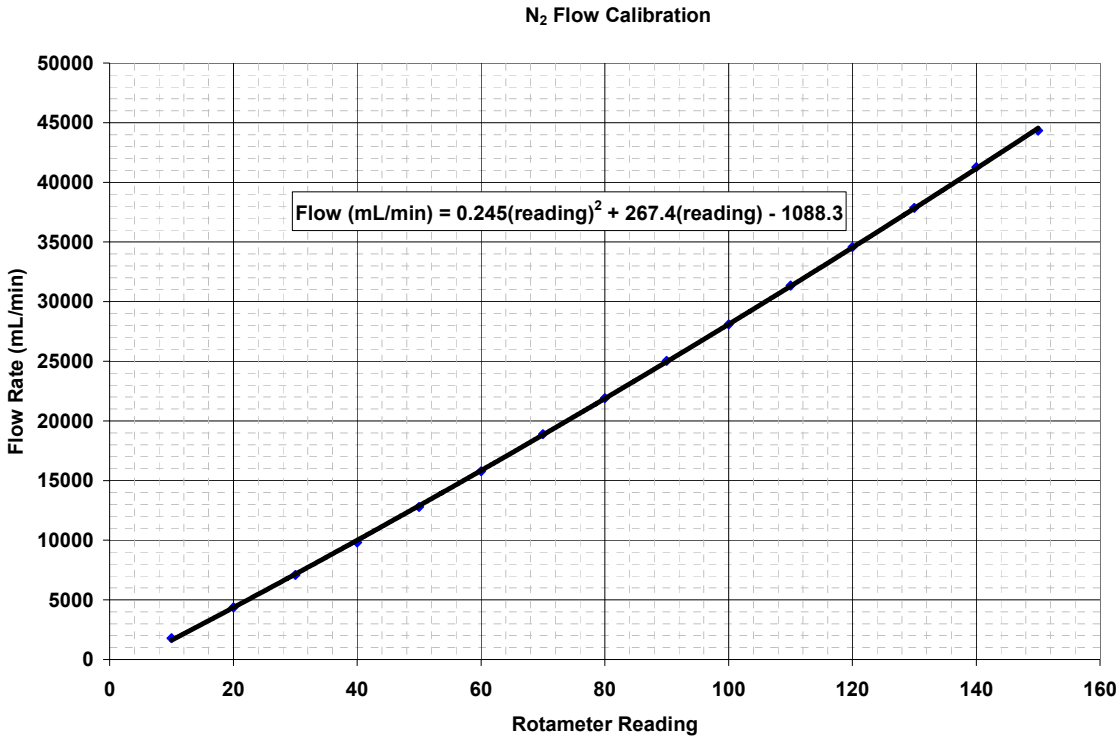

Figure **B.1**: Flow calibration for main N_2 flow-meter.

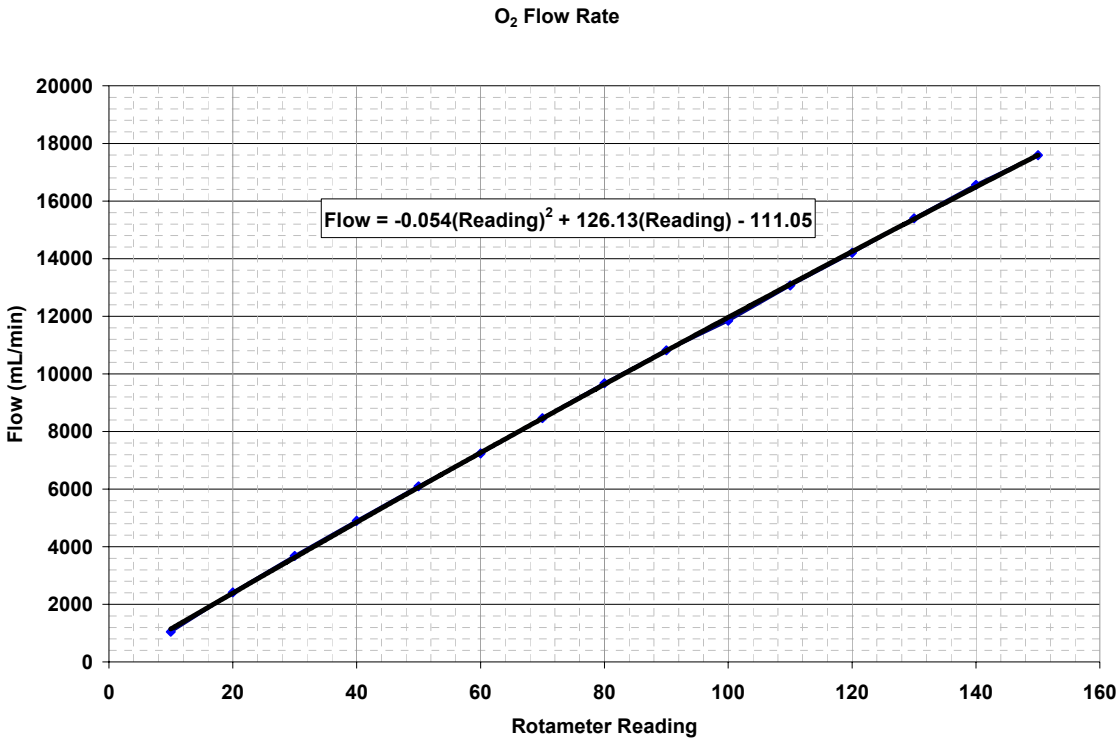

Figure **B.2**: Flow calibration for main O_2 flow-meter.

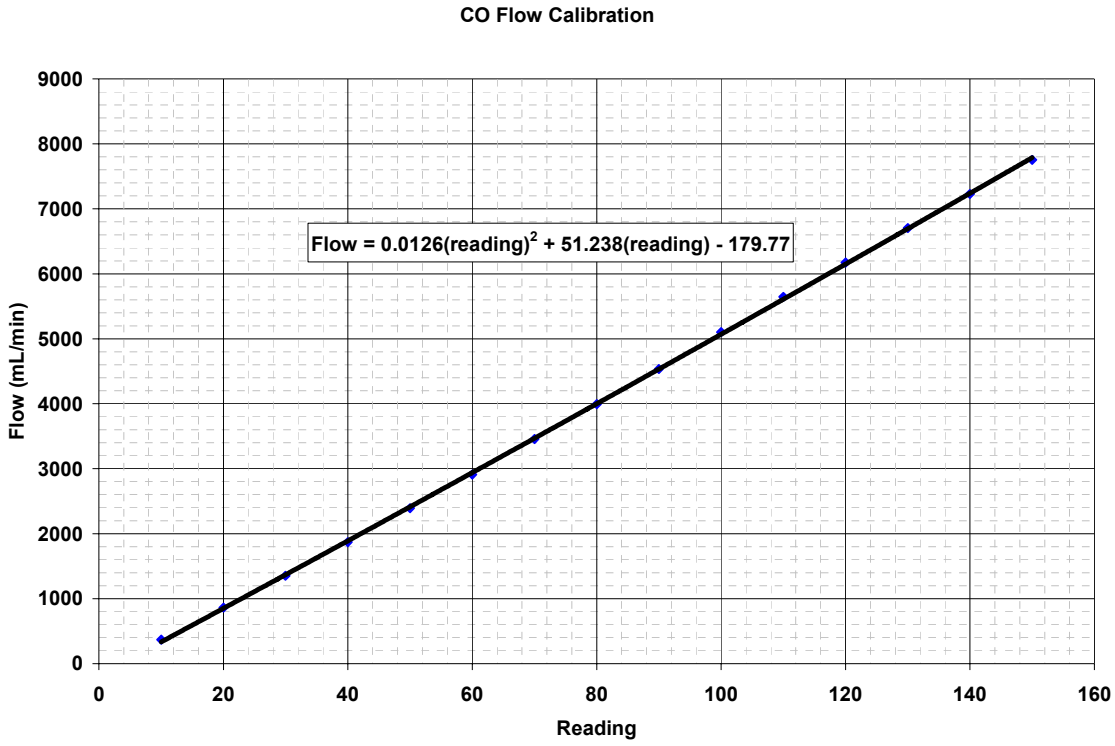

Figure **B.3**: Flow calibration for main CO flow-meter.

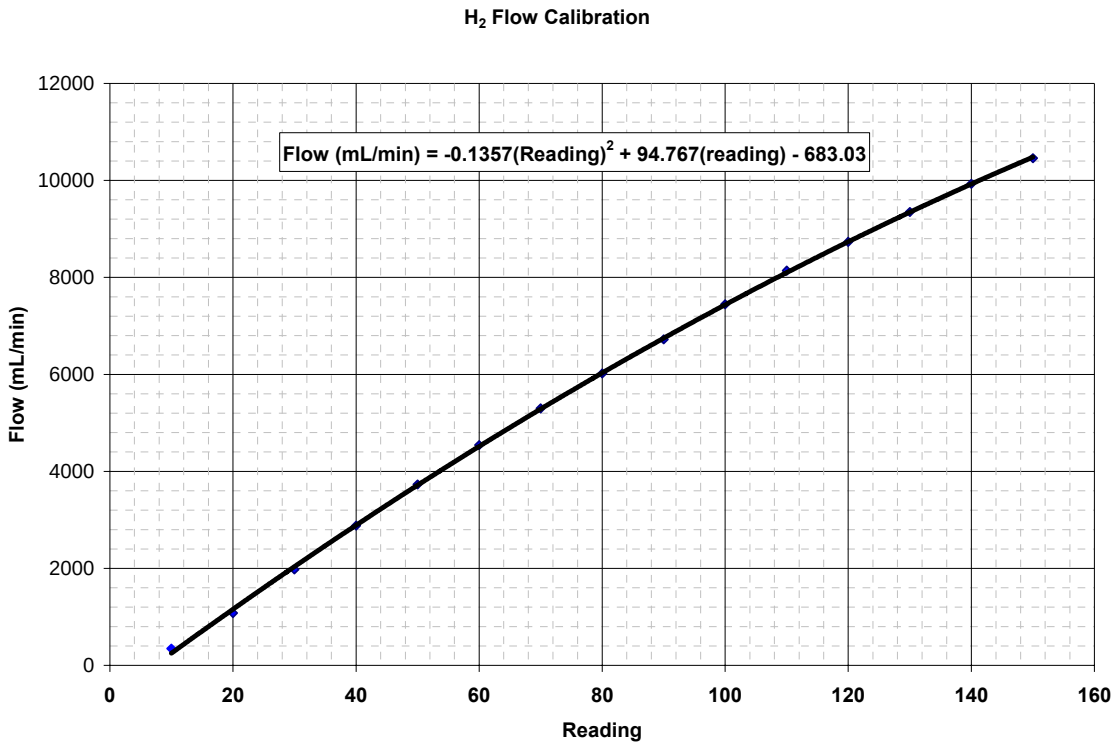

Figure **B.4**: Flow calibration for main H_2 flow-meter.

Figure **B.5**: Flow calibration for H_2 entrainment flow meter. Meant to be fed into the fluidized bed feeder.

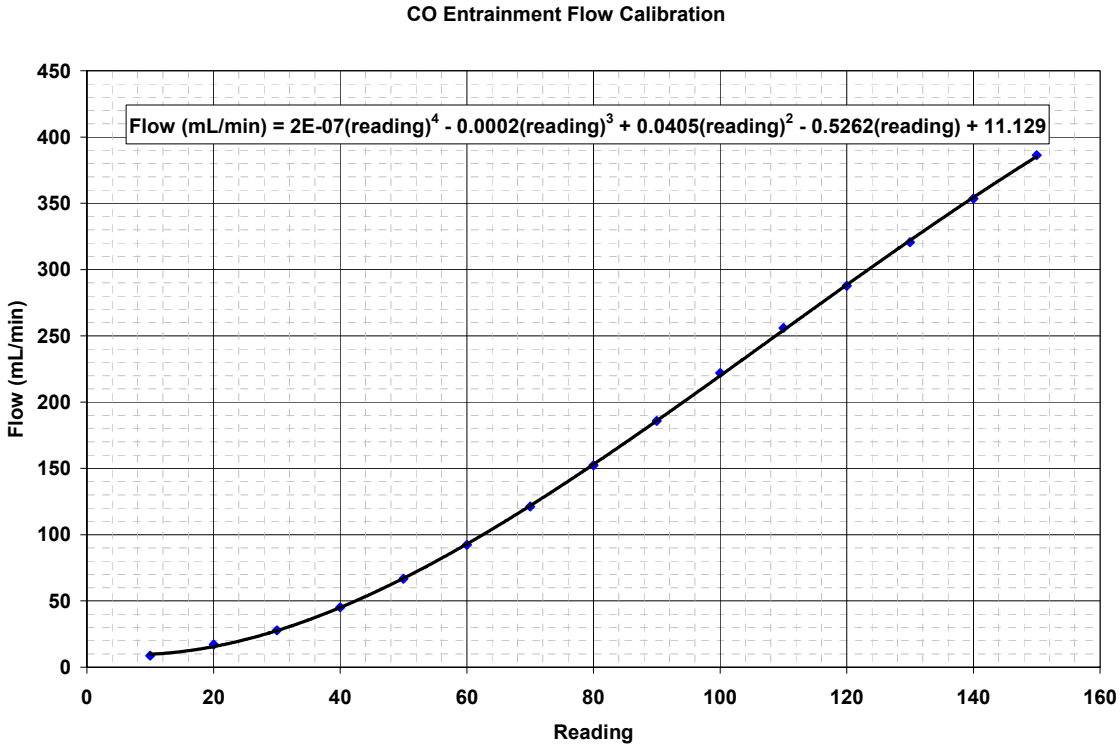

Figure **B.6**: Flow calibration for CO entrainment flow meter. Meant to be fed into the fluidized bed feeder.

Appendix C

Hazard Analysis

Hazard Analysis

of an

Experiment or System

at the

High Pressure Combustion Laboratory

The Pennsylvania State University

Project Name: Aluminum Combustion

Prepared by: Ryan Houim/Eric Boyd

Version:2.1

Reviewed and Approved by:

Director of the HPCL:_____

HPCL Safety Officer:_____

Table **C.1**: Hazard review mandatory mishap checklist

- ☐ Fuels and propellants
- ☐ Chemical initiators
- ☐ Explosive charges
- ☐ Chemical reactions
- ☐ Electrical current
- ☐ Shock (mechanical)
- ☐ Stored electrical sources
- ☐ Energy in any form
- ☐ High concentrations of toxicity
- ☐ Stress reversals or concentrations
- ☐ Radiation sources
- ☐ Heat or toxicity sources
- ☐ Oxidation /corrosion
- ☐ Moisture conditions
- ☐ OSHA violations
- ☐ Spring-loaded devices
- ☐ Objects that can be catapulted
- ☐ Objects that can disintegrate
- ☐ Falling, moving, or catapulted objects
- ☐ Elements which have become defective
- ☐ Initiation sensitivity
- ☐ Rate of burning or deflagration
- ☐ Protection capabilities of shields
- ☐ Prevent propagation due to blast overpressure
- ☐ Possible spillage of reactive materials
- ☐ Pressure Sources
  - ☐ high pressure
  - ☐ low pressure
  - ☐ dynamic pressure
- ☐ Electrical Conditions
  - ☐ energized surfaces
  - ☐ inadvertent activation
  - ☐ power source failure
- ☐ Actuating devices
- ☐ Noise or vibrations
- ☐ High velocities
- ☐ Contamination
- ☐ Unbalanced objects
- ☐ Excessive friction
- ☐ Penetrating or lacerating surfaces
- ☐ Moving mechanisms or machinery
- ☐ Condition which can lead to fire
- ☐ Structural weakness, damage, or failure
- ☐ Incompatible chemicals
- ☐ High levels of noise
- ☐ High levels of vibrations
- ☐ Objects that can move or fall
- ☐ Static-generating sources
- ☐ Mechanical power sources
- ☐ Leakage of fluids or electrical current
- ☐ Condition which can lead to explosion
- ☐ Hazards where controls may have been removed
- ☐ Hazards which personnel might be exposed
- ☐ Potential ignition sources
- ☐ Quantity of Ammunition and Explosives (A&E)
- ☐ A&E and personnel resource exposures
- ☐ Contain all fragmentation or direct fragments away from areas requiring protection
- ☐ Contain thermal effects to prevent propagation
- ☐ Hazardous Pressures
  - ☐ unusually high pressure
  - ☐ unusually low pressure
  - ☐ unusually dynamic pressure
- ☐ Hazardous Temperatures
  - ☐ unusually high temperatures
  - ☐ unusually low temperatures
  - ☐ unusually dynamic temperatures

Table **C.2:** Risk assessment levels

Mishap Risk Assessment Value	Mishap Risk Category	Suggested Criteria
1 – 5	High Risk	Unacceptable (Director of the HPCL Review and Decision Required)
6 – 9	Serious Risk	Undesirable (Director of the HPCL Decision Required)
10 – 17	Medium Risk	Acceptable (with Safety Officer's Review)
18 – 20	Low Risk	Acceptable

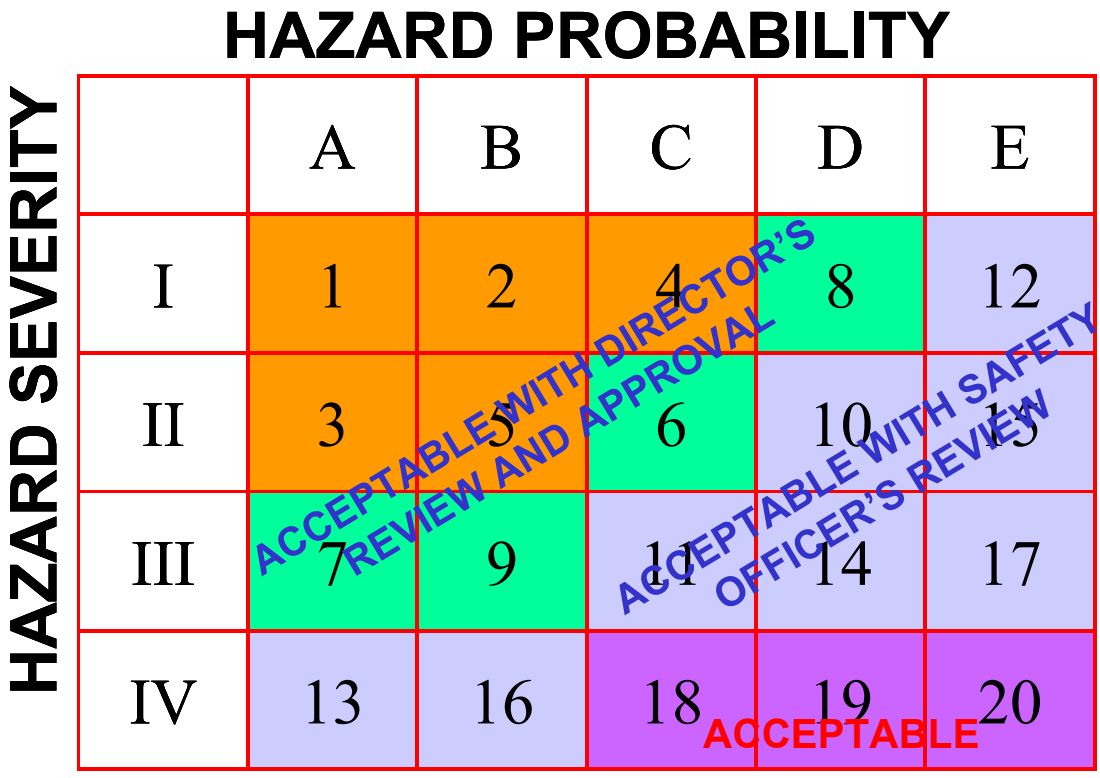

Figure **C.1:** Risk assessment matrix

Table **C.3**: Hazard severity

Category	Description	Environmental,Safety, and Health Result Criteria
I	Catastrophic	Could result in death, permanent total disability, loss exceeding $1M, or irreversible severe environmental damage that violates law or regulation
II	Critical	Could result in permanent partial disability, injuries or occupational illness that may results in loss exceeding $200K but less than $1M, hospitalization of at least 3 personnel, or reversible environmental damage causing a violation of law or regulation
III	Marginal	Could results in injury or occupational illness resulting in 1 or more lost work day(s), loss exceeding $10K but less than $200K, or mitigatible environmental damage without violation of law or regulation where restoration activities can be accomplished
IV	Negligible	Could result in injury or illness not resulting in a lost day of work, loss exceeding $2K but less $10K, or minimal environmental damage not violating law or regulation

Table **C.4**: Hazard probability

Category	Description	Specific Individual Item	Probability
A	Frequent	Likely to occur often in the life of an item	$P \geq 10^{-1}$
B	Probable	Will occur several times in the life of an item	$10^{-2} \leq P \leq 10^{-1}$
C	Occasional	Likely to occur some time in the life of an item	$10^{-3} \leq P \leq 10^{-2}$
D	Remote	Unlikely but possible to occur in the life of an item	$10^{-6} \leq P \leq 10^{-3}$
E	Improbable	So unlikely, it can be assumed occurrence may not be experienced	$P \leq 10^{-6}$

Table **C.5**: Potential Sources of Hazards

Hazard No.	**Energy Source and Hazard Description**	Potential Effects	**Potential Causal Factors**	**Initial Risk**	**Recommended Control Mechanisms/ Barriers**	**Final Risk**
1	hydrogen, oxygen, carbon monoxide, and nitrogen tanks in lab	See below	See below	See below	See below	See below
	(a) Leak	Suffocation/ poisoning, fire, explosion, pressure leaks	Broken junctions, loose fittings, slipped hose, etc.	I-C	Keep flow rates low, perform leak tests, after servicing parts	II-E
	(b) Tank fall	Explosion, fire	Failure to chain tank to wall, carelessness or accident	I-D	Keep tanks secured by chain, use caution in replacements	I-E
	(c) Line Rupture	Similar to severe leak	Over-pressurizing, kinks in the lines, damage to tube	I-D	Keep pressures below 80 psi, keep lines straight, inspect for wear	I-E

	(d) Uncontrolled high flow	Uncontrolled fire on table	Failure of flow regulator or pressure regulator	III-D	Replace problematic regulators, keep extinguisher on hand	III-E
2	Hand held lighter full of propane	Could leak, rupture or explode	Leaving lighter in or near flame region, dropping, etc.	III-D	Keep lighter from hot areas, use caution	III-E
3	Electric lines throughout	Could shock user, or short and cause damage	Stripped or disconnected lead, power surge	II-C	Continue to use surge protector, inspect lines regularly	II-D
4	Combustion burst when oxygen is activated	Could scatter hot particles, injure user	Probably due to burst of oxygen into flame during transitional period	III-C	Wear goggles and coat, turn on oxygen slowly	III-E
5	Detonation of SAVIT charges next door	Vibrations to system; damage	Unsecured or loose equipment on cart	III-D	Keep cart need and keep all components tightened	III-D
6	Aluminum particles form explosive aerosol	Explosion, fire, injury	Large spill of aluminum particles	II-C	Take great care moving Al; only transport small vials	III-D

7	Accumulation of fuels, oxidizers over burner	Fire, explosion	Failure of fan, or failure to use fan	II-D	Use the fan; if fan becomes inoperative, discontinue experiment	III-E
8	Use of lasers	Eye injury, burns, accidental ignition	Failure to heed laser warnings, unexpected reflection	III-C	Use beam block, eye protection, secure all optics and take care with reflective surfaces	III-D
9	Hot burner	Burns, fire hazard	Accident or careless use of equipment	III-D	Use purge and shielding gases, use caution with heated surfaces	III-E
10	Rust/water from vent shaft (roof leak)	Equipment damage	There seems to be a leak in the vent ducting	IV-B	Monitor leakage; fix leak if problem persists or worsens	IV-B
11	Glass tube full of aluminum flakes (shatters)	Glass shards, inhalants, and a flammable Al aerosol	Collision of cart with other table, similar accident	III-D	Remove or secure cylinder when moving cart	III-E

12	Equipment and other items fall from cart	Minor damage, minor injury	Messiness	IV-B	Keep area reasonably clean	IV-C
13	Bad regulators	Loss of pressure control	Regulator failure	III-C	Order new regulators; turn off pressure after tests	III-D
14	Overlarge flame	Damage to mesh, optics; uncontrolled fire	Oversupply of methane or hydrogen	III-B	Keep fuel flows low; and diluting gas	III-D
15	Dust/debris in Al feed	Unexpected energetic burning, fire	Failure to keep Al/bead mixture sealed	III-D	Keep feed mixture sealed	IV-E
16	Banging head on cowl	Pain	Carelessness	IV-A	Possibly paint or tape the hood's cowl with something bright and visible	IV-C
17	Static buildup in lines	Arcing, shocks, possible ignition	Particle abrasion on line	III-E	If needed, coat lines with foil and ground and test them	IV-E
18	Physical damage to tubing	Serious gas leak	Lines get caught or tripped over	II-B	Clean, sort, and tie off line, control foot traffic near stand	II-D

19	Photo-multiplier and steel base knocked off	Pain, damage to equipment, loss of P.M. tube	Clamps loosened, accident, etc.	III-C	Keep that clamp on, perhaps add a second. Don't tip or jar this equipment	III-D
20	Carbon monoxide leak	Death or serious injury from CO inhalation	Caused from leaking, line rupture, or uncontrolled high CO flow. See items 2, 4, 5 for more details	III-C	Use CO detector. If CO levels are above 200ppm close CO bottle and evacuate premises immediately; alert others of hazard	I-E
21	Shattering of quartz tube	Serious injury or damage to equipment	Caused premixture of fuel and oxygen in hot quartz tube after experiment or flame blowout	II-C	Do not flow O2 and fuel simultaneously when burner is not ignited When venting do not allow fuel to be in tube without running diluent flow at a high flow rate	II-D

Appendix D

STANDARD OPERATIONAL PROCEDURE

FOR

SINGLE METAL PARTICLE COMBUSTION TESTS

High Pressure Combustion Laboratory
Department of Mechanical and Nuclear Engineering
The Pennsylvania State University

Prepared by: Date:

_____ _____

Ryan Houim
Research Associate

Revised by: Date:

_____ _____

Eric Boyd
Research Assistant

Approved by: **Date:**

_____ _____

Prof. Kenneth K. Kuo
Director of HPCL

February 2009

THE PENNSYLAVANIA STATE UNIVERSITY

HIGH PRESSURE COMBUSTION LABORATORY

UNIVERSITY PARK, PA 16802

STANDARD OPERATING PROCEDURE Spring, 2009

VERSION: 3.1

SAFETY

SINGLE METAL PARTICLE COMBUSTION TESTS

I. Purpose

To establish safe operating procedures associated with combustion of ultra-fine metal particles in the post-flame region of a flat-flame burner which uses O_2 oxidizers and to assign responsibilities for the operation of single metal particle combustion experimental setup.

II. Scope

This SOP applies to operations associated with combustion of ultra-fine metal particles in the post-flame region of a flat-flame burner which uses O_2 oxidizers, Room 107, at the High Pressure Combustion Laboratory (Bldg 430). Operations that are not adequately covered by this SOP will be addressed in a separate SOP or a supplement to this SOP.

III. Applicability

This SOP applies to all Penn State, HPCL, and visiting personnel and all other personnel assigned to support the operation of the LGCP experiment.

IV. Responsibility

A. The Director of the High Pressure Combustion Laboratory and Distinguished Professor of Mechanical Engineering, Dr. Kenneth K. Kuo, is responsible for the overall enforcement of this SOP. Dr. Kuo is further responsible that only trained personnel are assigned to these operations and that all personnel are informed of all of the hazards associated with this experimental procedure.

B. The Experimentalist/Researcher/Graduate Student (E/R/GS) is responsible for application and enforcement of this SOP and overall on-site supervision of the experiments, to include taking necessary actions to protect all personnel, equipment, and facilities from any blast, fragmentation, or fire resulting from an experiment under his (or her) control. The E/R/GS is responsible that all personnel assigned to the testing programs have been adequately trained. Also, prior to any operation, they have been thoroughly briefed on duties, responsibilities, and hazards that mat be involved.

V. Personnel Limits

A. Personnel will be limited to the minimum required for safe and efficient operation of each experiment

B. A minimum of two trained persons must be present for any hazardous operation.

C. Observing personnel will be limited to those having an official interest in the experiment.

VI. Hazardous Material Limits

Hazardous material at least at the test site and fuel processing site will be limited to the amount necessary for safe and efficient operation of the program. All material not involved in the current test will be adequately protected and located so that it is not exposed to any personnel. Bulk aluminum stock will be maintained in the chemical or flammable cabinets; samples in use will be kept to a minimum and located in the flat flame burner cabinet in appropriate containers. All gas cylinders will be sealed when not in use.

VII. General Safety Requirements

A. Oxygen, hydrogen, carbon monoxide, argon, and nitrogen gases will be used in experiments. CO detectors and the exhaust fan will be turned on prior to each test involving CO. During tests not involving toxic gases, the exhaust fan must still be employed to prevent the accumulation of product or flammable gases.

VIII. Personal Protective Equipment Requirements

A. Safety glasses will be worn for all eye hazard operations.

IX. Sequence of Operations

A. Preparation of Metal Particle/Glass Bead Mixture:

1) Clean the glass tube with soap and water. Then put it in an oven until it is completely dry.
2) Mix metal particles and glass beads in the ratio between 1:15 to 1:20. The amount of metal particles should be about 5 gr.

3) Place the O-ring gasket between the glass tube and the bottom flange and tighten it using four bolts. Then put the metal particle/glass bead mixture into the glass tube. Install another Teflon gasket between the glass tube and the top flange and tighten it using bolts.
4) Connect the particle carrying gas ($N_2/H_2/CO$) line to the bottom flange.
5) Connect the particle feeding line to the top flange.

B. Preparation prior to Test:

If the Xybion Camera is used

1) When CO gas is used as a part of the oxidizer, turn on the CO monitor by plugging it in and testing in by pressing the test button located on the front panel of the instrument.
2) Turn on the exhaust fan by pressing the green START key on the panel display mounted on the wall next to the thermocouple room. During the test, the speed of the fan should be adjusted so that it does not disturb the burner flame.
3) Open one of the exit doors next to the test area to have fresh air and good ventilation.
4) If the test includes ignition-delay-time measurements, turn on the Cu-Vapor laser at least one hour before the test following the instructions given in the laser operation manual.
5) Open the valves on gas bottles and verify there are enough gases in the cylinders.
6) Turn on the He-Ne laser.

7) Using a low flowrate of particle carrying gas ($N_2/H_2/CO$), let some metal particles flow through the particle feeding tube.
8) Align the He-Ne laser so that the laser beam hits the metal particles and scatters light. Make sure that the laser beam is about 1 mm (or less) above the burner surface. The focus of the laser can be adjusted by moving the focusing lens back and forth.
9) Remove the cover on the top of the photo-multiplier tube to install the eyepiece.
10) Using the eyepiece adjust the location of the lens in front of the photo-multiplier tube to have a focused image of the boron particles on the eyepiece.
11) Take the eyepiece out and replace it with the top cover.
12) Turn on the power to the photo-multiplier tube. Set the knob to ¾ position. Note: Do not turn on the power to photo-multiplier tube unless the top cover is installed in its place.
13) Turn on the function generator. Check the width of the gating signal to the Xybion camera. The streak photography mode (combustion time measurements) needs a longer gating signal whereas multi-exposure mode (particle velocity measurements) needs short gating signal.
14) Stop the flow of particle carrying gas.
15) Turn on the control box for the Xybion camera.
16) Turn on the TV and VCR.
17) Connect the Xybion camera to VCR.

18) Position the Xybion camera at a desirable location such that its viewing area can see the completely burning particle streak. Adjust the focus of the Xybion camera by placing a ruler at the center of the burner where metal particles are being fed.

19) Put a DVD into the DVD recorder. Using the function generator write the necessary information about the test on the TV screen.

20) Open the water valve for cooling the premixed flat-flame burner (skip this step if multi-diffusion flat flame burner is used).

21) Turn on the amplifier, which amplifies the signal from the photo-multiplier tube.

If the PMT is to be used directly for measurement

1) Make sure the PMT is aligned with path traveled by the metal particles.

2) When CO gas is used as a part of the oxidizer, turn on the CO monitor by plugging it in and testing in by pressing the test button located on the front panel of the instrument.

3) Turn on the exhaust fan by pressing the green START key on the panel display mounted on the wall next to the thermocouple room. During the test, the speed of the fan should be adjusted so that it does not disturb the burner flame.

4) Open one of the exit doors next to the test area to have fresh air and good ventilation.

5) Open the valves on gas bottles and verify there are enough gases in the cylinders.
6) Start the data acquisition program.
7) Begin to increase the gain slowly on the PMT controller until voltage peaks can be seen from the particle combustion.

C. During the Test:

1) Care must be taken when selecting flow rates for the test conditions. If the oxidizer and diluent flow rates are too high, the resonance frequency of the quartz tube can be reached potentially causing the tube to shatter. If a high-pitched loud noise from the tube begins to occur, immediately back off the all flow rates.
2) Make an announcement of the test to warn the people in the lab about the use of CO toxic gas.
3) Open the valves on the regulators of each gas and set the pressures to 40 psig on pressure gages at the control panel.
4) Open the purge valve to ensure that the fuel lines are clear of all fuel and diffused oxidizing gases.
5) Slowly turn open the H_2 valve while holding a lighter over the fuel ports until a barely visible flame is ignited. The flame on the lighter may go out, just reignite it until the burner is ignited.

6) Open the oxidizer valve to high level so that there is an abundance of oxygen in the flame preventing it from being extinguished when the tube is placed onto the burner.
7) Holding around the top of the quartz tube place it onto the burner now. (This absolutely must be done after the flame is ignited to prevent a hard ignition and subsequent shattering of the quartz tube.)
8) Adjust the flow rates of the O_2 and diluent based on desired conditions.
9) After setting up the flame, open the hand valve on the CO line and start adding CO slowly according to the desired flow rate.
10) Wait until all the flow rates reach the steady state.
11) Start injecting Al flakes into the flame with enough carrying gas flow rate such that the number density of particles is not too high.
12) Start the DVD recorder to record the particle combustion event if the camera is used or start recording data with the data acquisition system if the PMT is to be used directly for the combustion time measurements.
13) If necessary, adjust the brightness of the picture by using the GAIN knob on the control box for the Xybion camera.
14) After recording sufficient amount of data, switch the mode of the function generator from streak photography to multi-exposure.
15) After the test is done, close the fuel and the oxidizer valves on the gas bottles respectively.
16) Purge N_2 through gas feeding lines and the burner for a couple of minutes to cool down the burner and to clean the lines.

17) Clean the top surface of the burner using a brush while purge is on.

D. After the Test:

1) Increase the diluent flow to and turn off the oxygen and fuel flows.
2) Leave the diluent flowing to prevent the fuels from premixing with any oxygen in the hot quartz tube.
3) Release the pressure of the fuels then purge the system with N_2.
4) Release the pressure of the oxidizer then purge the system N_2.
5) Turn off diluent and release its pressure.
6) Wait at least 15 minutes to remove the quartz tube, as it is still very hot from running the test.
7) Turn off the He-Ne laser.
8) Stop recording the VCR/DVD-R.
9) Turn off the control box for the Xybion camera.
10) Turn off the amplifier.
11) Turn off the power to the photo-multiplier tube.
12) Let the exhaust fan run for at least 15 minutes and then shut it off.
13) Check all the gas bottles and flowmeters and make sure they are all tightly closed. Release the valves on the regulators.

X. Malfunction

The E / R / GS will perform the following steps if the CO detector alarms are on in case there is a gas leak.

A. Close all the gas bottles to turn the burner flame off.

B. Increase the speed of the exhaust fan to the maximum to withdraw fresh air to the test cell.

C. Leave the test area for a couple of minutes.

D. Purge the system with nitrogen to remove any fuel or oxidizer gases in the lines.

E. Diagnose the problems.

XI. Posting Requirements

A copy of this SOP, and any other related SOPs, will be prominently displayed at the site of this experimental operation. (Test Cell Room 127, HPCL, Bldg 430).

Appendix E

Data Sheets

Aluminum Particle Combustion Tests

Particle Type: _____
Coating: _____
Date: _____
Operator Initials: _____

Main Panel Gas Composition for Ignition Tests (meter readouts)
CO main flow: _____
H_2 main flow: _____
O_2 main flow: _____
N_2 main flow: _____

Entrainment Panel Gas Composition Mixture:
N_2 entrainment: _____
H_2 entrainment: _____
CO entrainment: _____

Ruler Track #: _____
Track #: _____
Disk Name:_____

Notes:

Aluminum Particle Ignition Tests

Particle Type: _____
Coating: _____
Date: _____
Operator Initials: _____

Fuel Mixture: _____ %H_2/_____ %CO
Phi: _____

Main Panel Gas Composition for Ignition Tests (meter readouts)
CO main flow: _____
H_2 main flow: _____
O_2 main flow: _____
N_2 main flow: _Variable (See Chart Below)_____

Entrainment Panel Gas Composition Mixture:
N_2 entrainment: _____
H_2 entrainment: _____
CO entrainment: _____

Disc Name: _____
Ruler Track #: _____
Track #: _____

Ignition Test:

N_2 Flow Reading	"Go" or "No Go"

Notes: